INTRINSIC DISORDER AND AMPHITROPISM IN THE MITOCHONDRIAL FISSION MECHANOENZYME DRP1

by
Ammon E. Posey

A dissertation submitted to Johns Hopkins University in conformity with the requirements for the degree of Doctor of Philosophy

Baltimore, Maryland
June, 2014

Abstract

The Dynamin superfamily is a class of large GTPases that perform essential membrane remodeling events via self-assembly stimulated GTP hydrolysis in a manner that is not well understood. Malfunction in these enzymes is the basis of a number of diseases. Dynamin superfamily enzymes hydrolyze GTP via a G domain, self-assemble via a stalk domain, and may couple assembly and hydrolysis via a "bundle signaling element" domain. An additional "variable domain" (VD) is present in many superfamily members and may enable specific targeting to sites of action, but the nature of VD function is unclear in most dynamins. While VDs are not conserved in amino acid sequence, they may have similarities in function, namely allosteric regulation and membrane interaction. We identify two modes of membrane interaction in the dynamin superfamily: (1) tethering to the membrane via a transmembrane helix or a lipophilic anchor and (2) untethered, reversible interaction with membranes (amphitropism). We propose a subclassification of the dynamin superfamily into these two categories. We employ the mitochondrial dynamin, Drp1 as a model of the amphitropic dynamins because of its relative simplicity and relevance to human health. Specifically, we seek to identify the role of the Drp1 VD, or B domain, anticipating that it will also inform understanding of VDs in other amphitropic dynamins. We find that removal of the B domain from Drp1 results in enhanced assembly and GTP hydrolysis, suggesting that the B domain has an auto-inhibitory role. We find that the B domain is intrinsically disordered (ID) and surprisingly, undergoes phase separation or coacervation under conditions that induce other IDPs to fold. Finally, we show that the B domain binds lipid membranes with a preference for cardiolipin, and that this interaction is enhanced under conditions that favor the coacervated state. Based on these findings we suggest the possibility that the B domain acts as an entropic bristle in order to inhibit Drp1 assembly, and that this auto-inhibition is relieved upon

interaction of the B domain with a lipid membrane, perhaps involving the process of coacervation. We suspect that this model may also be applicable to other amphitropic dynamins.

Thesis advisers and readers: Dr. R. Blake Hill and Dr. Vincent J. Hilser
Thesis committee members: Dr. Juliette Lecomte, Dr. Karen Fleming, Dr. Tom Woolf

Dedication

To my wife and children

Acknowledgments

Working toward a doctoral degree has been one of the most challenging experiences of my life. Without the support of mentors, colleagues, family and friends, I would have failed. I express my sincere gratitude to each of you.

I could not have asked for a more attentive mentor than Dr. Blake Hill, who has provided thoughtful guidance and perspective at every step of my graduate career, from my first expression of interest in his lab to the final draft of my dissertation. I continue to be amazed by his ability to step back from a problem and assess it from nearly every angle possible. I have grown tremendously as a scientist under his instruction.

I express appreciation to my labmates Rob Wells, Lora Picton, Jonathan Lees, Marijke Koppenol-Raab and C. M. Manlandro for offering instruction, expert advice, constructive feedback and friendship throughout our time together in the Hill lab. I learned many important experimental skills as a result of their generous sharing of knowledge and expertise.

When the Hill Lab moved to the Medical College of Wisconsin and my personal circumstances made it difficult for me to follow, Dr. Vince Hilser was kind enough to take me under his wing, for which I will be forever grateful. The completion of my thesis research would have been very difficult if not impossible without his generosity. I also sincerely appreciate his assistance in securing teaching assistantships and a postdoctoral position.

I greatly appreciate the members of the Hilser lab for being my adoptive lab family and accepting me as one of their own. They shared their lab benches, freezer space, lab equipment and sharp minds with me. I am fortunate to have associated with and learned from each of them. I am especially grateful to Jing Li, who shared with me her expertise regarding intrinsically disordered proteins, fluorescence and osmolytes.

My committee members, Drs. Juliette Lecomte, Karen Fleming and Tom Woolf, have been exceptionally supportive. I appreciate the time they have taken to ask thoughtful questions, offer advice and provide assistance with experiments.

Many others have been generous in sharing their expert knowledge. I am particularly grateful to Drs. Dima Toptygin and Arne Schön for many enlightening conversations.

I am deeply indebted to my parents, David and Lorie Posey, for instilling in me a love of learning. I cannot thank them enough for their continual encouragement and endless concern for my success. I also thank my wife's parents, Brad and Kathy Jensen, for their unwavering support of me and my family. Quick weekend getaways to their home in West Virginia provided us with much needed repose.

I would not have succeeded without the support of my wife, Juliana, who has shouldered more than her share of parenting and household burdens while I completed this degree. Words are insufficient to express my gratitude for the sacrifices she has made.

Finally, I express my appreciation to my children, Ryley, Jensen, Evelyn and Eugene for being their bright, rambunctious, adorable selves. Each one of them is a source of inspiration and motivation to me.

Table of Contents

List of Tables

List of Figures

Chapter 1

Introduction: Lipid membrane remodeling, the dynamin superfamily, Drp1 and mitochondrial fission

Lipid membrane remodeling

A lipid membrane (i.e. the plasma membrane) forms the boundary that defines the basic unit of life, the cell. In eukaryotes, lipid membranes not only separate a cell from its surroundings, but also enclose subcellular spaces in the form of organelles. The nucleus, the endoplasmic reticulum (ER), the Golgi, mitochondria and peroxisomes are all delineated by lipid membranes. Eukaryotic intracellular and plasma membranes are dynamic structures that continually undergo remodeling events that are critical to cellular function[1–3]. A common vehicle by which lipids and proteins are transported throughout the cell, e.g., from the ER to the Golgi and from the Golgi to a variety of final destinations, involves the budding and detachment (scission) of a lipid vesicle from one membrane, and the eventual fusion of the vesicle with another membrane[4]. Signaling molecules, nutrients, plasma membrane proteins and other cargo from the extracellular environment are internalized through invagination and vesiculation of the plasma membrane[2]. Conversely, cytoplasmic cargo, encapsulated in lipid vesicles, is exported as the vesicles fuse with the plasma membrane and release their contents externally[5]. Mitochondria multiply through growth and division[6] and also divide to facilitate being transported throughout the cell[7] or to enable selective degradation through mitophagy[8]. Mitochondria fuse to form networks[9]. Peroxisomes bud from the ER and also divide and fuse during the course of their function of metabolizing fatty acids and other biomolecules[10–12]. Each of these membrane remodeling events requires protein machinery[13–15], which we refer to here collectively as membrane-remodeling enzymes.

The dynamin superfamily

While there are many types of membrane remodeling enzymes, this dissertation will focus on a protein in the dynamin superfamily. Dynamins are a functionally diverse group of

multi-domain GTPases involved in wide variety of membrane remodeling events throughout the cell. Phylogenetically, the dynamin superfamily divides into several clades (Figure 1.1). These clades have traditionally been grouped into three major subfamilies based on their cellular function and similarity in sequence and/or structure to the prototypical classical dynamins (dynamin-1, -2 and -3): (1) the classical dynamins (2) the dynamin-related proteins and (3) the guanylate binding proteins (GBPs) and atlastins[16]. We use the traditional subgrouping here for the sake of convenience, but note that it is somewhat equivocal for reasons described below. Classical dynamins are generally responsible for mediating vesicle scission in the endocytic and secretory pathways[16]. The prototypical superfamily members, dynamin-1 and dynamin-2, catalyze the scission of endocytic vesicles during clathrin-mediated endocytosis[17,18]. Dynamin-2 has also been implicated in mediating vesicle transport from the late endosome to the Golgi[19]. Yeast do not have a classical dynamin, and this role is instead fulfilled by Vps1[20], which is more similar to the dynamin-related protein subfamily than the classical dynamins. Vps1 is also involved in Golgi-to-vacuole transport and peroxisome fission[21–23]. The dynamin-related protein subfamily includes several clades of proteins that are primarily involved in mediating fission and fusion of mitochondria and peroxisomes, including dynamin-related proteins proper (Drps), OPA1 and mitofusins. Drp1 catalyzes mitochondrial and peroxisomal fission[7,24–26], while OPA1 and the mitofusins mediate the fusion of the inner and outer mitochondrial membranes, respectively. In addition to these proteins that act on the mitochondria, the interferon-induced Mx proteins are also grouped with the dynamin-related protein subfamily, due to their similarity in sequence and structure to the classical dynamins[27]. Functionally, however, the MxA proteins are an exception in this subfamily as they are involved in viral resistance rather than organellar remodeling[27,28]. They do exhibit membrane remodeling ability[29], but the role of membrane remodeling in viral resistance is unclear. The third subfamily of dynamin proteins is comprised

of the guanylate binding proteins (GBPs) and the atlastin GTPases. Guanylate-binding proteins (GBPs) have a similar function as Mx proteins in that they are involved in pathogen resistance[30], but unlike the Mx proteins they are a more distant relative to the classical dynamins. Atlastin GTPases, on the other hand, have a function more similar to the mitofusins, as they mediate

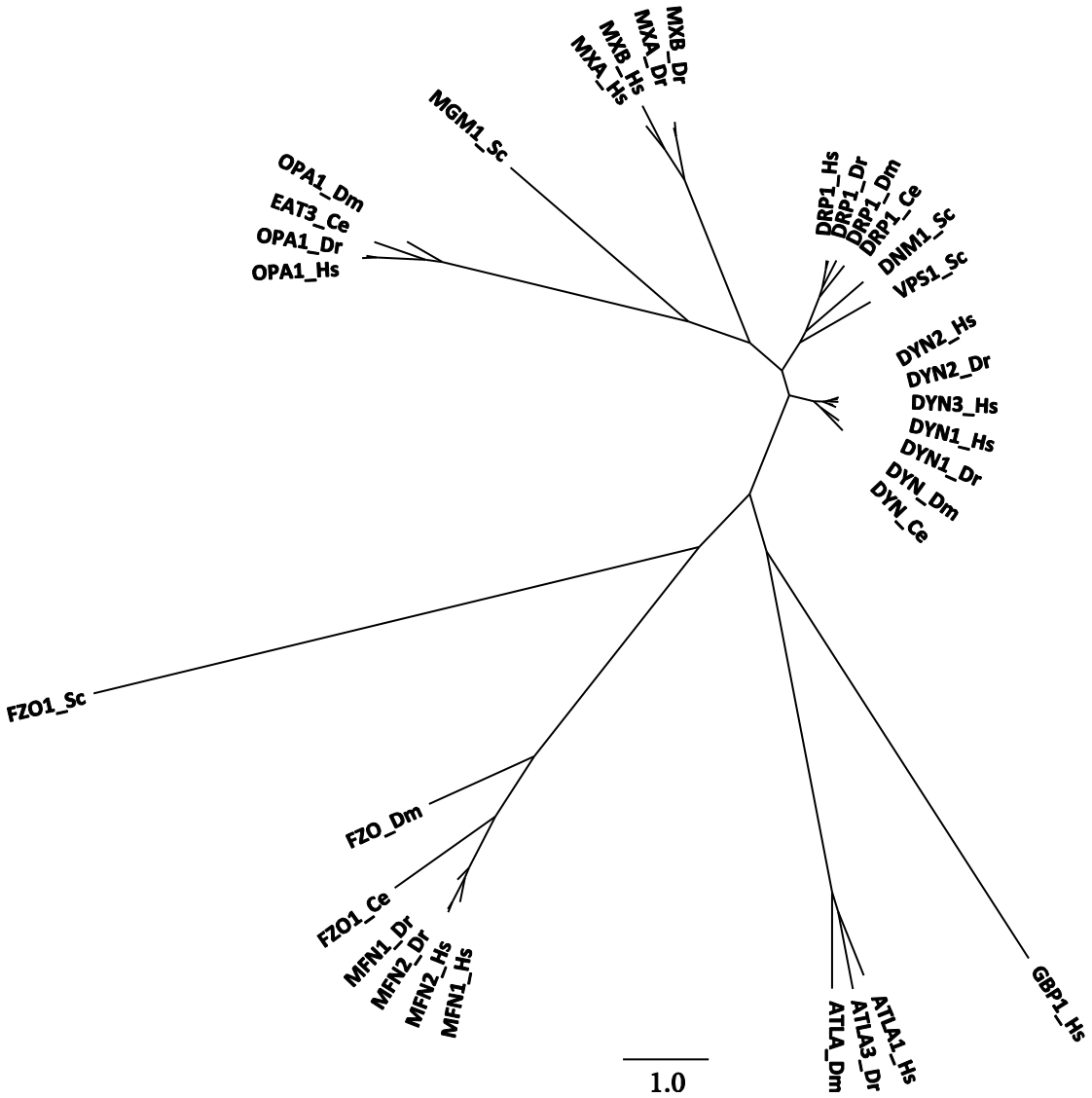

Figure 1.1 Phylogenetic tree of the dynamin superfamily with selections from fungi to humans. The tree suggests a close relationship between classical dynamins (Dyn), dynamin-related proteins (Drp) and myxovirus resistance (Mx) proteins. The phylogenetic tree was produced from sequences aligned by MUSCLE using the PhyML (maximum likelihood) algorithm as implemented in SeaView. The figure was generated using the FigTree software package. Scale bar denotes average number of substitutions per site. Abbreviations: Ce = Caenorhabditis elegans; Dm = Drosophila melanogaster; Dr = Danio rerio; Hs = Homo sapiens; Sc = Saccharomyces cerevisiae

homotypic fusion of the ER and of the Golgi[31,32]. Our phylogenetic analysis suggests that mitofusins are as distantly related to classical dynamins as the GBPs and atlastins, and perhaps belong in their own subfamily rather than in the dynamin-related protein subfamily.

Pathology related to the dynamin superfamily

Given the importance of membrane remodeling to a multitude of cellular functions, perhaps it is not surprising that defects in dynamin proteins have dire consequences for human health. In fact, mutations in every dynamin superfamily member have been linked to severe phenotypes and pathologies in humans (Table 1.1). Mutations in the three classical dynamins – dynamin-1, dynamin-2 and dynamin-3 – have been linked to severe neurological diseases, including centronuclear myopathy[33–36]; Charcot-Marie-Tooth disease, a sensory and motor neuropathy[37,38]; Alzheimer disease[39]; and proteinuric kidney disease[40]. Dynamin-related proteins are also implicated in severe human pathologies. For example, increased susceptibility to viral pathogens is linked to malfunction of MxA[41]. Mutations in the mitofusins, Mfn1 and Mfn2, cause Charcot-Marie-Tooth disease[42,43], likely due to altered mitochondrial trafficking in the axons of neurons[44–46]. Mutations in OPA1, the dynamin-related protein responsible for fusion of the inner mitochondrial membrane, cause dominant optic atrophy, which results in a progressive loss of the nerve cells that line the retina[47–49]. Optic atrophy has also been linked to defects in Drp1[50,51]. Defects in Drp1 has also been implicated in neonatal lethality[50,51], cardiomyopathy[52], embryonic lethality[53,54], Parkinson's disease[55,56], among others. Human disease has also been reported for protein in the third sub-family of dynamins, the atlastins and guanylate binding proteins. Spastic paraplegia is caused by malfunction of Atlastin-1[32], presumably due to the disruption of ER fusion[57]. Finally, mutations in GBP proteins, similar to MxA, have been linked to increased susceptibility to pathogens[58]. A summary of these and

other pathogenic phenotypes associated with defects in dynamin superfamily proteins is provided in Table 1.1.

Table 1.1

Protein	Intracellular targets	Function	Related pathology
Dynamin(1-3)	plasma membrane endosomes Golgi	scission of endocytic bud necks	Centronuclear Myopathy (CNM)
Vps1 (yeast)	plasma membrane endosomes Golgi	scission of endocytic bud necks vesicle scission and transport	endocytic defects accumulation of protein in Golgi
MxA	cytoplasm smooth ER	antiviral	no inactivating mutations reported virus susceptibility in knock-out mice
Drp1	mitochondrial outer membrane	mitochondrial fission	abnormal brain development optic atrophy neonatal lethality
Mfn(1-2)	mitochondrial outer membrane	mitochondrial fusion	Charcot-Marie-Tooth disease (CMT) (sensory and motor neuron degeneration)
OPA1	mitochondrial inner membrane	mitochondrial fusion	autosomal dominant optic atrophy degeneration of retinal ganglion cells and optic nerve; loss of visual acuity
GBP(1-7)	cytoplasm Golgi	antipathogenic (Listeria, Mycobacteria)	no inactivating mutations reported
Atlastin-1	ER	fusion of ER tubules	hereditary spastic paraplegia (shortened axons in corticospinal

Domain architecture in the dynamin superfamily

Members of the dynamin superfamily are (1) multi-domain GTPases that (2) utilize assembly-dependent GTP hydrolysis to (3) remodel cellular membranes[16,59]. Dynamin superfamily members share a specific domain architecture that includes, at a minimum, a G domain that binds GTP with low affinity and hydrolyzes it to GDP and a coiled-coil Stalk domain which is responsible for self-assembly (Figure 1.2). Upon enzyme assembly, GTP hydrolysis has

been shown to be enhanced in several dynamin superfamily members[48,51,60], and this phenomenon is best characterized in the classical dynamins, where the assembly-dependent increase in GTP hydrolysis can be up to 100-fold[61–63]. Many superfamily members also have a three-helix bundle known as the bundle signaling element (BSE), which may be involved in allosteric coordination of assembly and hydrolysis[63,64]. Additional domains vary between family members and may impart specificity. For example, classical dynamins have a Pleckstrin homology (PH) domain that binds phosphoinositides and a proline-rich (PR) domain that interacts with SH3 binding partners. In place of the PH domain in classical dynamins, Drp1 has a domain of unknown structure and function called the B domain. In Mx proteins this region is a loop known as L4. OPA1 and mitofusins have a transmembrane helix or helices, respectively, that anchor them to their target membranes, and OPA1 also has a mitochondrial targeting sequence at its N terminus.

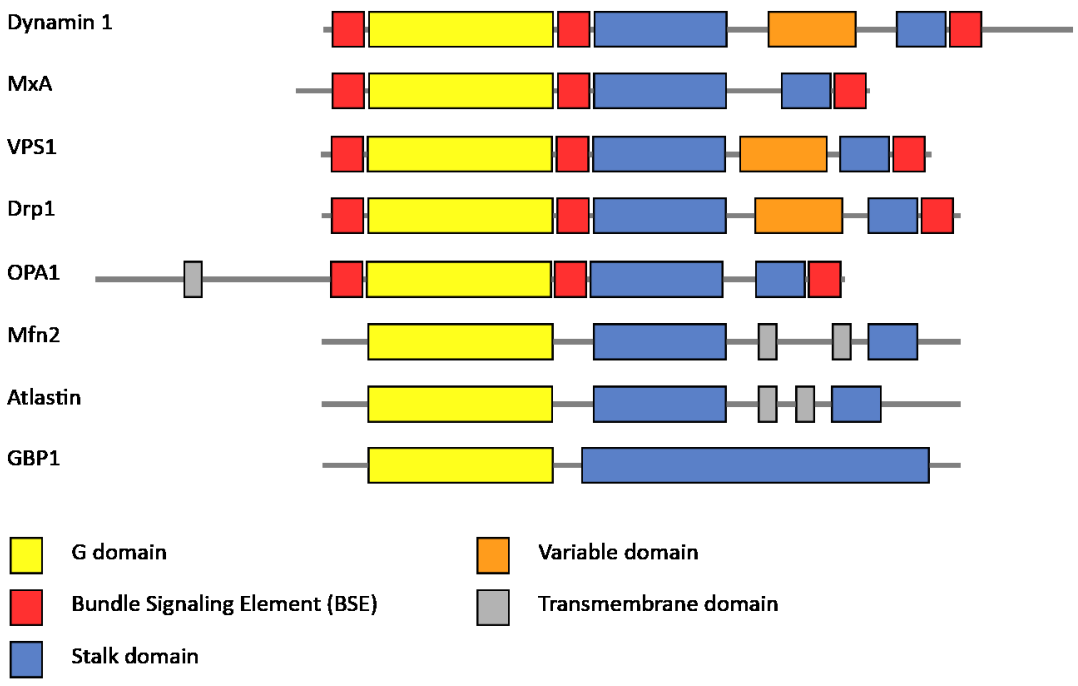

Figure 1.2 Comparison of domain architecture in the dynamin superfamily. All superfamily members possess a G domain and a stalk domain. Most superfamily members also possess a BSE.

Membrane interaction in the dynamin superfamily

As membrane-remodeling enzymes, all dynamin superfamily members interact with membranes in some capacity, typically at the end of the stalk, opposite the GTPase domain. Two modes of membrane interaction are apparent in the dynamin superfamily: (1) tethering to the membrane via a transmembrane (TM) helix (OPA1)[65,66] or helices (mitofusins and Atlastins)[32,67,68] or a covalently-attached lipophilic anchor (GBPs)[69], and (2) untethered reversible interaction with membranes (classical dynamins, Vps1, Drps and Mx proteins). Soluble proteins that interact reversibly with lipid membranes can be described as amphitropic, a term coined by Paul Burn to reflect the dual preference of these proteins for aqueous and lipid environments[70]. Based on the mode of membrane interaction, we propose a subclassification of the dynamin superfamily into two categories: (1) tethered dynamins and (2) untethered amphitropic dynamins (Figure 1.3). Interestingly, OPA1 could potentially be classified in both categories, as it has a proteolytic cleavage site in the tether that anchors it to the membrane, and both the tethered and untethered forms have been shown to be essential[65,66,71]. Furthermore, the untethered form of OPA1 reversibly binds anionic lipid membranes[48] presumably through the variable domain at the end of the stalk[59]. For the purposes of this dissertation we will focus on untethered amphitropic dynamins, and specifically the mitochondrial fission dynamin Drp1 because of its importance in human health and its known structural detail.

Drp1 and mitochondrial fission

Drp1 is the primary mechanoenzyme responsible for mitochondrial fission. Drp1 is recruited from the cytosol, where it exists primarily in dimeric/tetrameric form, to foci on the mitochondria, where it assembles further into rings or spirals that putatively extend around the circumference of the organelle[26,72]. The number of rings necessary for membrane scission is

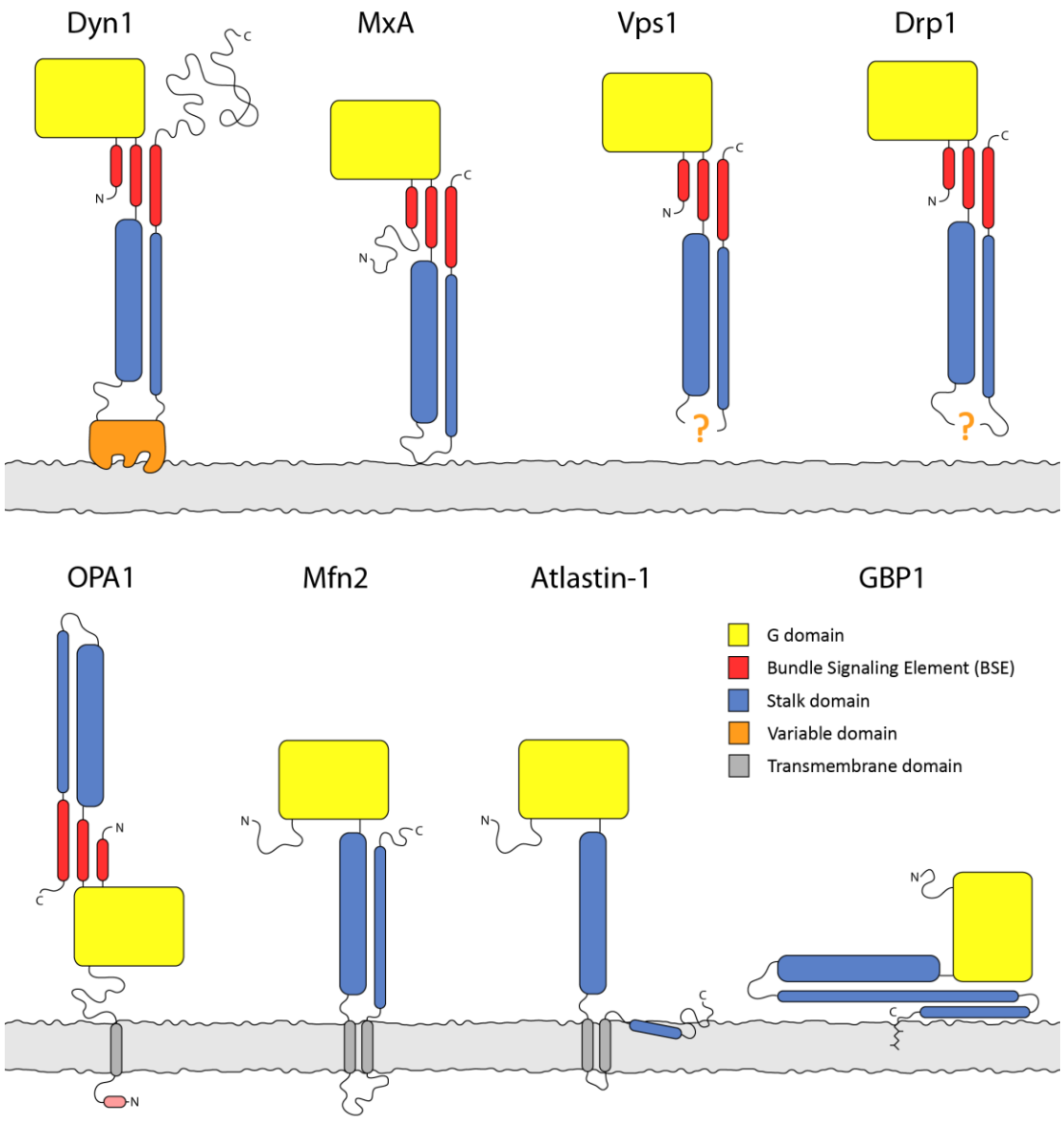

Figure 1.3 Comparison of structure and orientation at the membrane in the dynamin superfamily. There appears to be a pattern of membrane interaction at the end of the stalk opposite the G domain. OPA1 can be cleaved from its tether and may also interact with membranes in the same orientation as the other superfamily members. The structural features of the Vps1 and Drp1 variable domains are unknown, as indicated by the "?" symbols.

unknown. Hydrolysis of GTP is thought induce powerstroke-like conformational rearrangements in the Drp1 oligomers that ultimately result in membrane scission[73–78]. Structurally, Drp1 is composed of the G domain and stalk that are common to the dynamin superfamily, as well as the BSE that is common to the other amphitropic dynamins (classical dynamins and Mx proteins)

(Figure 1.4). Mx proteins and Drp1 lack the PH and PR domains that are found in classical dynamins. In the place of the PH domain, MxA has a loop known as L4, whereas Drp1 has a unique domain of unknown function called the B domain.

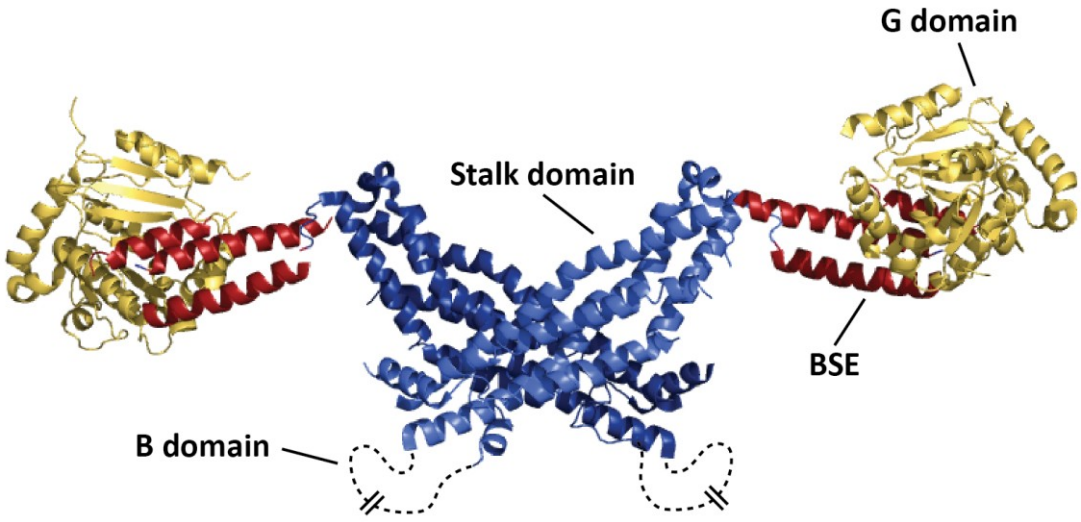

Figure 1.4 High resolution crystal structure of Drp1 (constitutive dimer). The B domain was removed to facilitate crystallization. PDB code 4BEJ

Assembly of Drp1 and the other amphitropic dynamins occurs through the stalk domain via three conserved interfaces (Figure 1.5A)[41,75,79]. Dimerization occurs through a central region of the stalk known as interface 2, with dimerized stalks forming an "X" shape. Higher-order oligomerization (filament extension) occurs through interactions at both ends of the stalks as dimers align side-by-side in a formation that resembles an accordion gate ("…XXXXXX…"). The interface near the G domain end of the stalk occurs near neighboring BSEs (interface 1), and the 3rd interface results from interactions near the tip of the stalk that is opposite the G domain (interface 3). In Drp1, a fourth interface is present in the crystal unit and is formed by a dimer of dimers, with the interface residing at the central crossing point of stalk dimers, on the opposite side as interface 2 (Figure 1.5B). This suggests the possibility of a four-stalk-thick filament[75], rather than the two-stalk-thick filament found in both dynamin and MxA[79–81], and is consistent

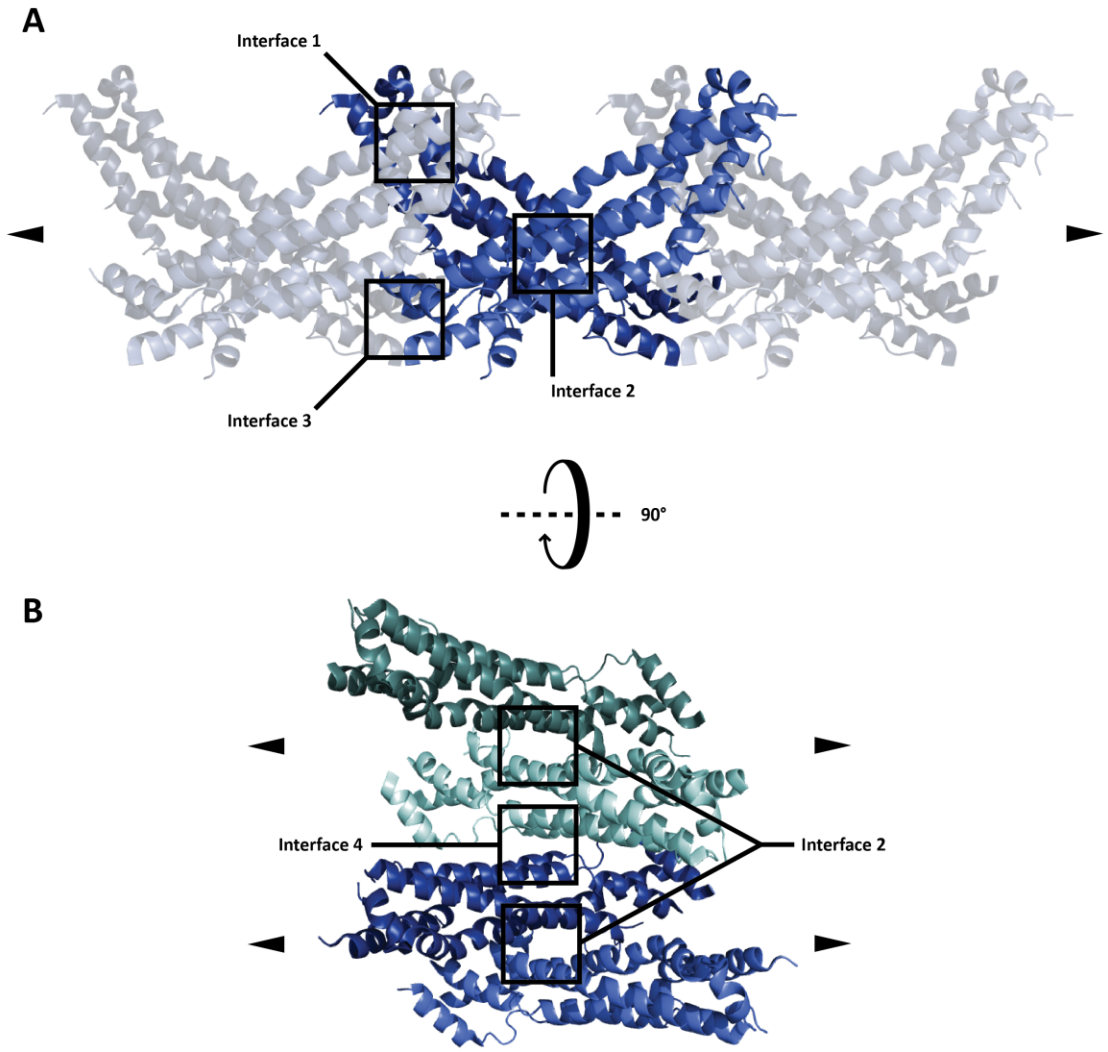

Figure 1.5 Assembly of Drp1 stalk domains. Filament formation occurs through three conserved interfaces (A). In Drp1, assembly on lipid membranes is thought to occur via a "double start" helix consisting of pairs of filaments interacting through a 4th interface (B). Wedge arrows indicate direction of filament extension. Adapted from Frohlich et al.[75]

with a cryo-EM study of the yeast Drp1 homolog, Dnm1, that identified a four-stalk-thick filament forming a "two-start" helical assembly of Dnm1 on lipid membrane tubules[76]. The two-start helical filaments of Drp1 and the single-start helical filaments both appear to form contacts between helical rungs through dimerization of G domains, consistent with G domain dimerization observed in the crystal structure of a G domain/BSE construct of dynamin[63]. A

model has been proposed in which a power stroke alters the angle between the G domain and the BSE, resulting in a cinching of helical rungs[73].

Potential allostery in Drp1 and the dynamin superfamily

Allostery may have an important role in Drp1 function and in the function of dynamin superfamily members in general. Allostery is energetic coupling between two distinct sites of a protein[82], such that an energetic perturbation (e.g. ligand binding) at one site results in a change in structure, binding or activity (e.g. catalysis) at the second site[83–85]. Historically, models of allostery were constructed to explain cooperative ligand binding in oligomeric proteins, and "distinct sites" referred to the structurally identical but physically separate active sites of a homo-oligomer, such as hemoglobin[86,87]. However, allostery within a monomer or a protomer is also possible[88], e.g., when a small molecule binds to a monomeric protein at a site distinct from the active site, resulting in either inhibition or enhancement of ligand binding (or catalysis) at the active site. As in this example, allostery is often used to describe the binding of small molecules. However, binding of proteins, lipids or other biological macromolecules by the protein of interest are equally relevant and the same principles of allostery apply[82].

The distinction between allostery involving cooperative binding in structurally identical but distinct sites in a homo-oligomer, and allostery within a monomer or protomer is important because the former does not appear to occur in Drp1, while the latter appears to be likely. For example, if Drp1 exhibited cooperative oligomerization, we would expect that Drp1 assembly would proceed such that an initial binding or nucleation event would be less favorable than the binding of subsequent protomers, or in other words, assembly would become increasingly favorable as oligomerization proceeded. In reality, it appears more likely that Drp1 assembles through an isodesmic mechanism, i.e. the association constant of all assembly events is the

same (C. M. Manlandro, unpublished results). As a second example, if Drp1 exhibited cooperativity between GTP binding sites in the G domains of an oligomer, we would expect that one G domain in the oligomer would bind GTP more readily once a neighboring G domain in the oligomer had bound GTP. This also does not appear to be true for Drp1 (C. M. Manlandro, unpublished results). Thus, allostery in Drp1, if it occurs, likely occurs within a protomer, with the "distinct sites" residing in different domains of that protomer.

Like classical dynamins, Drp1 exhibits enhanced GTP hydrolysis under assembly-promoting conditions, and reduced activity when assembly is disrupted by stalk domain mutations or solvent conditions[89]. Furthermore, an isolated dynamin-1 G domain construct dimerizes but does not exhibit concentration-dependent GTP hydrolysis. Given that assembly occurs primarily through the stalk domain, and hydrolysis occurs in the G domain, coupled hydrolysis and assembly is consistent with a role for allostery in dynamin and Drp1 function. Allostery is also implied by mutagenesis studies in classical dynamins[90] where reduced GTP hydrolysis was measured in dynamin variants with single-point mutations in the stalk domain[33,62], BSE[64], or the PH domain[34]. One study proposed that classical dynamins exhibit V-type allostery[77], but deliberate studies of allostery have not generally been pursued with members of the dynamin superfamily. In Drp1, further allosteric regulation may occur through the B domain, just as the PH domain may provide a source of allosteric regulation in classical dynamins. Potential allosteric regulation of Drp1 by the B domain was evident at the cellular level as reported by Strack and Cribbs, who observed differences in mitochondrial morphology in cells transfected with various Drp1 ΔB constructs[91]. All of the constructs reported co-immunoprecipitated with wild-type Drp1, suggesting that they were properly folded and were capable of at least dimerization with wild-type enzyme. Depending on how much of the B domain was removed in these Drp1 constructs, and also the nature of the linker that the B

domain was replaced with, mitochondria exhibited morphologies consistent with either excess or disrupted fission.

Unanswered questions

Many questions remain unanswered regarding Drp1, some of which also apply to the dynamin superfamily in general. How do assembly and membrane interaction stimulate hydrolysis? How is hydrolysis coupled to membrane remodeling? Is Drp1 truly a mechanoenzyme that exerts force in order to execute scission of a membrane, or does it carry out membrane scission through some other means? How is Drp1 function regulated? Finally, what is the role of the B domain in Drp1 function? Does it have an allosteric role? Does it bind lipid membranes? What role do post-translational modifications and alternative splicing (in the B domain) play in enzyme function?

In this dissertation we focus specifically on the role of the B domain in Drp1 function. In chapter 2 we present enzymatic evidence for allosteric regulation of Drp1 assembly and GTP hydrolysis by the B domain, and find that the B domain is intrinsically disordered and exhibits the unexpected property of coacervation under conditions that typically cause intrinsically disordered proteins to fold. In chapter 3 we provide evidence that the B domain binds lipid membranes with a preference for the mitochondrial lipid cardiolipin and suggest a relationship between coacervation and membrane interaction. In chapter 4 we present preliminary data examining whether alternative splicing and phosphorylation tune B domain structure and function. Finally, in chapter 5 we conclude with a discussion on the role of intrinsic disorder and amphitropism in Drp1 and more broadly in the dynamin superfamily.

REFERENCES

(1) Klausner, R. D., Donaldson, J. G., and Lippincott-Schwartz, J. (1992) Brefeldin A: insights into the control of membrane traffic and organelle structure. *J. Cell Biol. 116*, 1071–80.

(2) Conner, S. D., and Schmid, S. L. (2003) Regulated portals of entry into the cell. *Nature 422*, 37–44.

(3) Jr, G. T., and Nozawa, Y. (1977) Tetrahymena: A system for studying dynamic membrane alterations within the eukaryotic cell. *… Biophys. Acta (BBA)-Reviews … 472*, 55–92.

(4) Bonifacino, J. S., and Glick, B. S. (2004) The mechanisms of vesicle budding and fusion. *Cell 116*, 153–66.

(5) Palade, G. (1975) Intracellular aspects of the process of protein synthesis. *Science (80-.). 189*, 347–358.

(6) Posakony, J., England, J., and Attardi, G. (1977) Mitochondrial growth and division during the cell cycle in HeLa cells. *J. Cell Biol. 74*, 468–491.

(7) Smirnova, E., Shurland, D. L., Ryazantsev, S. N., and van der Bliek, A. M. (1998) A human dynamin-related protein controls the distribution of mitochondria. *J. Cell Biol. 143*, 351–8.

(8) Chen, H., and Chan, D. C. (2009) Mitochondrial dynamics--fusion, fission, movement, and mitophagy--in neurodegenerative diseases. *Hum. Mol. Genet. 18*, R169–76.

(9) Chevrollier, A., Cassereau, J., Ferré, M., Alban, J., Desquiret-Dumas, V., Gueguen, N., Amati-Bonneau, P., Procaccio, V., Bonneau, D., and Reynier, P. (2012) Standardized mitochondrial analysis gives new insights into mitochondrial dynamics and OPA1 function. *Int. J. Biochem. Cell Biol. 44*, 980–8.

(10) Motley, A. M., and Hettema, E. H. (2007) Yeast peroxisomes multiply by growth and division. *J. Cell Biol. 178*, 399–410.

(11) Opaliński, Ł., Kiel, J. A. K. W., Williams, C., Veenhuis, M., and van der Klei, I. J. (2011) Membrane curvature during peroxisome fission requires Pex11. *EMBO J. 30*, 5–16.

(12) Thoms, S., and Erdmann, R. (2005) Dynamin-related proteins and Pex11 proteins in peroxisome division and proliferation. *FEBS J. 272*, 5169–81.

(13) Gurkan, C., Koulov, A. V, and Balch, W. E. An Evolutionary Perspective on Eukaryotic Membrane Trai cking.

(14) Dacks, J. B., and Field, M. C. (2007) Evolution of the eukaryotic membrane-trafficking system: origin, tempo and mode. *J. Cell Sci. 120*, 2977–85.

(15) D'Souza-Schorey, C., and Chavrier, P. (2006) ARF proteins: roles in membrane traffic and beyond. *Nat. Rev. Mol. Cell Biol. 7*, 347–58.

(16) Praefcke, G. J. K., and McMahon, H. T. (2004) The dynamin superfamily: universal membrane tubulation and fission molecules? *Nat. Rev. Mol. Cell Biol. 5*, 133–47.

(17) Henley, J. R., Krueger, E. W., Oswald, B. J., and McNiven, M. A. (1998) Dynamin-mediated internalization of caveolae. *J. Cell Biol. 141*, 85–99.

(18) Oh, P., McIntosh, D. P., and Schnitzer, J. E. (1998) Dynamin at the neck of caveolae mediates their budding to form transport vesicles by GTP-driven fission from the plasma membrane of endothelium. *J. Cell Biol. 141*, 101–114.

(19) Nicoziani, P., Vilhardt, F., Llorente, A., Hilout, L., Courtoy, P. J., Sandvig, K., and van Deurs, B. (2000) Role for dynamin in late endosome dynamics and trafficking of the cation-independent mannose 6-phosphate receptor. *Mol. Biol. Cell 11*, 481–495.

(20) Smaczynska-de Rooij, I. I., Allwood, E. G., Aghamohammadzadeh, S., Hettema, E. H., Goldberg, M. W., and Ayscough, K. R. (2010) A role for the dynamin-like protein Vps1 during endocytosis in yeast. *J. Cell Sci. 123*, 3496–506.

(21) Nothwehr, S. E., Conibear, E., and Stevens, T. H. (1995) Golgi and Vacuolar Membrane Proteins Reach the Vacuole in *129*, 35–46.

(22) Lukehart, J., Highfill, C., and Kim, K. (2013) Vps1 , a recycling factor for the traffic from early endosome to *465*, 455–465.

(23) Kuravi, K., Nagotu, S., Krikken, A. M., Sjollema, K., Deckers, M., Erdmann, R., Veenhuis, M., and van der Klei, I. J. (2006) Dynamin-related proteins Vps1p and Dnm1p control peroxisome abundance in Saccharomyces cerevisiae. *J. Cell Sci. 119*, 3994–4001.

(24) Koch, A., Thiemann, M., Grabenbauer, M., Yoon, Y., McNiven, M. A., and Schrader, M. (2003) Dynamin-like protein 1 is involved in peroxisomal fission. *J. Biol. Chem. 278*, 8597–8605.

(25) Koch, A., Schneider, G., Lüers, G. H., and Schrader, M. (2004) Peroxisome elongation and constriction but not fission can occur independently of dynamin-like protein 1. *J. Cell Sci. 117*, 3995–4006.

(26) Smirnova, E., Griparic, L., Shurland, D. L., and van der Bliek, A. M. (2001) Dynamin-related protein Drp1 is required for mitochondrial division in mammalian cells. *Mol. Biol. Cell 12*, 2245–56.

(27) Haller, O., and Kochs, G. (2002) Interferon-Induced Mx Proteins : Dynamin-Like GTPases with Antiviral Activity 710–717.

(28) Haller, O., and Kochs, G. (2011) Human MxA protein: an interferon-induced dynamin-like GTPase with broad antiviral activity. *J. Interferon Cytokine Res. 31*, 79–87.

(29) Accola, M. A., Huang, B., Al Masri, A., and McNiven, M. A. (2002) The antiviral dynamin family member, MxA, tubulates lipids and localizes to the smooth endoplasmic reticulum. *J. Biol. Chem. 277*, 21829–35.

(30) Anderson, S. L., Carton, J. M., Lou, J., Xing, L., and Rubin, B. Y. (1999) Interferon-induced guanylate binding protein-1 (GBP-1) mediates an antiviral effect against vesicular stomatitis virus and encephalomyocarditis virus. *Virology 256*, 8–14.

(31) Hu, J., Shibata, Y., Zhu, P.-P., Voss, C., Rismanchi, N., Prinz, W. A., Rapoport, T. A., and Blackstone, C. (2009) A class of dynamin-like GTPases involved in the generation of the tubular ER network. *Cell 138*, 549–61.

(32) Zhu, P.-P., Patterson, A., Lavoie, B., Stadler, J., Shoeb, M., Patel, R., and Blackstone, C. (2003) Cellular localization, oligomerization, and membrane association of the hereditary spastic paraplegia 3A (SPG3A) protein atlastin. *J. Biol. Chem. 278*, 49063–71.

(33) Wang, L., Barylko, B., Byers, C., Ross, J. A., Jameson, D. M., and Albanesi, J. P. (2010) Dynamin 2 mutants linked to centronuclear myopathies form abnormally stable polymers. *J. Biol. Chem. 285*, 22753–7.

(34) Kenniston, J. A., and Lemmon, M. A. (2010) Dynamin GTPase regulation is altered by PH domain mutations found in centronuclear myopathy patients. *EMBO J. 29*, 3054–67.

(35) Bitoun, M., Maugenre, S., Jeannet, P.-Y., Lacène, E., Ferrer, X., Laforêt, P., Martin, J.-J., Laporte, J., Lochmüller, H., Beggs, A. H., Fardeau, M., Eymard, B., Romero, N. B., and Guicheney, P. (2005) Mutations in dynamin 2 cause dominant centronuclear myopathy. *Nat. Genet. 37*, 1207–1209.

(36) Bitoun, M., Bevilacqua, J. A., Prudhon, B., Maugenre, S., Taratuto, A. L., Monges, S., Lubieniecki, F., Cances, C., Uro-Coste, E., Mayer, M., Fardeau, M., Romero, N. B., and Guicheney, P. (2007) Dynamin 2 mutations cause sporadic centronuclear myopathy with neonatal onset. *Ann. Neurol. 62*, 666–670.

(37) Züchner, S., Noureddine, M., Kennerson, M., Verhoeven, K., Claeys, K., De Jonghe, P., Merory, J., Oliveira, S. A., Speer, M. C., Stenger, J. E., Walizada, G., Zhu, D., Pericak-Vance, M. a, Nicholson, G., Timmerman, V., and Vance, J. M. (2005) Mutations in the pleckstrin homology domain of dynamin 2 cause dominant intermediate Charcot-Marie-Tooth disease. *Nat. Genet. 37*, 289–94.

(38) Niemann, A., Berger, P., and Suter, U. (2006) Pathomechanisms of mutant proteins in Charcot-Marie-Tooth disease. *Neuromolecular Med. 8*, 217–242.

(39) Kelly, B. L., Vassar, R., and Ferreira, A. (2005) Beta-amyloid-induced dynamin 1 depletion in hippocampal neurons. A potential mechanism for early cognitive decline in Alzheimer disease. *J. Biol. Chem. 280*, 31746–31753.

(40) Sever, S., Altintas, M. M., Nankoe, S. R., Möller, C. C., Ko, D., Wei, C., Henderson, J., del Re, E. C., Hsing, L., Erickson, A., Cohen, C. D., Kretzler, M., Kerjaschki, D., Rudensky, A., Nikolic, B., and Reiser, J. (2007) Proteolytic processing of dynamin by cytoplasmic cathepsin L is a mechanism for proteinuric kidney disease. *J. Clin. Invest. 117*, 2095–2104.

(41) Gao, S., von der Malsburg, A., Paeschke, S., Behlke, J., Haller, O., Kochs, G., and Daumke, O. (2010) Structural basis of oligomerization in the stalk region of dynamin-like MxA. *Nature 465*, 502–6.

(42) Chung, K. W., Kim, S. B., Park, K. D., Choi, K. G., Lee, J. H., Eun, H. W., Suh, J. S., Hwang, J. H., Kim, W. K., Seo, B. C., Kim, S. H., Son, I. H., Kim, S. M., Sunwoo, I. N., and Choi, B. O. (2006) Early onset severe and late-onset mild Charcot-Marie-Tooth disease with mitofusin 2 (MFN2) mutations. *Brain 129*, 2103–2118.

(43) Züchner, S., Mersiyanova, I. V, Muglia, M., Bissar-Tadmouri, N., Rochelle, J., Dadali, E. L., Zappia, M., Nelis, E., Patitucci, A., Senderek, J., Parman, Y., Evgrafov, O., De Jonghe, P., Takahashi, Y., Tsuji, S., Pericak-Vance, M. A., Quattrone, A., Battaloglu, E., Polyakov, A. V, Timmerman, V., Schröder, J. M., Vance, J. M., and Battologlu, E. (2004) Mutations in the mitochondrial GTPase mitofusin 2 cause Charcot-Marie-Tooth neuropathy type 2A. *Nat. Genet. 36*, 449–51.

(44) Baloh, R. H., Schmidt, R. E., Pestronk, A., and Milbrandt, J. (2007) Altered axonal mitochondrial transport in the pathogenesis of Charcot-Marie-Tooth disease from mitofusin 2 mutations. *J. Neurosci. 27*, 422–430.

(45) Cartoni, R., and Martinou, J. C. (2009) Role of mitofusin 2 mutations in the physiopathology of Charcot-Marie-Tooth disease type 2A. *Exp. Neurol.*

(46) Calvo, J., Funalot, B., Ouvrier, R. A., Lazaro, L., Toutain, A., De Mas, P., Bouche, P., Gilbert-Dussardier, B., Arne-Bes, M.-C., Carrière, J.-P., Journel, H., Minot-Myhie, M.-C., Guillou, C., Ghorab, K., Magy, L., Sturtz, F., Vallat, J.-M., and Magdelaine, C. (2009) Genotype-phenotype correlations in Charcot-Marie-Tooth disease type 2 caused by mitofusin 2 mutations. *Arch. Neurol. 66*, 1511–1516.

(47) Delettre, C., Lenaers, G., Griffoin, J. M., Gigarel, N., Lorenzo, C., Belenguer, P., Pelloquin, L., Grosgeorge, J., Turc-Carel, C., Perret, E., Astarie-Dequeker, C., Lasquellec, L., Arnaud, B., Ducommun, B., Kaplan, J., and Hamel, C. P. (2000) Nuclear gene OPA1, encoding a mitochondrial dynamin-related protein, is mutated in dominant optic atrophy. *Nat. Genet. 26*, 207–10.

(48) Ban, T., Heymann, J. A. W., Song, Z., Hinshaw, J. E., and Chan, D. C. (2010) OPA1 disease alleles causing dominant optic atrophy have defects in cardiolipin-stimulated GTP hydrolysis and membrane tubulation. *Hum. Mol. Genet. 19*, 2113–22.

(49) Alavi, M. V, and Fuhrmann, N. (2013) Dominant optic atrophy, OPA1, and mitochondrial quality control: understanding mitochondrial network dynamics. *Mol. Neurodegener. 8*, 32.

(50) Waterham, H. R., Koster, J., van Roermund, C. W. T., Mooyer, P. A. W., Wanders, R. J. A., and Leonard, J. V. (2007) A lethal defect of mitochondrial and peroxisomal fission. *N. Engl. J. Med. 356*, 1736–41.

(51) Chang, C.-R., and Blackstone, C. (2010) Dynamic regulation of mitochondrial fission through modification of the dynamin-related protein Drp1. *Ann. N. Y. Acad. Sci. 1201*, 34–9.

(52) Ashrafian, H., Docherty, L., Leo, V., Towlson, C., Neilan, M., Lygate, C. A., Hough, T., Townsend, S., Williams, D., Wells, S., Glyn-jones, S., Land, J., Barbaric, I., Lalanne, Z., Denny, P., Bhattacharya, S., Griffin, J. L., Hargreaves, I., Fernandez-fuentes, N., Cheeseman, M., Watkins, H., and Dear, T. N. (2010) A Mutation in the Mitochondrial Fission Gene Dnm1l Leads to Cardiomyopathy *6*, 1–18.

(53) Ishihara, N., Nomura, M., Jofuku, A., Kato, H., Suzuki, S. O., Masuda, K., Otera, H., Nakanishi, Y., Nonaka, I., Goto, Y.-I., Taguchi, N., Morinaga, H., Maeda, M., Takayanagi, R., Yokota, S., and Mihara, K. (2009) Mitochondrial fission factor Drp1 is essential for embryonic development and synapse formation in mice. *Nat. Cell Biol. 11*, 958–966.

(54) Wakabayashi, J., Zhang, Z., Wakabayashi, N., Tamura, Y., Fukaya, M., Kensler, T. W., Iijima, M., and Sesaki, H. (2009) The dynamin-related GTPase Drp1 is required for embryonic and brain development in mice. *J. Cell Biol. 186*, 805–16.

(55) Wang, H., Song, P., Du, L., Tian, W., Yue, W., Liu, M., Li, D., Wang, B., Zhu, Y., Cao, C., Zhou, J., and Chen, Q. (2011) Parkin ubiquitinates Drp1 for proteasome-dependent degradation: implication of dysregulated mitochondrial dynamics in Parkinson disease. *J. Biol. Chem. 286*, 11649–11658.

(56) Oettinghaus, B., Licci, M., Scorrano, L., and Frank, S. (2012) Less than perfect divorces: dysregulated mitochondrial fission and neurodegeneration. *Acta Neuropathol.*

(57) Orso, G., Pendin, D., Liu, S., Tosetto, J., Moss, T. J., Faust, J. E., Micaroni, M., Egorova, A., Martinuzzi, A., McNew, J. A., and Daga, A. (2009) Homotypic fusion of ER membranes requires the dynamin-like GTPase atlastin. *Nature 460*, 978–983.

(58) Vöpel, T., Syguda, A., Britzen-Laurent, N., Kunzelmann, S., Lüdemann, M.-B., Dovengerds, C., Stürzl, M., and Herrmann, C. (2010) Mechanism of GTPase-activity-induced self-assembly of human guanylate binding protein 1. *J. Mol. Biol. 400*, 63–70.

(59) Faelber, K., Gao, S., Held, M., Posor, Y., Haucke, V., Noé, F., and Daumke, O. (2013) Oligomerization of dynamin superfamily proteins in health and disease. *Prog. Mol. Biol. Transl. Sci.* 1st ed., pp 411–43. Copyright © 2013, Elsevier Inc. All Rights Reserved.

(60) Flohr, F., Schneider-Schaulies, S., Haller, O., and Kochs, G. (1999) The central interactive region of human MxA GTPase is involved in GTPase activation and interaction with viral target structures. *FEBS Lett. 463*, 24–8.

(61) Warnock, D. E., Hinshaw, J. E., and Schmid, S. L. (1996) Dynamin self-assembly stimulates its GTPase activity. *J. Biol. Chem. 271*, 22310–4.

(62) Ramachandran, R., Surka, M., Chappie, J. S., Fowler, D. M., Foss, T. R., Song, B. D., and Schmid, S. L. (2007) The dynamin middle domain is critical for tetramerization and higher-order self-assembly. *EMBO J. 26*, 559–66.

(63) Chappie, J. S., Acharya, S., Leonard, M., Schmid, S. L., and Dyda, F. (2010) G domain dimerization controls dynamin's assembly-stimulated GTPase activity. *Nature 465*, 435–40.

(64) Chappie, J. S., Acharya, S., Liu, Y., Leonard, M., Pucadyil, T. J., and Schmid, S. L. (2009) An Intramolecular Signaling Element that Modulates Dynamin Function In Vitro and In Vivo *20*, 3561–3571.

(65) Ishihara, N., Fujita, Y., Oka, T., and Mihara, K. (2006) Regulation of mitochondrial morphology through proteolytic cleavage of OPA1. *EMBO J. 25*, 2966–77.

(66) Song, Z., Chen, H., Fiket, M., Alexander, C., and Chan, D. C. (2007) OPA1 processing controls mitochondrial fusion and is regulated by mRNA splicing, membrane potential, and Yme1L. *J. Cell Biol. 178*, 749–55.

(67) Rojo, M., Legros, F., Chateau, D., and Lombès, A. (2002) Membrane topology and mitochondrial targeting of mitofusins, ubiquitous mammalian homologs of the transmembrane GTPase Fzo. *J. Cell Sci. 115*, 1663–74.

(68) Rismanchi, N., Soderblom, C., Stadler, J., Zhu, P.-P., and Blackstone, C. (2008) Atlastin GTPases are required for Golgi apparatus and ER morphogenesis. *Hum. Mol. Genet. 17*, 1591–604.

(69) Modiano, N., Lu, Y. E., and Cresswell, P. (2005) Golgi targeting of human guanylate-binding protein-1 requires nucleotide binding, isoprenylation, and an IFN-gamma-inducible cofactor. *Proc. Natl. Acad. Sci. U. S. A. 102*, 8680–5.

(70) Burn, P. (1988) Amphitropic proteins: a new class of membrane proteins. *Trends Biochem Sci 13*, 79–83.

(71) Mishra, P., Carelli, V., Manfredi, G., and Chan, D. C. (2014) Proteolytic cleavage of opa1 stimulates mitochondrial inner membrane fusion and couples fusion to oxidative phosphorylation. *Cell Metab. 19*, 630–41.

(72) Ingerman, E., Perkins, E. M., Marino, M., Mears, J. A., McCaffery, J. M., Hinshaw, J. E., and Nunnari, J. (2005) Dnm1 forms spirals that are structurally tailored to fit mitochondria. *J. Cell Biol. 170*, 1021–7.

(73) Chappie, J. S., Mears, J. A., Fang, S., Leonard, M., Schmid, S. L., Milligan, R. A., Hinshaw, J. E., and Dyda, F. (2011) A pseudoatomic model of the dynamin polymer identifies a hydrolysis-dependent powerstroke. *Cell 147*, 209–22.

(74) Ford, M. G. J., Jenni, S., and Nunnari, J. (2011) The crystal structure of dynamin. *Nature 477*, 561–6.

(75) Fröhlich, C., Grabiger, S., Schwefel, D., Faelber, K., Rosenbaum, E., Mears, J. A., Rocks, O., and Daumke, O. (2013) Structural insights into oligomerization and mitochondrial remodelling of dynamin 1-like protein. *EMBO J. 32*, 1280–92.

(76) Mears, J. A., Lackner, L. L., Fang, S., Ingerman, E., Nunnari, J., and Hinshaw, J. E. (2011) Conformational changes in Dnm1 support a contractile mechanism for mitochondrial fission. *Nat. Struct. Mol. Biol. 18*, 20–6.

(77) Stowell, M. H., Marks, B., Wigge, P., and McMahon, H. T. (1999) Nucleotide-dependent conformational changes in dynamin: evidence for a mechanochemical molecular spring. *Nat. Cell Biol. 1*, 27–32.

(78) Roux, A., Uyhazi, K., Frost, A., and De Camilli, P. (2006) GTP-dependent twisting of dynamin implicates constriction and tension in membrane fission. *Nature 441*, 528–31.

(79) Faelber, K., Posor, Y., Gao, S., Held, M., Roske, Y., Schulze, D., Haucke, V., Noé, F., and Daumke, O. (2011) Crystal structure of nucleotide-free dynamin. *Nature 477*, 556–60.

(80) Zhang, P., and Hinshaw, J. E. (2001) Three-dimensional reconstruction of dynamin in the constricted state. *Nat. Cell Biol. 3*, 922–6.

(81) Gao, S., von der Malsburg, A., Dick, A., Faelber, K., Schröder, G. F., Haller, O., Kochs, G., and Daumke, O. (2011) Structure of myxovirus resistance protein a reveals intra- and intermolecular domain interactions required for the antiviral function. *Immunity 35*, 514–25.

(82) Fenton, A. W. (2008) Allostery: an illustrated definition for the “second secret of life”. *Trends Biochem. Sci. 33*, 420–5.

(83) Hilser, V. J., Wrabl, J. O., and Motlagh, H. N. (2012) Structural and energetic basis of allostery. *Annu. Rev. Biophys. 41*, 585–609.

(84) England, J. L. (2011) Allostery in protein domains reflects a balance of steric and hydrophobic effects. *Structure 19*, 967–75.

(85) Gunasekaran, K., Ma, B., and Nussinov, R. (2004) Is Allostery an Intrinsic Property of All Dynamic Proteins ? *Cancer 443*, 433– 443.

(86) Monod, J., Wyman, J., and Changeux, J. P. (1965) On the nature of allosteric transitions: a plausible model. *J. Mol. Biol. 12*, 88–118.

(87) Koshland, D. E., Némethy, G., and Filmer, D. (1966) Comparison of experimental binding data and theoretical models in proteins containing subunits. *Biochemistry 5*, 365–85.

(88) Cui, Q., and Karplus, M. (2008) Allostery and cooperativity revisited. *Protein Sci. 17*, 1295–307.

(89) Chang, C.-R., Manlandro, C. M., Arnoult, D., Stadler, J., Posey, A. E., Hill, R. B., and Blackstone, C. (2010) A lethal de novo mutation in the middle domain of the dynamin-related GTPase Drp1 impairs higher order assembly and mitochondrial division. *J. Biol. Chem. 285*, 32494–503.

(90) Schmid, S. L., and Frolov, V. A. (2011) Dynamin: functional design of a membrane fission catalyst. *Annu. Rev. Cell Dev. Biol. 27*, 79–105.

(91) Strack, S., and Cribbs, J. T. (2012) Allosteric modulation of Drp1 mechanoenzyme assembly and mitochondrial fission by the variable domain. *J. Biol. Chem. 287*, 10990–1001.

Chapter 2

The B domain of Drp1 auto-inhibits assembly and GTP hydrolysis, is intrinsically disordered and coacervates in protecting osmolyte

INTRODUCTION

Dynamin-related protein 1 (Drp1) is a member of the Dynamin superfamily responsible for the remodeling of mitochondrial membranes, a process that is important for the maintenance of mitochondrial homeostasis[1,2] including the regulation of mitophagy[3] and apoptosis[4,5]. Drp1 is thought to execute mitochondrial fission through extensive self-assembly into massive spiral-like structures around the circumference of a mitochondrion, accompanied by the conversion of energy from GTP hydrolysis into mechanical constriction (force), ultimately resulting in scission of mitochondria[6].

In addition to the canonical GTPase (G), stalk and bundle signaling element (BSE) domains found in other dynamin superfamily members, Drp1 has a domain known as the B domain, whose function is poorly understood. Interestingly, the B domain contains several experimentally-confirmed sites of post-translational modification, including two phosphorylation sites[7–11] and eight SUMOylation sites[12,13]. Alternative splicing of the Drp1 gene gives rise to at least eight known isoforms[14], five of which are the result of truncations of the B domain alone[15]. The Drp1 isoforms appear to be differentially expressed in human tissues[14,16,17]. These traits suggest that the B domain is a region of great importance for the regulation of Drp1 function.

It was recently shown by Strack and Cribbs that various Drp1ΔB constructs expressed in HeLa cells resulted in either punctuate or elongated mitochondria compared to wild-type, indicative of either excess or disrupted mitochondrial fission, respectively[18]. The phenotypes varied depending on how much of the B domain sequence was removed and the length and properties of the linker used to replace the removed segment. These findings suggest that the B domain could be involved in both positive and negative regulation of Drp1 activity.

It has been theoretically demonstrated using a statistical thermodynamic model (the ensemble allosteric model or EAM) that positive and negative allostery can occur through the same domain, particularly for proteins with at least three allosterically coupled domains[19]. Furthermore, this model suggests that regions of intrinsic disorder may be uniquely poised to execute an allosteric response[19,20]. Central to the EAM and its experimental validation is the difference in energy between relaxed and tensed states, or in other words the stability, of each domain. The stability of alternatively spliced intrinsically disordered domains in the glucocorticoid receptor (GR) transcription factor have been shown correlate with GR activity (gene expression) using an experimental approach[21]. The dual effects of tamoxifen on the estrogen receptor in different tissues is a potential example of a single ligand acting as both an agonist and antagonist through the same protein domain, but this has not been experimentally verified[19].

We suspect that the B domain of Drp1 may be involved in the allosteric regulation of Drp1 and here test if the B domain is important for GTP hydrolysis and assembly of Drp1 by measuring these properties in a Drp1ΔB construct. We then attempt to measure the thermodynamic properties of the B domain in isolation in order to evaluate its potential for thermodynamic coupling. We find that the B domain is intrinsically disordered, and to our surprise, we discover that the B domain undergoes phase separation (coacervation) under conditions that typically induce intrinsically disordered proteins to fold. These findings are consistent with the notion that intrinsically disordered regions may be uniquely poised for allosteric regulation of enzymes, and also identify a novel property of the B domain, encouraging further exploration of the relationship between intrinsic disorder and coacervation in other systems.

MATERIALS AND METHODS

Drp1 and Drp1ΔB cloning - Drp1 isoform 1 (Genbank accession number AB006965) was PCR amplified with Pfu Turbo DNA polymerase (Stratagene, La Jolla, CA) as an *NdeI/XhoI* fragment, with a Tobacco Etch Virus (TEV) protease site (ENLYFQS) preceeding the *XhoI* restriction site. The resulting DNA fragment was then ligated into the bacterial expression vector pET29b (EMD Millipore, Billerica, MA), which contains a C-terminal hexa-histadine (His_6) tag. To clone a Drp1ΔB-His_6 fusion protein, the gene sequence corresponding to residues 1-525 of Drp1 isoform 1 was fused to the gene sequence corresponding to residues 637-736 of Drp1 isoform 1 with a "GGGSGGG" linker. The Drp1ΔB-His_6 fusion protein was created by PCR amplifying two fragments. The first fragment contained an *NdeI* restriction site, the Drp1 GTPase domain (residues 1-525), and the "GGGSGGG" linker. The second fragment contained the same linker, residues 637-736 of the GED domain, a TEV cleavage site (ENLYFQS) and an *XhoI* restriction site. 100 ng of each fragment were mixed together to form the template of a third PCR reaction, which was amplified with the forward primer of reaction 1 and the reverse primer of reaction 2. The resulting 1100 bp PCR product was gel extracted, digested with *NdeI*/*XhoI* and ligated into pet29b.

Drp1 and Drp1ΔB expression and purification - pET29b-Drp1-His_6 or pET29b-Drp1ΔB-His_6 were transformed into *Escherichia coli* BL21 (DE3). Cells were grown at 37°C in Super Broth (SB) with kanamycin (30 µg/ml) to an A_{600} of ~1.5 with shaking at 250 rpm, the temperature was lowered to 14°C and after 30 minutes, protein expression was induced with 0.5 mM isopropyl 1-thio-β-D-galactopyranoside for 12-16 hours. Cells were harvested by centrifugation using a Sorvall JLA-8.1000 rotor at 5,000 rpm for 10 minutes at 4°C and were resuspended in column buffer A (50 mM 4-(2-hydroxyethyl)-1-piperazineethanesulfonic acid (HEPES), pH 7.4, 400 mM NaCl, 5 mM $MgCl_2$, 40 mM imidazole) containing protease inhibitors (Complete, EDTA-free

Protease Inhibitor Mixture, Roche Applied Science, Indianapolis, IN). Cells were lysed by four passes through a French press (Thermo Scientific, Pittsburgh, PA), DNAse was added to a final concentration of 1 μg/ml and lysates were clarified by centrifugation using a Sorvall SS34 rotor at 15,000 rpm for 30 minutes at 4°C. His_6-tagged fusion proteins were isolated from the resulting supernatant by affinity chromatography using Ni^{2+} Sepharose High Performance beads (GE Healthcare, Pittsburgh, PA). Bound fusion proteins were washed with 200-300 mL of column Buffer A, 100 mL of column buffer B (50 mM HEPES, pH 7.4, 400 mM NaCl, 5 mM $MgCl_2$, 40 mM imidazole, 1 mM ATP, 10 mM KCl), 200 mL of column buffer C (50 mM HEPES, pH 7.4, 80 mM imidazole, 400 mM NaCl, 0.5% (w/v) 3-[(3-cholamicopropyl)dimethylammonio]-1-propanesulfonate (CHAPS)), and 100 mL of column buffer A. Bound fusion proteins were then eluted with column buffer D (50 mM HEPES, pH 7.4, 800 mM NaCl, 5 mM $MgCl_2$, 500 mM imidazole). Fractions containing His_6-tagged fusion proteins were pooled and dialyzed overnight at 4°C into buffer containing 50 mM HEPES, pH 7.4, 5 mM $MgCl_2$, 1 M NaCl with Spectra/Por Biotech Cellulose Ester dialysis membrane with a 100,000 molecular weight cut-off (Spectrum Laboratories, Rancho Dominguez, CA). Proteins were concentrated by centrifugation in Vivaspin 20 ultrafiltration devices with a 100,000 molecular weight cut-off (GE Healthcare). Protein concentrations were quantified by UV spectroscopy with an extinction coefficient of 36380 M^{-1} cm^{-1} (Drp1) or 30870 M^{-1} cm^{-1} (Drp1ΔB) after incubation for 3 hours in 6M guanidium hydrochloride at 65°C. Purified protein was stored at 4°C until use and was used with 72 hours of cell lysis.

B domain cloning, expression and purification - A B domain construct representing amino acids 501 – 637 of human Drp1 isoform 1 was PCR amplified from a full-length Drp1 template as an Nde1/Xho1 fragment with a Tobacco Etch Virus (TEV) protease site (ENLYFQS) preceding the XhoI restriction site, and subcloned into the pET29b expression vector (EMD

Biosciences) including a C-terminal 6xHis tag. All constructs were verified by DNA sequencing (GENEWIZ, South Plainfield, NJ). Plasmids were transformed into chemically competent *Escherichia coli* Rosetta cells (Novagen) and grown at 37°C in Super Broth with kanamycin (30mg/mL) and chloramphenicol (34mg/mL) to A600 of 1.0. Protein expression was induced by addition of 0.5 mM isopropyl 1-thio-b-dgalactopyranoside (IPTG) at 18°C and harvested by centrifugation 15–18 h after induction. The resulting cell pellets were resuspended in Ni column buffer (25 mM Tris HCl, 50 mM NaCl, 30 mM imidazole pH 7.4) containing protease inhibitors (Roche Applied Science). Cells were lysed with 4 passes through an Emulsiflex C3 (Avestin), DNase was added to 1 mg/mL and lysates were clarified by centrifugation using a Sorvall SS34 rotor at 15,000 rpm for 30 minutes at 4°C. Protein was isolated from the resulting supernatant by affinity chromatography using Ni-Sepharose 6 Fast Flow beads (GE Healthcare), and eluted with a 100 mL linear gradient of column buffer with 500 mM imidazole. Fractions containing His-tagged proteins were pooled, TEV protease was added at 1/100 molar ratio, and the solution was dialyzed against SP column buffer (50 mM KPhos, 50 mM KCl, 1 mM DTT, pH 7.4) using Spectra/Por Biotech Cellulose Ester dialysis membrane with a 12 – 14 kDa molecular weight cut-off (Spectrum Laboratories, Rancho Dominguez, CA) at 4°C for 24 hours or until the protease reaction reached completion, as determined by SDS-PAGE. B domain was separated from TEV protease and further purified on a HiTrap SP XL column (GE Healthcare). Flow-through fractions containing B domain were pooled and concentrated to ~ 1 mM by centrifugation in Amicon Ultra-15 ultrafiltration devices with a 10 kDa molecular weight cut-off (EMD Millipore, Billerica, MA). Sample purity was checked by coomassie-stained SDS-PAGE and was typically greater than 95%. Protein concentrations were determined by UV spectroscopy using an extinction coefficient of 6990 mol^{-1} cm^{-1}. Concentrated protein stocks were divided into 50 µL aliquots, flash frozen in liquid nitrogen, lyophilized and stored under dry conditions at -20°C until use.

Immediately prior to use, lyophilized stocks were reconstituted using 50 µL of deionized water, and protein concentration was re-measured.

Sedimentation assay - A sedimentation assay to quantitatively measure Drp1 and Drp1ΔB self-assembly into oligomeric structures was adapted from a previously established protocol for human dynamin-1[22,23]. Briefly, Drp1-His_6 or Drp1ΔB-His_6 in 50 mM HEPES, pH 7.4, 1M NaCl, 5 mM $MgCl_2$ was diluted at the indicated protein concentration into various buffer conditions on ice. The sedimentation assays were incubated at 37°C for 30 minutes. Supernatant and pellet fractions were obtained after centrifugation at 50,000x*g* for 30 minutes at 4°C in a TLA-45 rotor (Beckman Instruments, Brea, CA). After centrifugation, the pellet was resuspended in an equal volume of buffer. Drp1-His_6 or Drp1ΔB-His_6 in each fraction was resolved by SDS-PAGE and immunoblotted as described above. Protein quantification was performed using ImageJ software to calculate intensities of Drp1 in supernatant and pellet fractions relative to an input fraction.

Coupled GTP hydrolysis assay - A continuous GTPase assay was used whereby the rate of GTP hydrolysis was determined through coupling to a GTP regeneration system, as previously described[24]. GTPase activity was assayed in 200 µL of GTPase reaction buffer (25 mM HEPES, pH 7.0, 7.5 mM KCl, 5 mM $MgCl_2$, 1 mM phosphoenolpyruvate, 20 units/mL pyruvate kinase/lactate dehydrogenase, 600 µM NADH), of which 150 µL was placed into the wells of a 96-well plate. Depletion of NADH over time was measured for 40 minutes at 25°C using a FlexStation 3 Multi-Detection Reader with Integrated Fluid Transfer (Molecular Devices, Sunnyvale, CA). GTPase assays were started by the addition of the indicated concentration of GTP. For determination of salt dependence, the final NaCl concentration was varied between 50 mM and 1M, as indicated.

Size Exclusion Chromatography (SEC) - B domain hydrodynamic properties were approximated by SEC using a HiLoad 16/60 Superdex 75 prep grade (S-75) column (GE Healthcare) in 20 mM Tris, 50 mM NaCl, 1 mM DTT, pH 7.4.

Sedimentation velocity AUC - Sedimentation velocity experiments were carried out in a Beckman XL-A analytical ultracentrifuge, using two-sector cells and an An60Ti rotor. Experiments were carried out at a speed of 50,000 rpm and 22°C. Sedimentation profiles were detected using absorbance optics operated in continuous mode. The sedimentation coefficient, apparent diffusion coefficient and MW were determined by fitting data to the Lamm equation using the DCDT+ software by John Philo[25,26].

NMR - NMR experiments were performed at 18.8 T on a Varian Inova 800 spectrometer outfitted with a TXI coldprobe. Two-dimensional ^{1}H–^{15}N heteronuclear single quantum correlation (HSQC) experiments were collected at pH 7.4 using WATERGATE for solvent suppression. Uniformly ^{15}N-labeled B domain samples were prepared by dialysis into 20 mM Tris-HCl pH 7.4. with 100 mM NaCl, 10 mM EDTA, 1 mM DTT and 10% D_2O. The protein concentration was 300 µM. HSQC spectra were collected at 4 scans per increment, 1280 (t_2) x 256 (t_1) complex points with acquisition times of 64 ms (^{1}H) and 71 ms (^{15}N). Carrier frequencies were centered on the chemical shift of water in ^{1}H and in the center of the amide region at 117.5 ppm in ^{15}N. NMR data were processed using NMRPipe[27] and analyzed with NMRView[28].

Preparation of TMAO buffers - Trimethylamine N-oxide dihydrate (98% pure; Sigma-Aldrich) was dissolved in 100 mM Tris, 200 mM NaCl, 50 mM arginine buffer to make 0, 0.8, 1.6, 2.4, 3.2, 4.0 and 4.8 M TMAO buffers. The pH was adjusted to 7.4 for each buffer separately. Impurities in the TMAO were removed by incubating each buffer solution with activated carbon (12–20 mesh; Sigma-Aldrich) for at least 4 hours while protected from light. The buffer was then filtered (0.22 µm filter; Millipore), aliquoted, flash frozen in liquid nitrogen and stored at -

80 °C until further use. At the time of sample preparation, TMAO buffers with similar concentrations were mixed in the appropriate ratios to obtain the target TMAO concentrations used in the fluorescence measurements. This minimized pH changes that could occur from mixing two TMAO buffers with a large concentration difference. Final TMAO concentrations were determined by refractive index and a standard curve, after the manner of Bolen[29].

Circular dichroism - Far UV circular dichroism spectra for the Drp1 isoform 1 B domain were recorded with an Aviv Model 215 CD spectrometer (Aviv Biomedical, Lakewood, NJ) from 260 nm to 195 nm with a bandwidth of 1.0 nm and scan step of 1 nm in a 0.1 cm quartz cuvette at 22°C. All spectra were recorded in CD buffer (10 mM sodium phosphate, 200 mM sodium fluoride, 1 mM TCEP, pH 7.4) and corrected for the contribution of buffer. Each spectrum shown is an average of three spectra. Data for which the HT voltage rose above 500 V were discarded. Molar ellipticity ([θ], deg cm^2/dmol) was calculated using the equation $[\theta] = \theta \times \mathrm{MRW}/(10 \times 0.1\ \mathrm{cm} \times [\mathrm{B}])$, where $\mathrm{MRW} = \mathrm{MW}/(\#\ \mathrm{residues} - 1)$. CD spectra were deconvoluted using CONTIN-LL in the CDPro software package[30,31].

Steady-state tryptophan fluorescence - Steady-state fluorescence emission spectra of the B domain were measured using an Aviv ATF-105 fluorometer (Aviv Biomedical, Lakewood, NJ) in TMAO buffers of varying concentrations. Fresh dithiothreitol (DTT) was added to a final concentration of 15 mM to a 15x protein stock solution, to be diluted to 1mM DTT upon sample preparation. Protein samples (ranging from 2 μM to 40 μM) were prepared in a final volume of 150 μL by combining 10 μL of 15x protein stock with 140 μL of TMAO buffer of the appropriate concentration. Samples were allowed to equilibrate in a "submicro" fluorometer cell at 22 °C (Santa Cells) for 5 min to allow for temperature stabilization and protein conformation equilibrium to be reached. Emission spectra were then recorded with excitation at 295 nm (5 nm slit width). All spectra were corrected for the contribution of buffer. Fluorescence emission

intensities at 338 nm (5 nm slit width) were recorded as a function of TMAO concentration. The resulting sigmoid curve was fit to a two-state cooperative folding transition using nonlinear least-squares analysis to determine the stability (ΔG) and m-value[32,33]. In order to maximize the amount of spectral information used for analysis, we calculated the center of spectral mass ⟨ν⟩ from fluorescence spectra using equation 2.1:

$$\langle \nu \rangle = \left(\frac{\sum I_n / \lambda_n}{\sum I_n} \right) \times 10^7 \qquad (2.1)$$

where λ is the wavelength in nm, I_n is the fluorescence emitted at wavelength λ_n, and the summation is carried out from $\lambda_n = 310$ nm to $\lambda_n = 480$ nm. The variable ν denotes the wavenumber, defined as $\nu = \frac{1}{\lambda} \times 10^7$, and has been used historically because it is directly proportional to energy. It has been shown that the center of spectral mass does not scale proportionally with fraction folded[34], but this can be corrected for when determining thermodynamic values from these data[35].

Light scattering - Right-angle light scattering near 350 nm was measured using an Aviv ATF-105 fluorometer (Aviv Biomedical, Lakewood, NJ) immediately following each fluorescence measurement. Excitation and emission wavelengths were set to 345 and 355 respectively, with both slit widths at 5 nm. Excitation and emission wavelengths had to be offset in this manner in order to keep the signal in a measurable range without altering the PMT settings used for fluorescence measurements. Additionally, samples were retained after fluorescence measurements and their absorbance spectra were measured with a Nanodrop 2000c UV/visible spectrophotometer (Thermo Scientific) in a quartz cuvette with a 1 cm pathlength. The absorbance at 350 nm was used as an indicator of scattered light since the B domain does not absorb light at this wavelength under native conditions. The two methods were found to give

comparable results. Light scattering data were fit to a two-state model after the same manner as outlined above for fluorescence data.

Electron microscopy - Samples were prepared for EM using samples retained from fluorescence measurements, or with fresh samples prepared in the same manner. 5 µL of protein sample was applied to freshly-ionized carbon-coated copper mesh grids (Electron Microscopy Science). After 15 minutes, the grids were rinsed quickly with four washes of deionized water, then floated face-down on a drop of 2% uranyl acetate solution for one minute before being air-dried. Images were taken on a FEI Tecnai 12 TWIN equipped with 16 bit 2K x 2K FEI Eagle bottom mount camera and SIS Megaview III wide-angle camera (Olympus).

RESULTS

Removal of the B domain stimulates GTP hydrolysis and assembly of Drp1

The fragmented mitochondria observed by Strack and Cribbs[18] in HeLa cells transfected with Drp1 lacking the B domain could have resulted from an increase in Drp1-mediated fission, or an inhibition of mitochondrial fusion activity. Conversely, the elongated mitochondria could be due to an inability of Drp1 to correctly assemble on mitochondria, or due to hydrolytically-deficient Drp1. To address how the B domain impacts the assembly and hydrolytic capabilities of Drp1, we expressed and isolated a construct lacking the B domain (Drp1ΔB) (Figure 2.1A) and compared its assembly and GTP hydrolysis activity to wild-type enzyme.

Since almost all of the Strack and Cribbs Drp1ΔB variants appeared to form either punctate or filamentous aggregates by *in vivo* fluorescence microscopy, we suspected that our Drp1ΔB construct would also exhibit enhanced assembly or aggregation. We performed a sedimentation assay as a function of salt concentration in order to compare the assembly properties of Drp1ΔB with wild-type Drp1 (Figure 2.1B). Quantification of the fraction of protein

pelleted indicated that 94% Drp1ΔB pelleted at the lowest salt concentration (150 mM NaCl), while only 51% of wild-type Drp1 pelleted under the same conditions (Figure 2.1C). At the highest salt concentration, the amount of Drp1ΔB in the pellet was still more than 70%, while pelleting of wild-type Drp1 was reduced to less than 20%. These results suggest that Drp1ΔB is more highly assembled than wild-type, and the Drp1ΔB assembled form may be slightly more resistant to disassembly by salt than wild-type. Thus, the B domain appears to have an auto-inhibitory effect on Drp1 assembly.

GTP hydrolysis is enhanced by assembly in all dynamin superfamily members, including Drp1[36,37]. Therefore, we might expect hyper-assembly to result in enhanced GTP hydrolysis. However, unregulated, chaotic assembly could potentially interfere with efficient GTP hydrolysis. To determine if the observed hyper-assembly of Drp1ΔB results in enhanced or depressed GTP hydrolysis, we measured GTP hydrolysis as a function of salt concentration for wild-type Drp1 and Drp1ΔB. The amount of GTP hydrolyzed per minute by Drp1ΔB was two-fold greater at the lowest salt concentration tested (100 mM NaCl), and was more than 20-fold greater at the highest salt concentration (Figure 2.1D). To facilitate easier comparison of the degree of salt sensitivity, we normalized the amount of GTP hydrolyzed per minute at each salt concentration against the amount of GTP hydrolyzed per minute at the lowest salt concentration. Observed this way, the difference in salt sensitivity between wild-type Drp1 and Drp1ΔB is more readily apparent, with the assembly-dependent GTP hydrolysis of wild-type Drp1 dropping dramatically with increasing salt concentration (95% decrease), while the assembly-dependent GTP hydrolysis of Drp1ΔB decreases much more modestly with increasing salt concentration (40% decrease)(Figure 2.1E). These results confirm that hyper-assembly of Drp1ΔB does indeed result in enhanced GTP hydrolysis.

While the salt-dependence of Drp1 GTP hydrolysis is consistent with the notion that salt

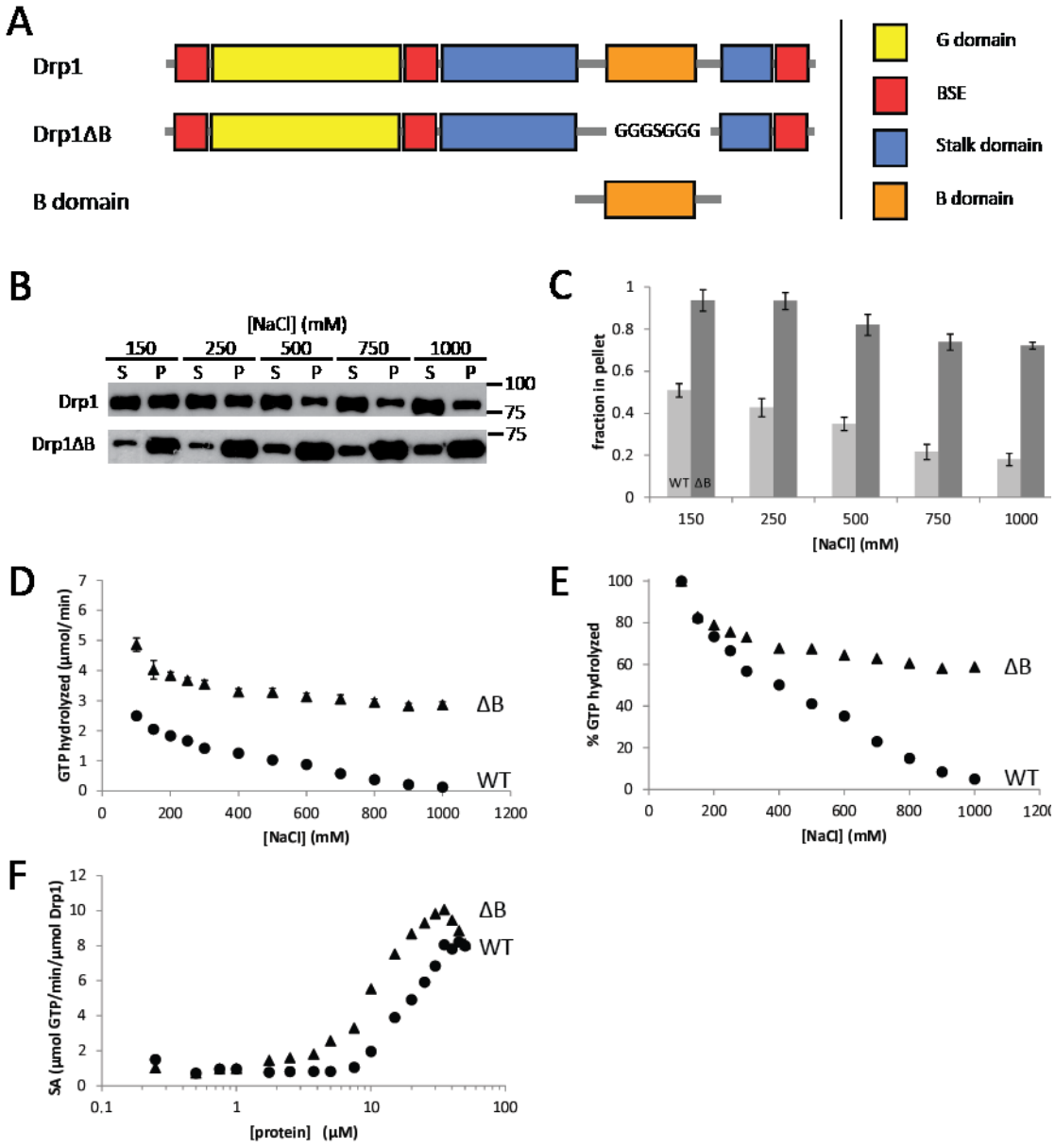

Figure 2.1 Assembly and GTP hydrolysis and of Drp1ΔB. (A) Constructs used in this study. The B domain is replaced by a seven amino acid flexible linker "GGGSGGG" in the Drp1ΔB construct. (B) Sedimentation of wild-type Drp1 and Drp1ΔB was performed at 100k x g for 30 minutes in NaCl concentrations ranging from 150 mM to 1000 mM. The supernatant (S) and pellet (P) were run on a gel for quantification by densitometry. (C) Quantification of fraction of wild-type Drp1 (light gray) or Drp1ΔB (dark gray) pelleted in (B). (D) GTP hydrolysis of 5 µM protein was measured using a coupled assay as a function of NaCl concentration for wild-type Drp1 (circles) and Drp1ΔB (triangles). (E) The amount of GTP hydrolyzed per minute at each salt concentration was normalized against the amount of GTP hydrolyzed per minute at 100 mM NaCl in order to compare the salt sensitivity of GTP hydrolysis in wild-type Drp1 (circles) and Drp1ΔB (triangles). (F) Specific activity (SA) of wild-type Drp1 (circles) and Drp1ΔB (triangles) measured as a function of protein concentration at a fixed salt concentration (500mM NaCl).

disrupts assembly and disrupted assembly reduces GTP hydrolysis, a decrease in GTP hydrolysis as a function of increasing salt concentration could also be explained by reduced GTP substrate binding. We sought further confirmation that the observed trends in GTP hydrolysis activity were due to assembly and not altered GTP binding. To this end, we measured GTP hydrolysis at a fixed salt concentration (500 mM NaCl) as a function of protein concentration (Figure 2.1F). The specific activity (SA, μmol GTP hydrolyzed/min/μmol protein) of wild-type Drp1 increased with increasing protein concentration, consistent with assembly-dependent enzymatic activity. The specific activity of Drp1ΔB similarly increased with increasing protein concentration, but with higher activity compared to wild-type at all protein concentrations above 1 μM. This supports that GTP hydrolysis is assembly-dependent in Drp1 and Drp1ΔB, and that Drp1ΔB hyper-assembles. In summary, these results are consistent with the hypothesis that the B domain influences GTP hydrolysis in Drp1 by influencing assembly.

Disorder predictions of the B domain are inconclusive

This enzymological data suggest that the B domain may play an inhibitory role in the wild-type enzyme. However, some of the cell biological data suggest that the opposite may also be the case[18]. The EAM predicts that positive and negative allostery can occur through a single domain that is allosterically coupled to at least two other domains, and that intrinsic disorder may play an important role allostery. To assess whether the B domain is intrinsically disordered, possibly enabling both a positive and a negative allosteric regulation of Drp1, we evaluated the amino acid sequence of the B domain by several metrics. The output of intrinsic disorder prediction algorithms suggests that the B domain is likely to be intrinsically disordered (Figure 2.2A). However, another widely used metric for the prediction of disorder is mean net charge vs mean hydrophobicity[38–41]. Interestingly, the B domain falls on the natively folded side of the

empirical division between natively folded and intrinsically disordered proteins, in disagreement with the other predictions (Figure 2.2B). Although The B domain has many ionizable residues, the relative abundance of basic and acidic residues is nearly equivalent (19 and 17 respectively), and assuming unshifted pKa values for all ionizable residues, the resulting net charge per residue is modest (~.022). Furthermore, the B domain appears to be slightly more hydrophobic on average than the "typical" IDP, perhaps due to the elevated frequency of alanine residues in its sequence (Figure 2.2C). In fact, the alanine frequency in the B domain is even elevated compared to a selection of natively folded globular proteins (Figure 2.2D). Thus, sequence-based cues for intrinsic disorder in the B domain are somewhat ambiguous.

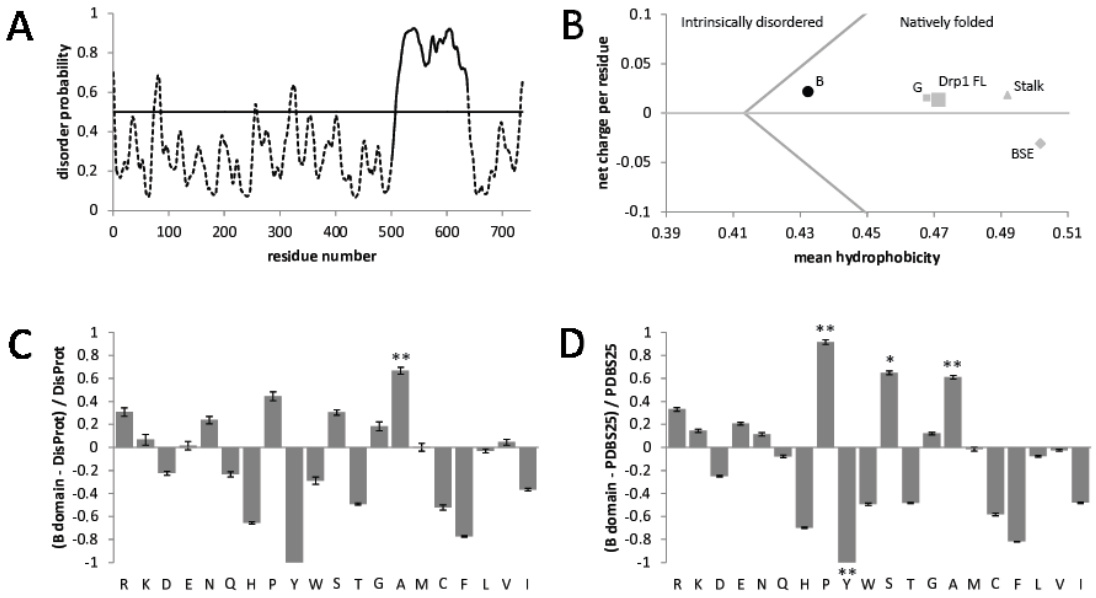

Figure 2.2 B domain sequence analysis. (A) PrDOS[79] disorder probability prediction for Drp1. The PrDOS prediction method creates a position-specific scoring matrix (PSSM) based on a multiple sequence alignment with the target protein. The PSSM is then is then analyzed using a support vector machine algorithm trained on disordered regions (missing residues) in a non-redundant set of proteins in the Protein Data Bank. The PSSM is also analyzed based on homologous proteins for which structural information is available. The final prediction is a combination of the two analyses. (B) Net charge vs. hydrophobicity plot for full-length Drp1 (Drp1 FL) and the individual Drp1 domains. Note that all domains, including the B domain, fall on the natively folded side of the empirical division between natively folded and intrinsically disordered proteins (dark gray line). (C-D) Amino acid composition profiles[80] of the B domain vs. the DisProt database (C), or a selection of globular proteins from the PDB (D). **significance level α = .05, *significance level α = .051

The B domain does not independently adopt a globular fold

To determine if the B domain is natively folded, we expressed and purified a B domain construct composed of residues 501-637 of Drp1 isoform 1 for further analysis. The protein was well-expressed into the soluble fraction of E. coli and was obtained in reasonable yields (~15 mg homogeneous protein/L rich media). In order to identify the boundaries of the B domain, we performed a multiple sequence alignment with classical dynamins and dynamin-related proteins and identified where sequence conservation was interrupted. We also analyzed the Drp1 sequence using the JPRED structure prediction algorithm to identify where the regular secondary structure of the stalk domain was predicted to be interrupted. This prediction was consistent with the multiple sequence alignment. Finally, we constructed a homology model using Swiss-Model, with the dynamin-1 crystal structure as a template and again identified where the helical stalk domain was interrupted. A high-resolution crystal structure for Drp1 (with the B domain removed) has since been solved. The termination of helices in the stalk domain at either terminus of the B domain observed in the crystal structure agrees with our multiple sequence alignment, JPRED structure prediction and homology model (data not shown).

When analyzed by size exclusion chromatography (SEC), the B domain eluted much earlier than would be expected for a globular protein of its molecular weight (Figure 2.3A). Using a standard curve composed of the S75 elution volumes of eight globular proteins of known molecular weight, we calculated an expected elution volume of 89 mL for a globular monomer with a molecular weight equivalent to that of our B domain construct (15.4 kDa). The observed elution volume for the B domain was 69 mL, which based on the standard curve equates to a molecular weight that is about 3.5 times larger than that expected for a globular monomer. This suggests that the B domain may elute as a globular oligomer (trimer or

tetramer), a result that was previously reported by Zhang et al. for a B domain construct[42]. However, SEC is a better measurement of hydrodynamic dimensions than molecular weight[43,44]. Therefore, the lower elution volume observed for the B domain could also indicate that it is a monomeric extended chain with a large hydrodynamic radius.

Sedimentation velocity of the B domain (Figure 2.3B) revealed that the B domain is indeed monomeric, with a sedimentation coefficient of 1.069 $S_{20,w}$ and an estimated molecular weight of 13,970 Da (vs. 15,363 Da calculated from sequence), thus eliminating the possibility of oligomerization. The maximum sedimentation coefficient S_{max}, calculated after the manner of Erickson[44], represents the sedimentation coefficient of the smallest non-hydrated smooth sphere that could contain the mass of a given protein. For our B domain construct, S_{max} = 2.231. By taking the ratio of S_{max} and the measured $S_{20,w}$, we obtained a semi-quantitative estimate of protein shape. By this measure, globular proteins typically have a ratio near 1.2 or 1.3, moderately elongated proteins have a ratio around 1.5 to 1.9, and highly elongated proteins have a ratio around 2.0 to 3.0[44]. The $S_{max}/S_{20,w}$ ratio for the B domain was 2.09, indicating that it likely populates moderate to highly elongated conformations.

Comparison of the measured B domain hydrodynamic dimensions to those published for other globular, premolten globule (PMG), random coil and denatured proteins[39] indicated that the hydrodynamic dimensions of the B domain lie between those of a natively unfolded PMG and a natively unfolded random coil (Figure 2.3C). However, we could not exclude that some portion of the B domain adopts regular secondary structure.

To evaluate this possibility, the secondary structure of the B domain was evaluated by circular dichroism (CD) (Figure 2.3D). The CD spectrum of the B domain showed a minimum near 200 nm, indicative of a random coil conformation. No minima were apparent at 208 nm or 222 nm, eliminating the possibility of a large helical content for this sequence. Deconvolution of

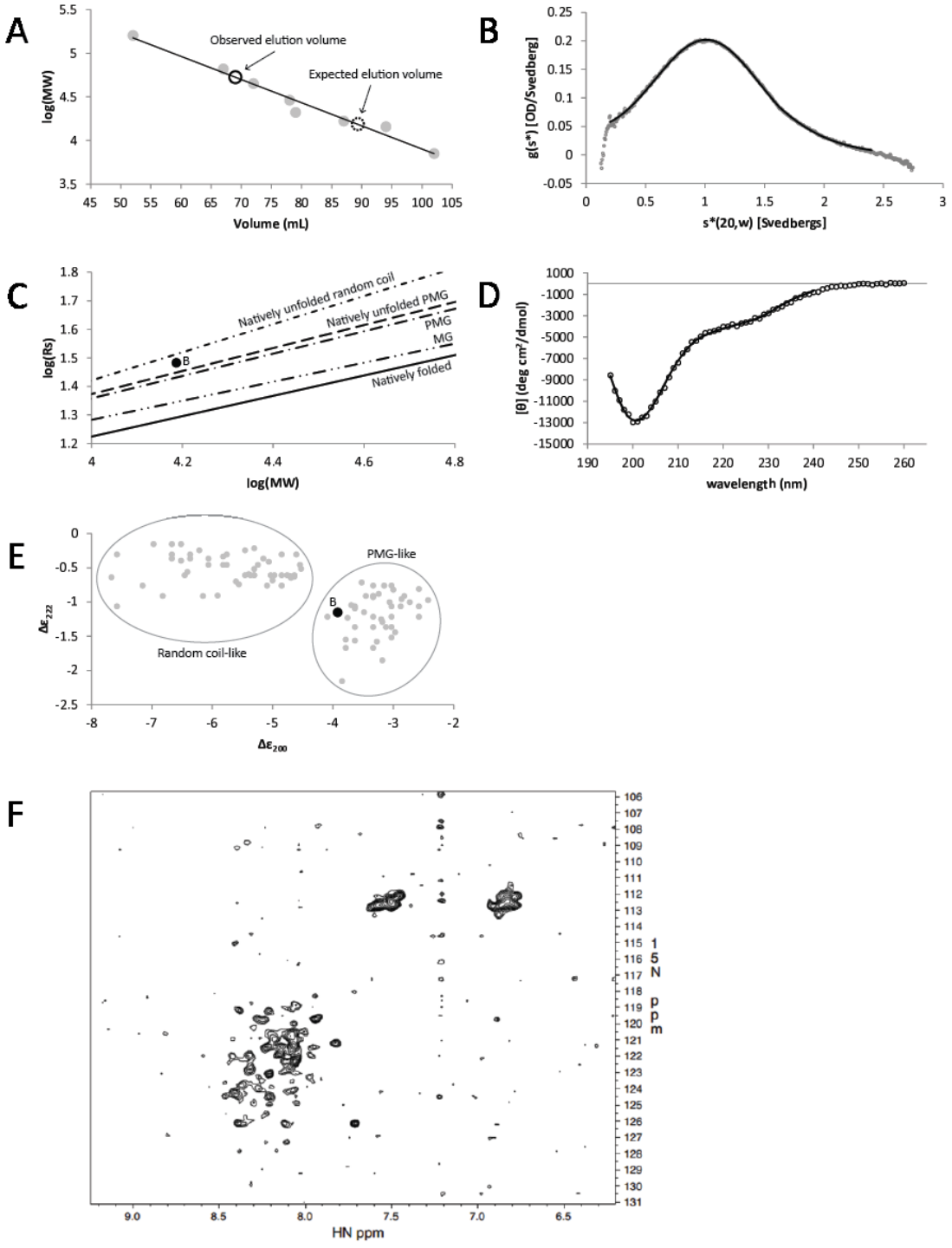

Figure 2.3 Structural properties of the isolated B domain. (A) The B domain eluted from an S75 SEC column at about 69 mL (open black circle), much earlier than the expected 89 mL elution volume for a globular protein of equivalent molecular weight (open gray circle) based on globular protein standards (filled gray circles). (B) Fit of sedimentation velocity data of the B domain to the Lamm equation using DCDT+ indicates that the B domain is monomeric, with a sedimentation coefficient of 1.069 $S_{20,w}$. Further analysis of this data suggests that the B domain adopts elongated conformations (see text). (C) The Stokes radius (Rs) of the B domain (filled black circle) lies between

(Figure 2.3, continued) **natively unfolded pre-molten globule (PMG) and a natively unfolded coil, according to standard curves published by Uversky (Uversky 2002). (D) Circular dichroism spectrum of the B domain is consistent with intrinsic disorder, with a characteristic minimum near 200 nm. (E) The B domain mean residual ellipticities at 200 and 222 nm are similar to PMG-like standards published by Uversky (Uversky 2002). (F) The ^{1}H-^{15}N HSQC spectrum of the B domain shows poor dispersion in both dimensions, consistent with intrinsic disorder.**

the CD spectrum using CONTIN-LL in the CDPro software package[30,31] suggests that the construct is just over 60% random coil, with the remainder being mostly beta turn and beta strand, and a small amount of alpha helix (Table 2.1). A small amount of helicity was expected based on the prediction of a slight helical propensity in the N terminal region of the B domain, as predicted by the secondary structure predictors PSIPRED, JPred and PredictProtein (data not shown). A comparison of the mean residue ellipticities at 200 and 222 nm to other proteins after the method of Uversky[45] is again consistent with the B domain adopting a PMG-like conformation (Figure 2.3E).

Given that the CD spectrum might be consistent with a significant fraction of beta structure, we collected site-specific information using NMR spectroscopy. We uniformly labeled the B domain with ^{15}N and collected a ^{1}H-^{15}N HSQC spectrum that primarily correlates amide protons to their attached amide nitrogens (Figure 2.3F). Beta structure would be expected to result in excellent chemical shift dispersion from the unique chemical environment experienced by backbone amides. However, the HSQC spectrum of the B domain showed poor chemical shift dispersion in both dimensions, indicating that the backbone amides experience a similar chemical environment, consistent with an intrinsically disordered conformation. Together, these data show that the B domain adopts an intrinsically disordered conformation in solution.

Many known IDPs undergo specific changes in secondary structure upon heating, as indicated by a positive shift in the CD spectrum around 200 nm and a negative shift in the spectrum near 222 nm[46–48]. We observed such a shift for the B domain (Figure 2.4A, 2.4B), although the magnitude was slightly less pronounced compared to that reported for other IDPs.

Furthermore, we discovered that at 10 µM protein, the spectral change as a function of temperature was more pronounced at 200 nm than at 222 nm (Figure 2.4C), whereas at a higher protein concentration (108 µM), the negative shift in the spectrum near 222 nm as a function of temperature was more pronounced than the change at 200 nm (Figure 2.4D). These findings suggest that the spectral changes at 200 and 222 nm as a function of temperature are dependent upon protein concentration, an observation that has not been reported previously (to our knowledge) for other IDPs. These data are consistent with the B domain being intrinsically disordered, but also suggest that the B domain may possess unique characteristics not typically observed in other IDPs, namely a concentration-dependent structural behavior.

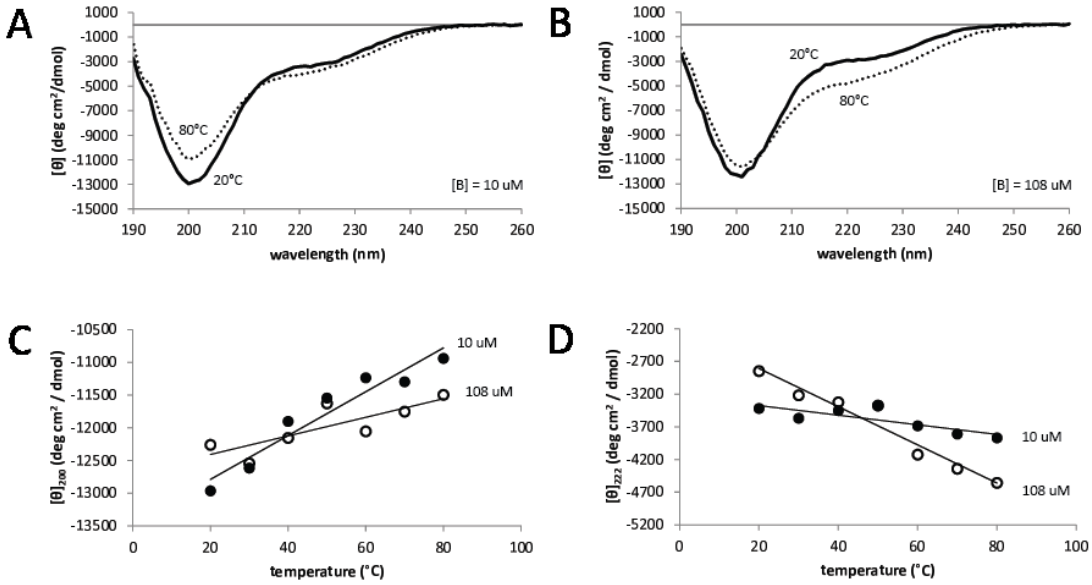

Figure 2.4 Temperature and concentration dependence of the B domain. (A) The endpoints of a CD thermal scan of 10 µM B domain, from 20°C (solid line) to 80°C (dotted line) . (B) The endpoints of a CD thermal scan of 108 µM B domain, from 20°C (solid line) to 80°C (dotted line). (C) Molar ellipticity at 200 nm for the CD thermal scan, indicates that 10 µM B domain undergoes greater changes in the spectrum at this wavelength than does 108 µM B domain. (D) Molar ellipticity at 222 nm for the CD thermal scan, indicates that 108 µM B domain undergoes greater changes in the spectrum at this wavelength than does 10 µM B domain.

The B domain exhibits peculiar behavior in the protecting osmolyte TMAO

Determination of B domain stability is central to evaluating its potential for allosteric function in terms of the EAM. Since the B domain is intrinsically disordered, we must first

determine if the B domain adopts a folded conformation. If it does, we must then determine the stability of that conformation. The protecting osmolyte trimethylamine-N-oxide (TMAO) has been used to induce folding of intrinsically disordered proteins and measure the free energy of folding for these proteins [49–52]. TMAO is a naturally occurring osmolyte that has been shown to favor native-like folded states of proteins by elevating the free energy of the unfolded state[49]. To determine the effect of TMAO on the B domain, we followed the B domain steady-state tryptophan fluorescence as a function of TMAO. A preliminary measurement of B domain tryptophan fluorescence intensity over time indicated that the tryptophan fluorescence signal reached a maximum quickly (< 30 seconds) and then very gradually decreased by a insignificant amount over the duration of the time-course measurement (30 minutes), consistent with the effect of photobleaching (data not shown). All subsequent fluorescence measurements were made following a two minute incubation period to ensure that equilibrium was attained. As a function of increasing TMAO concentration, the λ_{max} of the tryptophan intensity showed a significant blue shift of ~12 nm, a strong indicator of tryptophan burial (Figure 2.5A, filled circles). The tryptophan intensity measured at a single wavelength (338 nm) as a function of TMAO concentration showed a cooperative transition consistent with folding (Figure 2.5A, open circles). These data are well fit by a two-state model (Figure 2.5A, solid line), giving an m-value of 2.9 ± 0.2 kcal/mol M, consistent with other IDPs of similar size[21,53–55]. However, the concentration midpoint (Cm) of the transition (2.8 ± 0.1 M) and the apparent free energy of folding (8.2 ± 0.5 kcal/mol) indicate that, if the observed change in fluorescence was indeed due to folding alone, the folded conformation of the B domain is highly destabilized under native conditions. As a control, we measured the fluorescence of free tryptophan in TMAO and observed no significant blue-shift of the λ_{max} , but rather a slight red-shift of about 4 nm at TMAO concentrations above 3 M, verifying that the blue-shift observed in the B domain was not

attributable to a change in solvent polarity (Figure 2.5B, filled squares). Furthermore, there was no sigmoidal transition observed in the free tryptophan fluorescence intensity measured at 338 nm (Figure 2.5B, open squares).

Two-state behavior can be assessed by measuring the reversibility of a process[56]. In this case this was achieved by reverse titration, i.e., starting with a 15x concentrated protein stock in a concentrated TMAO buffer that was then diluted into buffers of lower TMAO concentrations. The resulting fluorescence intensity and λ_{max} curves (Figure 2.5C, open and filled diamonds, respectively) indicate that the process is indeed reversible. However, they show hysteresis with respect to the forward titration (Figure 2.5D). The stock solution of concentrated protein in concentrated TMAO that was used in these experiments was noticeably turbid, but the turbidity vanished upon 15x dilution to the final protein concentration. To verify that the observed reduction in fluorescence intensity was not due to precipitation of protein aggregates, we measured the protein concentration by UV spectroscopy following 15x dilution from native buffer and from concentrated TMAO buffer. In both cases, all protein was recovered (Figure 2.5E), verifying that the previously observed change in fluorescence was due to reversal of tryptophan burial, and not to loss of protein. Hysteresis is clearly evident in a comparison of normalized fluorescence data from the forward and reverse TMAO titrations (Figure 2.6A). The presence of hysteresis suggests that the observed process is not two-state, and a kinetic component in the process is implied[56]. Furthermore, this indicates that the parameters obtained from the fit to a two-state model do not accurately represent the energetics of the process. For the purpose of comparing processes on the basis of "fraction completed," we have normalized the TMAO-induced process to a two-state fit. However, since the measurements were taken at pseudo-equilibrium, we forgo using these fits to determine thermodynamic parameters of the process, as this would give incorrect and misleading values. Without a direct

measure of the stability of the B domain, we were unable to evaluate the capacity of the B domain for allosteric regulation in terms of the EAM. However, we continued to investigate further as we suspected the hysteresis and the reversible turbidity observed at higher protein concentrations in the presence of TMAO could be indicative of a self-assembly capability that has not been previously appreciated in the B domain.

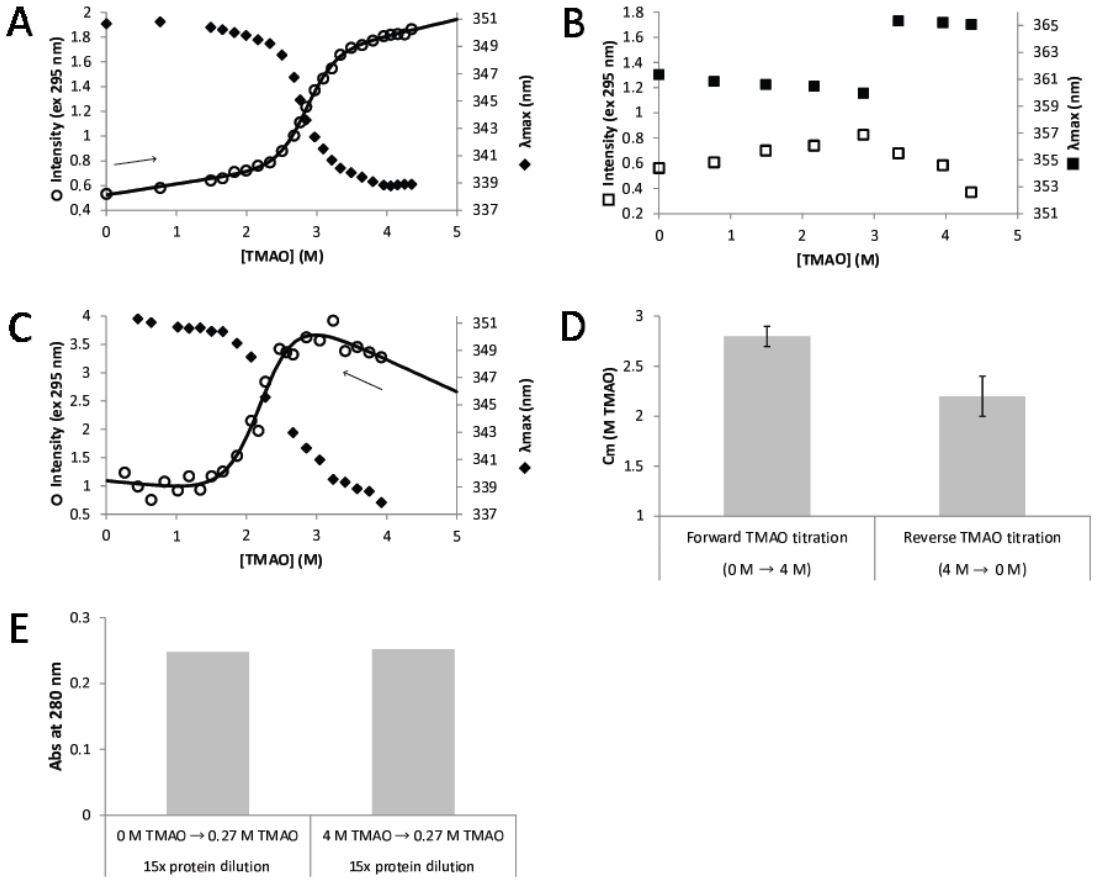

Figure 2.5 Steady-state tryptophan fluorescence of the B domain in the protecting osmolyte TMAO. (A) Forward titration (direction indicated by arrow) in TMAO resulted in a 12 nm blue-shift of the λ_{max} (filled diamonds), and a transition in the fluorescence intensity at 338 nm (open circles) that is well-fit by a two-state model (solid line). (B) Free tryptophan exhibits a slight red-shift of the λ_{max} in TMAO (filled squares) and does not undergo a two-state increase in fluorescence intensity at 338 nm (open squares). (C) Reverse titration (direction indicated by arrow) in TMAO, like the forward titration, resulted in a 12 nm blue-shift of the λ_{max} (filled diamonds), and a transition in the fluorescence intensity at 338 nm (open circles) that is well-fit by a two-state model (solid line). However, the concentration midpoint (Cm) of the transition was shifted to a lower concentration of TMAO (D). (E) UV/Vis absorbance measurements following 15x dilution from native buffer and from concentrated TMAO buffer (corresponding to forward and reverse titration, respectively) indicates that all protein is recovered, regardless of titration direction.

As a verification of assembly or aggregation, we observed static right-angle light scattering (RALS) in the same samples used for fluorescence measurements. As a control, we also measured RALS as a function of TMAO for Lysozyme, which is similar to the B domain in amino acid sequence length and molecular weight, but is a natively folded protein. Lysozyme showed no sign of aggregation (as measured by light scattering) even at high concentrations of TMAO (Figure 2.6B). The B domain, on the other hand, showed significant light scattering across the same range of TMAO concentrations that the fluorescence transition was observed (Figure 2.6B). This contrast with lysozyme suggests that the assembly/aggregation behavior observed in the B domain may be an inherent property of the B domain, possibly attributable to its intrinsically disordered properties. Interestingly, the normalized light scattering data we

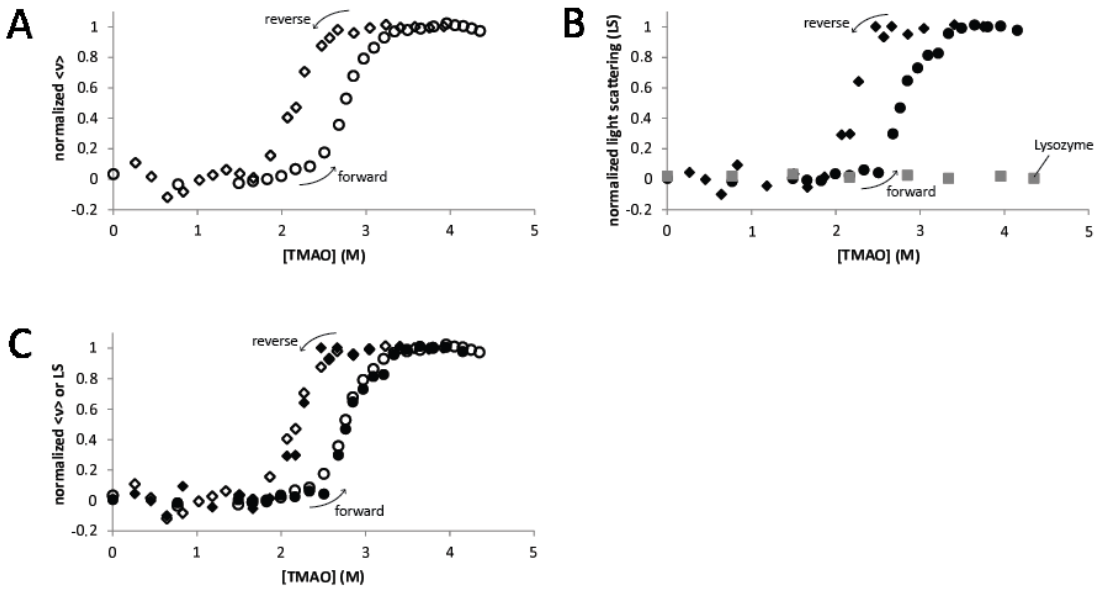

Figure 2.6 Comparison of forward and reverse titrations in TMAO by fluorescence and light scattering (LS). (A) The reverse titration (open diamonds) exhibits hysteresis with respect to the forward titration (open circles). (B) TMAO titration of the B domain followed by light scattering gives a two-state transition similar to that observed by fluorescence, with similar hysteresis between forward (filled circles) and reverse (filled diamonds) titrations. Lysozyme, used here as a negative control, does not scatter light in TMAO (gray squares). (C) The light scattering data (filled shapes) aligns with the fluorescence data (open shapes) for both the forward (circles) and reverse (diamonds) titrations.

measured are essentially superimposable on the fluorescence data in both the forward and reverse titrations (Figure 2.6C), suggesting that these observables (fluorescence and light scattering) are reporting on the same process, or if not a single process, then two processes occurring concomitantly.

To further confirm the presence of self-assembly, we repeated the fluorescence experiments in TMAO at several protein concentrations. We found that the midpoint of the transition decreased by 0.6 M, from a Cm of 2.8 M at 2 µM protein concentration to a Cm of 2.2 M at 40 µM protein concentration (Figure 2.7A). RALS of the same samples showed the same shifts in Cm, and the normalized RALS curves were again superimposable on the normalized fluorescence curves (Figure 2.7B). A monomeric folding reaction would not be dependent on protein concentration, thus the observed dependence of the Cm on protein concentration indicates that the process involves self-assembly. In the absence of TMAO, tryptophan burial, as

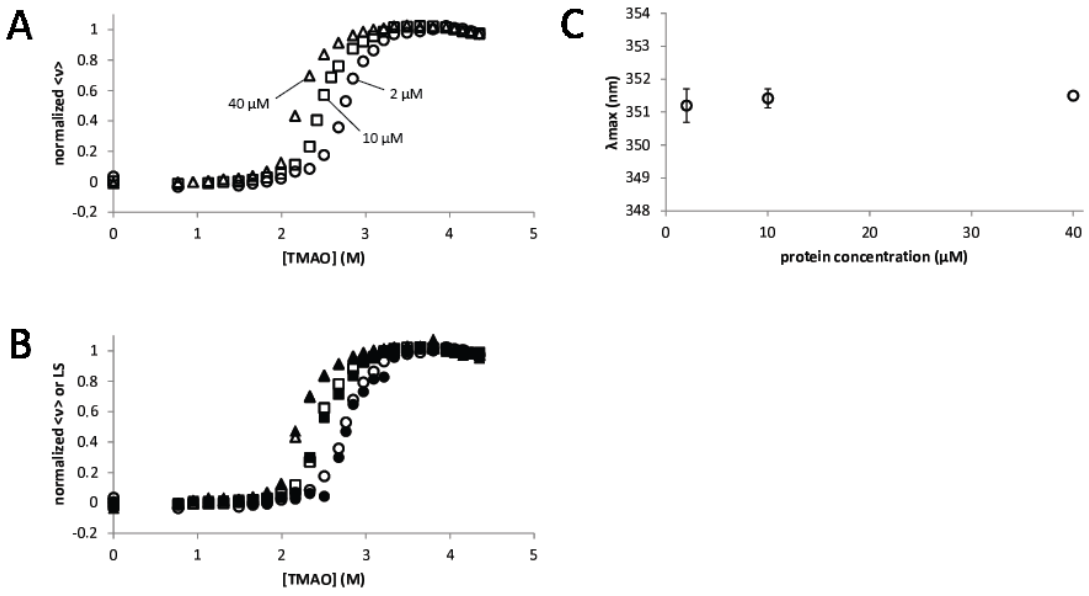

Figure 2.7 Concentration dependence of the B domain in TMAO. (A) TMAO titrations carried out with 2 µM (circles),10 µM (squares) and 40 µM (triangles), followed by fluorescence, show a concentration dependence. (B) The same samples followed by light scattering (LS) (filled shapes) show the same concentration dependence, and align with the fluorescence data (open shapes). (C) The λ_{max} does not change with B domain concentration in the absence of TMAO.

measured by λ_{max} , did not show concentration dependence for this range of protein concentrations (Figure 2.7C), indicating that TMAO is required to induce self-assembly at these protein concentrations.

Given the superimposability of the RALS and fluorescence curves, we questioned to what extent the B domain was folding, if at all, since the change in fluorescence could also be explained by burial of the tryptophan in an assembly interface without significant autonomous folding of monomers. Alternatively, the tryptophan may become buried within an independently folded (or partially folded) conformation that subsequently assembles or aggregates. To determine if the putative folding and assembly/aggregation could be separated, we tested various solution conditions to see if light scattering could be reduced or eliminated without completely preventing tryptophan burial (as indicated by a shift in λ_{max}). We tested three strategies that we anticipated would reduce protein aggregation compared to the original buffer condition: (1) maximization of protein net charge (and therefore electrostatic repulsion between proteins) by titrating the buffer pH to points further above or below the isoelectric point of the B domain (calculated to be 7.85), (2) stabilization of monomers through preferential shielding of hydrophobic regions by glycerol[57], and (3) disruption of protein-protein interactions by influencing both hydrophobic and electrostatic interactions through the addition of arginine hydrochloride[58,59]. For each buffer condition, we measured the tryptophan fluorescence spectrum and light scattering of the B domain in the absence and presence of 4 M TMAO and plotted the change in light scattering (ΔLS) vs the change in λ_{max} ($\Delta\lambda_{max}$). All data points were normalized to the ΔLS and $\Delta\lambda_{max}$ of the original buffer condition.

All of the conditions tested reduced the light scattering compared to the original buffer condition (Figure 2.8A). The pH 8.5 condition and the 40% glycerol condition exhibited reduced light scattering by 29% and 43% respectively, without significantly altering tryptophan burial, i.e.

they exhibited nearly the same blue shift of the λ_{max} . The pH 6.5 condition and the 1 M arginine hydrochloride conditions reduced scattering even further, by 74% and 96% respectively, but did so at the expense of tryptophan burial. A linear relationship between ΔLS and $\Delta\lambda_{max}$ was apparent upon comparison of the conditions tested. A linear fit of these data points gave a slope of 1.08 and an intercept of 0.34. The slope near unity is consistent with the superimposability of the fluorescence and light scattering curves observed previously (see Figure 2.6B), but also raises the concern that the shift in λ_{max} could be an artifact induced by light scattering. However, we still observed the strong blue-shift of the λ_{max} when polarizers were crossed to eliminate scattered light (Figure 2.8B), confirming that the observed change in tryptophan fluorescence was not due to a light scattering artifact. The non-zero intercept (0.34) of the $\Delta LS/\Delta\lambda_{max}$ linear fit in Figure 2.8A may suggest that some fraction (perhaps one third) of the total blue-shift observed in the original condition is due to tryptophan burial in the absence of significant assembly or aggregation, i.e. within a monomeric fold or low-order oligomeric collapsed state. We attempted to determine the oligomeric state of the B domain in TMAO with

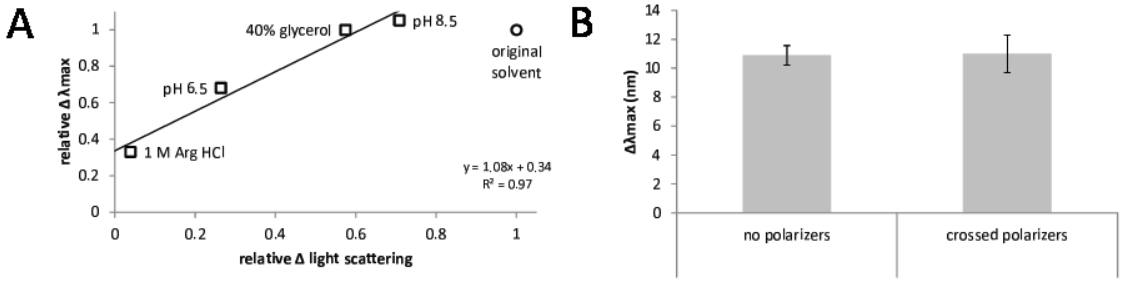

Figure 2.8 Relationship between tryptophan burial and self-assembly. (A) Extent of tryptophan burial (as measured by $\Delta\lambda_{max} = |\lambda_{max,\ 4\ M\ TMAO} - \lambda_{max,\ 0\ M\ TMAO}|$), and extent of self-assembly (as measured by Δlight scattering = $|\text{light scattering}_{4\ M\ TMAO} - \text{light scattering}_{,\ 0\ M\ TMAO}|$) were measured under different solvent conditions intended to reduce self-assembly without reducing putative folding induced by TMAO. The $\Delta\lambda_{max}$ and Δlight scattering data were normalized to the $\Delta\lambda_{max}$ and Δlight scattering data under the original solvent conditions (pH 7.4, 50 mM Arg HCl, no glycerol, with and without 4 M TMAO). There appears to be a linear relationship between tryptophan burial and self-assembly, with a slope near 1 and an intercept of 0.34. (B) The $\Delta\lambda_{max}$ was measured with and without crossed polarizers and resulted in the same value, indicating that the $\Delta\lambda_{max}$ was not attributable to scattered light.

1 M arginine hydrochloride by sedimentation velocity, but the experiment was unsuccessful because the protein assembled and began to scatter light a few hours into the experiment (data not shown). This indicates that arginine does not permanently prevent protein-protein interaction; rather it slows the kinetics of assembly/aggregation.

The TMAO-induced changes include an increase in beta strands and beta turns

We explored the secondary structural characteristics of the TMAO-induced form of the B domain by circular dichroism. A plot of the change in ellipticity at 222 nm at three TMAO concentrations aligned with the transition observed by fluorescence (Figure 2.9A), indicating that the tryptophan burial is accompanied by change in secondary structure. The change in the B domain CD spectrum in increasing concentrations of TMAO appeared quite dramatic, resulting in a minimum at 230 nm (Figure 2.9B). However, deconvolution of the spectra using CONTIN-LL from the CDPro analysis software estimated modest changes in structure, with the most notable change being a 10 point increase in beta-strand and a nearly 7 point decrease in helicity (Table 2.1). It should be noted that we were only able to deconvolute a small portion of the spectra in samples that contained TMAO because the intrinsic optical properties of TMAO buffers interfered with collection of data below 210 nm. A CONTIN-LL fit of this small range of wavelengths will be less accurate than one performed on a larger portion of the spectrum.

To alleviate the problem of optical interference by TMAO, and also to determine whether the B domain would exhibit similar behavior in the presence of other cosolvents, we repeated fluorescence, RALS and CD measurements of the B domain in the kosmotropic salt, ammonium sulfate. The B domain exhibited similar two-state-like behavior as measured by fluorescence and light scattering (Figure 2.10A), although the midpoint of the light scattering curve was slightly shifted toward higher ammonium sulfate concentration compared to the

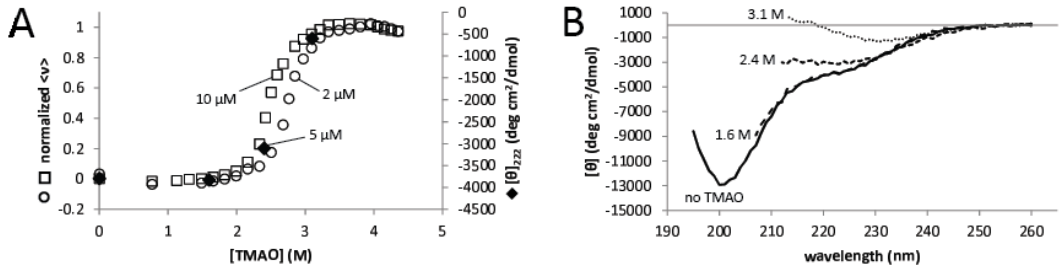

Figure 2.9 Change in B domain secondary structure in TMAO. (A) B domain molar ellipticity at 222 nm measured at 5µM protein concentration (filled diamonds) falls between the fluorescence intensity transitions measured previously (see Figure 2.7) at protein concentrations of 2 µM (open circles) and 10 µM (open squares). (B) CD spectra of the B domain in increasing concentrations of TMAO.

Table 2.1

	CONTIN-LL fit structural composition				
[TMAO] (M)	**Helix**	**Strand**	**Turn**	**Unrd**	RMSD
0	8.4	18.5	12.5	60.6	0.037
3.1	1.7	28.6	11.6	58.1	0.031
Δ	-6.7	10.1	-0.9	-2.5	

fluorescence curve. This may reflect a slight kinetic lag between folding and assembly/aggregation of the B domain in ammonium sulfate. The mean residual ellipticity at 200 nm in increasing concentrations of ammonium sulfate overlays with the fluorescence curve (Figure 2.10B), indicating that these observables are reporting on the same process or concomitant processes. The full CD spectra in ammonium sulfate follow a similar trend as in TMAO, with a minimum appearing near 230 nm, but we were also able to observe a maximum around 200 nm since the absence of optical interference in ammonium sulfate buffers allowed us to make measurements at much lower wavelengths (Figure 2.10C). The CONTIN-LL fit estimated a 16 point increase in beta-strand and a 5 point decrease in helicity, and also a 4 point increase in beta-turn not previously estimated from the TMAO fit (Table 2.2).

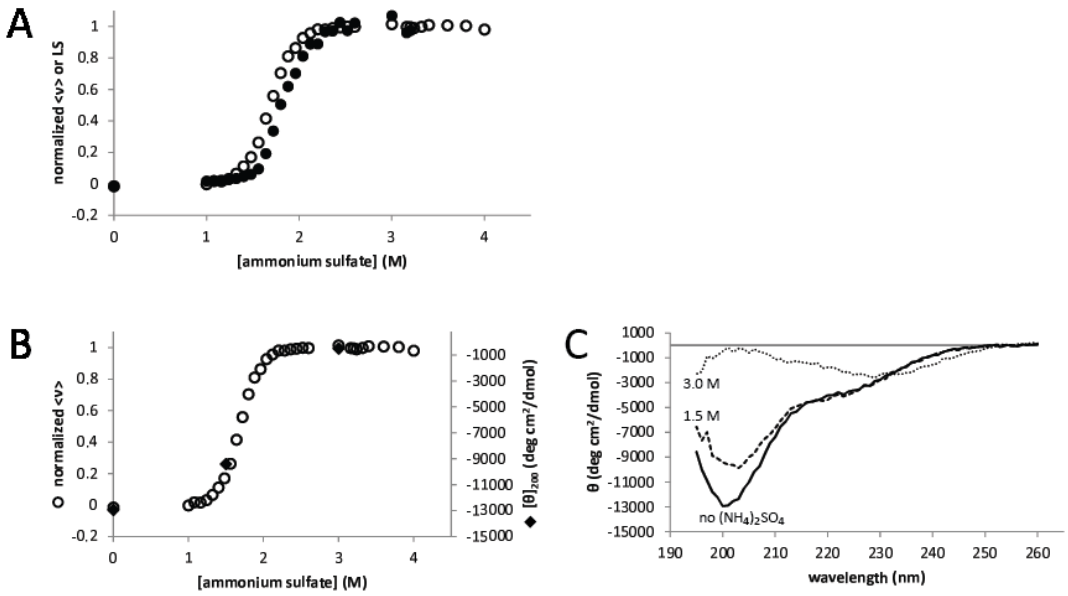

Figure 2.10 Steady-state tryptophan fluorescence, light scattering and circular dichroism of the B domain in the kosmotropic salt, ammonium sulfate. (A) The B domain exhibits a two-state transition by fluorescence (open circles) and light scattering (LS) (filled circles), similar to what was observed in TMAO, except that the light-scattering is slightly shifted to higher ammonium sulfate concentrations. (B) Molar ellipticity of the B domain at 200 nm (filled diamonds) aligns with the transition observed by fluorescence (open circles). Both measurements were made at 2 µM protein concentration. (C) CD spectra of the B domain in increasing concentrations of ammonium sulfate ($(NH_4)_2SO_4$).

Table 2.2

	CONTIN-LL fit structural composition				
$[(NH_4)_2SO_4]$ (M)	**Helix**	**Strand**	**Turn**	**Unrd**	RMSD
0	8.4	18.5	12.5	60.6	0.037
3	3.3	34.6	16.3	45.8	0.073
Δ	-5.1	16.1	3.8	-14.8	

The B domain also exhibited a response similar to what was observed in TMAO and ammonium sulfate in another protecting osmolyte, sarcosine. As a function of increasing sarcosine concentration, we observed an apparent two-state-like change in mean residual ellipticity that was superimposable on the normalized fluorescence curve (data not shown).

Taken together, these data suggest that the observed folding and self-assembly behavior is intrinsic to the B domain and is independent of kosmotropic cosolvent. As the solvent quality decreases (due to increasing kosmotropic cosolvent), the B domain undergoes changes in secondary structure with concomitant assembly/aggregation.

The B domain coacervates in the presence of TMAO

Because the observed assembly or aggregation phenomenon exhibited the unique properties of being reversible and deceptively similar to two-state, we suspected it may represent ordered assembly rather than amorphous non-native aggregation. In order to distinguish between amorphous aggregation and ordered assembly, we used transmission electron microscopy (TEM) to observe the B domain in the presence of TMAO. The same samples used for fluorescence and RALS measurements were applied to grids and imaged by TEM (Figure 2.11). The TMAO-induced state was neither an amorphous aggregate nor fibril-like ordered assembly. Rather, we consistently observed darkly stained spherical assemblies, 100-200 nm in diameter, with negatively stained globular textures within, a morphology that we never observed in the TMAO-only or protein-only controls. We observed these assemblies in samples that were prepared minutes to hours before being applied to the grid, and the assemblies appeared to be increasingly abundant in samples that were incubated in TMAO for longer periods (many hours to days). We suspect that these assemblies represent a coacervate, i.e. a phase separation resulting in a protein-rich phase (the coacervate) and a protein-poor phase (the bulk or equilibrium solution). The spherical droplet morphology is distinct from amorphous aggregation and is similar in appearance to the liquid-liquid phase separation observed in other coacervating systems such as tropoelastin[60].

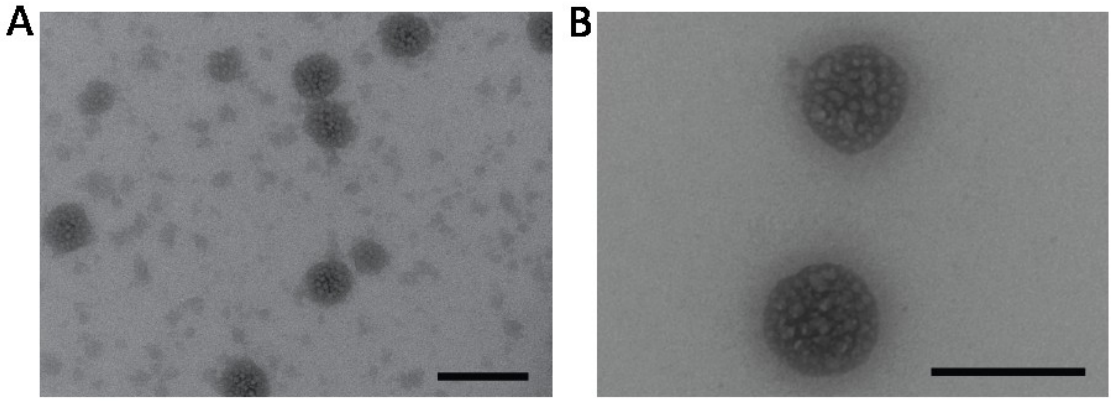

Figure 2.11 TEM images of B domain in TMAO. (A) 2 µM B domain in 3 M TMAO was applied to a carbon-coated copper grid and stained with 2% uranyl acetate. (B) An independently prepared sample under the same conditions as (A). The darkly-stained spherical coacervates are roughly 50 – 150 nm in diameter and appear to be formed by the coalescence of smaller globules (negatively-stained texture within the larger spheres). Scale bar is 200 nm in both images.

DISCUSSION

Here we have shown that removal of the B domain results in hyper-assembly and elevated GTP hydrolysis, suggesting an auto-inhibitory or allosteric role for the B domain. Furthermore, we have shown that the B domain does not adopt a folded conformation in isolation, exhibits concentration-dependent structural changes in response to elevated temperature, and undergoes conformational change and self-assembly in the presence of protecting osmolyte or kosmotropic cosolvent. We suspect that the self-assembled form is a coacervate.

The B domain may influence GTP hydrolysis in the G domain indirectly by regulating assembly in the stalk domain. Nearly all of the fission-deficient constructs examined by Strack and Cribbs[18] exhibited some form of aggregation. In their cell-based assay, GTP hydrolysis of Drp1 was not measurable, thus the enzymatic activity of the variants was unknown. Our Drp1ΔB variant exhibited hyper-assembly, probably similar in nature to the aggregates observed by Strack and Cribbs. We showed that hyper-assembly in our Drp1ΔB variant was accompanied

by elevated GTP hydrolysis compared to wild-type Drp1. We suspect that fission-deficient variants of Strack and Cribbs may also have had elevated enzymatic activity, But were prevented from productively associating with the mitochondrial membrane by aberrant assembly, so the GTP hydrolysis was futile and did not result in mitochondrial fission. Given that assembly-stimulated GTP hydrolysis is a hallmark of dynamin superfamily members, and that GTP-hydrolysis is attenuated by point mutations in the stalk domain that inhibit assembly, we suspect that the B domain may influence GTP hydrolysis in the G domain indirectly by regulating assembly in the stalk domain.

The influence of the B domain on the stalk domain may be through an allosteric mechanism wherein the energetics of the B domain are coupled to the stability of the stalk domain. We favored this hypothesis upon finding that the B domain is intrinsically disordered, in light of the ensemble allosteric model (EAM) which suggests that intrinsically disordered domains are uniquely poised for allosteric regulation of enzymes[20]. However, since the B domain self-assembled under conditions that typically induce IDPs to fold, we were unable to cleanly identify an equilibrium folded state of the B domain and therefore could not evaluate the capacity of the B domain for allosteric regulation in terms of the EAM. This hypothesis remains valid, and the observed B domain self-assembly may play a role in allosteric regulation.

Alternatively, the B domain may exert its effects on stalk domain assembly more directly, e.g., through physical occlusion of assembly interfaces in the stalk domain. The pleckstrin homology (PH) domain of dynamin has been proposed to interact directly with the dynamin stalk domain, based on contacts identified in the crystal structure[61]. Given the overall similarity between Drp1 and dynamin, and the similar location and size of B and PH domains, it may be that the B domain likewise forms contacts with the stalk domain in Drp1, preventing its assembly.

Regardless of the mechanism of auto-inhibition by the B domain, coacervation may play a role. In terms of allostery, the energy of coacervation could be coupled to stalk domain stability. In terms of physical occlusion, homotypic B domain interactions (coacervation) could compete with heterotypic B domain-stalk interactions, thereby relieving occlusion of stalk domain assembly interfaces. In both cases, relief of auto-inhibition must be triggered at the appropriate time so that Drp1 assembly occurs productively at the mitochondrial membrane surface.

Charge neutralization and the ability to form multivalent interactions are essential components of the mechanism of coacervation[62–68]. The B domain is well equipped to simultaneously undergo charge neutralization and form multiple contacts through homotypic interactions. The multiple positive and negative charges in the B domain polypeptide chain offer many opportunities for multivalent interactions through ion pairing, and when ion pairs form, the participating charges are neutralized. Since the B domain has only a few more positive than negative charges, it is capable of neutralizing nearly all of its charges through homotypic interactions. It has been shown for other coacervating proteins that a combination of "stiff" and "flexible" residues prevent chain collapse and maximize conformational dynamics, thereby favoring "fuzzy" intermolecular interactions over intramolecular interactions[69]. A combination of "stiff" and "flexible" residues are relatively abundant in the B domain in the form of proline and serine respectively. Finally, the few excess positive charges in the B domain may facilitate interactions with negatively charged lipid headgroups, resulting in complete charge neutralization at the membrane surface.

TMAO has been used to drive coacervation of other proteins that are known to naturally coacervate. Here we have used TMAO to elevate the energy of the unfolded state in an attempt to drive the B domain into a natural folded conformation. It is not clear if the

resulting coacervation represents a natural state of the protein. TMAO has been used to drive coacervation of other proteins that are known to naturally coacervate, such as tropoelastin[70] and nucleoporins[71]. Additionally, many IDPs have been shown to adopt monomeric folded states in TMAO[21,49,51,52,72–74]. In these examples, whether the final state is coacervation or folded monomer, TMAO does not appear to force proteins into non-native states. This is in contrast to other cosolvents such as trifluoroethanol (TFE), which most certainly does induce non-native protein conformations. Unlike TFE, TMAO does not preferentially or directly interact with the polypeptide backbone or sidechains, and thus does not lower the energy of a particular conformation [75–77]. Rather, it appears to destabilize unfolded conformations by altering the solvation of the protein backbone[49,78], allowing the protein to move into a lower energy state that is already part of its energy landscape. However, while several lines of evidence suggest TMAO favors natural or native-like states, it remains to be determined if TMAO can induce unnatural coacervation in some types of intrinsically disordered proteins. Future work will seek to verify whether coacervation is a natural state of the B domain and how coacervation might contribute to membrane remodeling and allosteric regulation in the context of Drp1 and more broadly in amphitropic proteins at large.

ACKNOWLEDGEMENTS

Assembly and GTP hydrolysis experiments relating to Drp1ΔB, as well as cloning, expression and purification of this construct were performed by Cara Marie Manlandro, to whom I express my sincere appreciation.

REFERENCES

(1) Cerveny, K. L., Tamura, Y., Zhang, Z., Jensen, R. E., and Sesaki, H. (2007) Regulation of mitochondrial fusion and division. *Trends Cell Biol. 17*, 563–9.

(2) Khacho, M., Tarabay, M., Patten, D., Khacho, P., MacLaurin, J. G., Guadagno, J., Bergeron, R., Cregan, S. P., Harper, M.-E., Park, D. S., and Slack, R. S. (2014) Acidosis overrides oxygen deprivation to maintain mitochondrial function and cell survival. *Nat. Commun. 5*, 3550.

(3) Mao, K., and Klionsky, D. J. (2013) Participation of mitochondrial fission during mitophagy. *Cell Cycle 12*, 3131–2.

(4) Frank, S., Gaume, B., Bergmann-Leitner, E. S., Leitner, W. W., Robert, E. G., Catez, F., Smith, C. L., and Youle, R. J. (2001) The role of dynamin-related protein 1, a mediator of mitochondrial fission, in apoptosis. *Dev. Cell 1*, 515–25.

(5) Landes, T., and Martinou, J.-C. (2011) Mitochondrial outer membrane permeabilization during apoptosis: the role of mitochondrial fission. *Biochim. Biophys. Acta 1813*, 540–5.

(6) Mears, J. A., Lackner, L. L., Fang, S., Ingerman, E., Nunnari, J., and Hinshaw, J. E. (2011) Conformational changes in Dnm1 support a contractile mechanism for mitochondrial fission. *Nat. Struct. Mol. Biol. 18*, 20–6.

(7) Chang, C.-R., and Blackstone, C. (2007) Cyclic AMP-dependent protein kinase phosphorylation of Drp1 regulates its GTPase activity and mitochondrial morphology. *J. Biol. Chem. 282*, 21583–7.

(8) Taguchi, N., Ishihara, N., Jofuku, A., Oka, T., and Mihara, K. (2007) Mitotic phosphorylation of dynamin-related GTPase Drp1 participates in mitochondrial fission. *J. Biol. Chem. 282*, 11521–9.

(9) Cribbs, J. T., and Strack, S. (2007) Reversible phosphorylation of Drp1 by cyclic AMP-dependent protein kinase and calcineurin regulates mitochondrial fission and cell death. *EMBO Rep. 8*, 939–44.

(10) Cereghetti, G. M., Stangherlin, A., Martins de Brito, O., Chang, C. R., Blackstone, C., Bernardi, P., and Scorrano, L. (2008) Dephosphorylation by calcineurin regulates translocation of Drp1 to mitochondria. *Proc. Natl. Acad. Sci. U. S. A. 105*, 15803–8.

(11) Han, X.-J., Lu, Y.-F., Li, S.-A., Kaitsuka, T., Sato, Y., Tomizawa, K., Nairn, A. C., Takei, K., Matsui, H., and Matsushita, M. (2008) CaM kinase I alpha-induced phosphorylation of Drp1 regulates mitochondrial morphology. *J. Cell Biol. 182*, 573–85.

(12) Figueroa-Romero, C., Iñiguez-Lluhí, J. A., Stadler, J., Chang, C.-R., Arnoult, D., Keller, P. J., Hong, Y., Blackstone, C., and Feldman, E. L. (2009) SUMOylation of the mitochondrial fission protein Drp1 occurs at multiple nonconsensus sites within the B domain and is linked to its activity cycle. *FASEB J. 23*, 3917–27.

(13) Chang, C.-R., and Blackstone, C. (2010) Dynamic regulation of mitochondrial fission through modification of the dynamin-related protein Drp1. *Ann. N. Y. Acad. Sci. 1201*, 34–9.

(14) Strack, S., Wilson, T. J., and Cribbs, J. T. (2013) Cyclin-dependent kinases regulate splice-specific targeting of dynamin-related protein 1 to microtubules. *J. Cell Biol. 201*, 1037–51.

(15) Apweiler, R., Bairoch, A., Wu, C. H., Barker, W. C., Boeckmann, B., Ferro, S., Gasteiger, E., Huang, H., Lopez, R., Magrane, M., Martin, M. J., Natale, D. A., O'Donovan, C., Redaschi, N., and Yeh, L.-S. L. (2004) UniProt: the Universal Protein knowledgebase. *Nucleic Acids Res. 32*, D115–D119.

(16) Howng, S.-L., Sy, W.-D., Cheng, T.-S., Lieu, A.-S., Wang, C., Tzou, W.-S., Cho, C.-L., and Hong, Y.-R. (2004) Genomic organization, alternative splicing, and promoter analysis of human dynamin-like protein gene. *Biochem. Biophys. Res. Commun. 314*, 766–772.

(17) Chen, C. H., Howng, S. L., Hwang, S. L., Chou, C. K., Liao, C. H., and Hong, Y. R. (2000) Differential expression of four human dynamin-like protein variants in brain tumors. *DNA Cell Biol. 19*, 189–94.

(18) Strack, S., and Cribbs, J. T. (2012) Allosteric modulation of Drp1 mechanoenzyme assembly and mitochondrial fission by the variable domain. *J. Biol. Chem. 287*, 10990–1001.

(19) Motlagh, H. N., and Hilser, V. J. (2012) Agonism/antagonism switching in allosteric ensembles. *Proc. Natl. Acad. Sci. U. S. A. 109*, 4134–9.

(20) Hilser, V. J., and Thompson, E. B. (2007) Intrinsic disorder as a mechanism to optimize allosteric coupling in proteins. *Proc. Natl. Acad. Sci. U. S. A. 104*, 8311–5.

(21) Li, J., Motlagh, H. N., Chakuroff, C., Thompson, E. B., and Hilser, V. J. (2012) Thermodynamic dissection of the intrinsically disordered N-terminal domain of human glucocorticoid receptor. *J. Biol. Chem. 287*, 26777–87.

(22) Warnock, D. E., Hinshaw, J. E., and Schmid, S. L. (1996) Dynamin self-assembly stimulates its GTPase activity. *J. Biol. Chem. 271*, 22310–4.

(23) Hinshaw, J. E., and Schmid, S. L. (1995) Dynamin self-assembles into rings suggesting a mechanism for coated vesicle budding. *Nature 374*, 190–192.

(24) Ingerman, E., and Nunnari, J. (2005) A continuous, regenerative coupled GTPase assay for dynamin-related proteins. *Methods Enzymol. 404*, 611–9.

(25) Philo, J. S. (2006) Improved methods for fitting sedimentation coefficient distributions derived by time-derivative techniques. *Anal. Biochem. 354*, 238–46.

(26) Stafford, W. F. (1992) Boundary analysis in sedimentation transport experiments: a procedure for obtaining sedimentation coefficient distributions using the time derivative of the concentration profile. *Anal. Biochem. 203*, 295–301.

(27) Delaglio, F., Grzesiek, S., Vuister, G. W., Zhu, G., Pfeifer, J., and Bax, A. (1995) NMRPipe: a multidimensional spectral processing system based on UNIX pipes. *J. Biomol. NMR 6*, 277–293.

(28) Johnson, B. A., and Blevins, R. A. (1994) NMRView: A computer program for the visualization and analysis of NMR data. *J. Biomol. NMR 4*, 603–614.

(29) Wang, A., and Bolen, D. W. (1997) A naturally occurring protective system in urea-rich cells: mechanism of osmolyte protection of proteins against urea denaturation. *Biochemistry 36*, 9101–8.

(30) Sreerama, N., and Woody, R. W. (2000) Estimation of protein secondary structure from circular dichroism spectra: comparison of CONTIN, SELCON, and CDSSTR methods with an expanded reference set. *Anal. Biochem. 287*, 252–60.

(31) Sreerama, N., Venyaminov, S. Y., and Woody, R. W. (2000) Estimation of protein secondary structure from circular dichroism spectra: inclusion of denatured proteins with native proteins in the analysis. *Anal. Biochem. 287*, 243–51.

(32) Pace, C. N. (1990) Measuring and increasing protein stability. *Trends Biotechnol. 8*, 93–8.

(33) Santoro, M. M., and Bolen, D. W. (1988) Unfolding free energy changes determined by the linear extrapolation method. 1. Unfolding of phenylmethanesulfonyl alpha-chymotrypsin using different denaturants. *Biochemistry 27*, 8063–8.

(34) Moon, C. P., and Fleming, K. G. (2011) Using tryptophan fluorescence to measure the stability of membrane proteins folded in liposomes. *Methods Enzymol.* 1st ed., pp 189–211. Elsevier Inc.

(35) Hong, H., and Tamm, L. K. (2004) Elastic coupling of integral membrane protein stability to lipid bilayer forces. *Proc. Natl. Acad. Sci. U. S. A. 101*, 4065–70.

(36) Chang, C.-R., Manlandro, C. M., Arnoult, D., Stadler, J., Posey, A. E., Hill, R. B., and Blackstone, C. (2010) A lethal de novo mutation in the middle domain of the dynamin-related GTPase Drp1 impairs higher order assembly and mitochondrial division. *J. Biol. Chem. 285*, 32494–503.

(37) Fröhlich, C., Grabiger, S., Schwefel, D., Faelber, K., Rosenbaum, E., Mears, J. A., Rocks, O., and Daumke, O. (2013) Structural insights into oligomerization and mitochondrial remodelling of dynamin 1-like protein. *EMBO J. 32*, 1280–92.

(38) Uversky, V. N., Gillespie, J. R., and Fink, A. L. (2000) Why are “natively unfolded” proteins unstructured under physiologic conditions? *Proteins 41*, 415–27.

(39) Uversky, V. (2002) What does it mean to be natively unfolded? *Eur. J. Biochem. 12*, 2–12.

(40) Prilusky, J., Felder, C. E., Zeev-Ben-Mordehai, T., Rydberg, E. H., Man, O., Beckmann, J. S., Silman, I., and Sussman, J. L. (2005) FoldIndex: a simple tool to predict whether a given protein sequence is intrinsically unfolded. *Bioinformatics 21*, 3435–8.

(41) Mao, A. H., Crick, S. L., Vitalis, A., Chicoine, C. L., and Pappu, R. V. (2010) Net charge per residue modulates conformational ensembles of intrinsically disordered proteins. *Proc. Natl. Acad. Sci. U. S. A. 107*, 8183–8188.

(42) Zhang, Y., Gao, X., and Garavito, R. M. (2011) Biochemical characterization of human dynamin-like protein 1. *J. Biochem. 150*, 627–33.

(43) Horiike, K., Tojo, H., Yamano, T., and Nozaki, M. (1983) Interpretation of the stokes radius of macromolecules determined by gel filtration chromatography. *J. Biochem. 93*, 99–106.

(44) Erickson, H. P. (2009) Size and shape of protein molecules at the nanometer level determined by sedimentation, gel filtration, and electron microscopy. *Biol. Proced. Online 11*, 32–51.

(45) Uversky, V. (2002) Natively unfolded proteins: a point where biology waits for physics. *Protein Sci. 11*, 739–756.

(46) Sánchez-Puig, N., Veprintsev, D. B., and Fersht, A. R. (2005) Human full-length Securin is a natively unfolded protein. *Protein Sci. 14*, 1410–1418.

(47) Kjaergaard, M., Nørholm, A.-B., Hendus-Altenburger, R., Pedersen, S. F., Poulsen, F. M., and Kragelund, B. B. (2010) Temperature-dependent structural changes in intrinsically disordered proteins: formation of alpha-helices or loss of polyproline II? *Protein Sci. 19*, 1555–64.

(48) Uversky, V. N. (2009) Intrinsically disordered proteins and their environment: effects of strong denaturants, temperature, pH, counter ions, membranes, binding partners, osmolytes, and macromolecular crowding. *Protein J. 28*, 305–25.

(49) Baskakov, I., and Bolen, D. W. (1998) Forcing thermodynamically unfolded proteins to fold. *J. Biol. Chem. 273*, 4831–4.

(50) Baskakov, I. V, Kumar, R., Srinivasan, G., Ji, Y. S., Bolen, D. W., and Thompson, E. B. (1999) Trimethylamine N-oxide-induced cooperative folding of an intrinsically unfolded transcription-activating fragment of human glucocorticoid receptor. *J. Biol. Chem. 274*, 10693–6.

(51) Mello, C. C., and Barrick, D. (2003) Measuring the stability of partly folded proteins using TMAO. *Protein Sci. 12*, 1522–9.

(52) Chang, Y.-C., and Oas, T. G. (2010) Osmolyte-induced folding of an intrinsically disordered protein: folding mechanism in the absence of ligand. *Biochemistry 49*, 5086–96.

(53) Ghosh, K., and Dill, K. A. (2009) Computing protein stabilities from their chain lengths. *Proc. Natl. Acad. Sci. U. S. A. 106*, 10649–54.

(54) Auton, M., and Bolen, D. W. (2005) Predicting the energetics of osmolyte-induced protein folding/unfolding. *Proc. Natl. Acad. Sci. U. S. A. 102*, 15065–8.

(55) Auton, M., Rösgen, J., Sinev, M., Holthauzen, L. M. F., and Bolen, D. W. (2011) Osmolyte effects on protein stability and solubility: a balancing act between backbone and side-chains. *Biophys. Chem. 159*, 90–9.

(56) Andrews, B. T., Capraro, D. T., Sulkowska, J. I., Onuchic, J. N., and Jennings, P. A. (2013) Hysteresis as a Marker for Complex, Overlapping Landscapes in Proteins. *J. Phys. Chem. Lett. 4*, 180–188.

(57) Vagenende, V., Yap, M. G. S., and Trout, B. L. (2009) Mechanisms of protein stabilization and prevention of protein aggregation by glycerol. *Biochemistry 48*, 11084–96.

(58) Tsumoto, K., Ejima, D., Kita, Y., and Arakawa, T. (2005) Review: Why is arginine effective in suppressing aggregation? *Protein Pept. Lett. 12*, 613–9.

(59) Arakawa, T., Ejima, D., Tsumoto, K., Obeyama, N., Tanaka, Y., Kita, Y., and Timasheff, S. N. (2007) Suppression of protein interactions by arginine: a proposed mechanism of the arginine effects. *Biophys. Chem. 127*, 1–8.

(60) Tu, Y., Wise, S. G., and Weiss, A. S. (2010) Stages in tropoelastin coalescence during synthetic elastin hydrogel formation. *Micron 41*, 268–72.

(61) Faelber, K., Posor, Y., Gao, S., Held, M., Roske, Y., Schulze, D., Haucke, V., Noé, F., and Daumke, O. (2011) Crystal structure of nucleotide-free dynamin. *Nature 477*, 556–60.

(62) Dobrynin, A. V., Colby, R. H., and Rubinstein, M. (2004) Polyampholytes. *J. Polym. Sci. Part B Polym. Phys. 42*, 3513–3538.

(63) Everaers, R., Johner, A., and Joanny, J. (1997) Complexation and precipitation in polyampholyte solutions. *Europhys. Lett. 37*, 275–280.

(64) Gupta, A., and Bohidar, H. (2005) Kinetics of phase separation in systems exhibiting simple coacervation. *Phys. Rev. E 72*, 011507.

(65) Cousin, F., Gummel, J., Combet, S., and Boué, F. (2011) The model Lysozyme-PSSNa system for electrostatic complexation: Similarities and differences with complex coacervation. *Adv. Colloid Interface Sci. 167*, 71–84.

(66) Kaibara, K., Okazaki, T., Bohidar, H. B., and Dubin, P. L. (2000) pH-induced coacervation in complexes of bovine serum albumin and cationic polyelectrolytes. *Biomacromolecules 1*, 100–7.

(67) Pathak, J., Rawat, K., and Bohidar, H. B. (2014) Surface patch binding and mesophase separation in biopolymeric polyelectrolyte-polyampholyte solutions. *Int. J. Biol. Macromol. 63*, 29–37.

(68) Kizilay, E., Kayitmazer, A. B., and Dubin, P. L. (2011) Complexation and coacervation of polyelectrolytes with oppositely charged colloids. *Adv. Colloid Interface Sci. 167*, 24–37.

(69) Rauscher, S., and Pomès, R. (2012) Structural disorder and protein elasticity. *Adv. Exp. Med. Biol. 725*, 159–83.

(70) Dyksterhuis, L. B., Carter, E. A., Mithieux, S. M., and Weiss, A. S. (2009) Tropoelastin as a thermodynamically unfolded premolten globule protein: The effect of trimethylamine N-oxide on structure and coacervation. *Arch. Biochem. Biophys. 487*, 79–84.

(71) Milles, S., Huy Bui, K., Koehler, C., Eltsov, M., Beck, M., and Lemke, E. A. (2013) Facilitated aggregation of FG nucleoporins under molecular crowding conditions. *EMBO Rep. 14*, 178–83.

(72) Kumar, R., Lee, J. C., Bolen, D. W., and Thompson, E. B. (2001) The conformation of the glucocorticoid receptor af1/tau1 domain induced by osmolyte binds co-regulatory proteins. *J. Biol. Chem. 276*, 18146–52.

(73) Lin, T., and Timasheff, S. (1994) Why do some organisms use a urea-methylamine mixture as osmolyte? Thermodynamic compensation of urea and trimethylamine N-oxide interactions with protein. *Biochemistry 33*, 12695–12701.

(74) Henkels, C. H., Kurz, J. C., Fierke, C. A., and Oas, T. G. (2001) Linked folding and anion binding of the Bacillus subtilis ribonuclease P protein. *Biochemistry 40*, 2777–89.

(75) Auton, M., Ferreon, A. C. M., and Bolen, D. W. (2006) Metrics that differentiate the origins of osmolyte effects on protein stability: a test of the surface tension proposal. *J. Mol. Biol. 361*, 983–92.

(76) Cho, S. S., Reddy, G., Straub, J. E., and Thirumalai, D. (2011) Entropic stabilization of proteins by TMAO. *J. Phys. Chem. B 115*, 13401–7.

(77) Zou, Q., Bennion, B. J., Daggett, V., and Murphy, K. P. (2002) The Molecular Mechanism of Stabilization of Proteins by TMAO and Its Ability to Counteract the Effects of Urea. *J. Am. Chem. Soc. 124*, 1192–1202.

(78) Bolen, D. W., and Baskakov, I. V. (2001) The osmophobic effect: natural selection of a thermodynamic force in protein folding. *J. Mol. Biol. 310*, 955–63.

(79) Ishida, T., and Kinoshita, K. (2007) PrDOS: prediction of disordered protein regions from amino acid sequence. *Nucleic Acids Res. 35*, W460–4.

(80) Vacic, V., Uversky, V. N., Dunker, A. K., and Lonardi, S. (2007) Composition Profiler: a tool for discovery and visualization of amino acid composition differences. *BMC Bioinformatics 8*, 211.

Chapter 3

The Drp1 B domain binds lipid membranes with specificity for cardiolipin and a membrane-binding-competent state is favored by TMAO

INTRODUCTION

Dynamin superfamily members demonstrate the ability to remodel membranes in vitro, in the absence of protein cofactors. Lipid membrane interaction resulting in membrane tubulation has been directly demonstrated in several members of dynamin superfamily, including classical dynamins[1,2], Mx proteins[3,4], Vps1[5], OPA1[6], the yeast homolog of Drp1, Dnm1[7,8] and Drp1[9].

Structurally, dynamin superfamily members are characterized by a coiled coil stalk that connects a G domain at one end of the stalk to a variable domain or motif located at the other end of the stalk. In dynamin, this variable region is a PH domain. Cryo EM of dynamin assembled on lipid tubules has revealed that the PH domains are located at the membrane surface and the G domains are oriented away from the surface[10]. Furthermore, the dynamin PH domain has been shown to specifically bind phosphoinositides[11], thus membrane interaction in classical dynamin is attributed to the PH domain.

Based on the similar domain organization across the dynamin superfamily, the variable domains of other dynamin superfamily members may also be involved in membrane binding. Indeed, the orientation of yeast Dnm1 on lipid tubules observed by cryo EM is similar to the orientation observed for dynamin[8]. Interestingly, the density of the Dnm1 B domain could not be resolved in the cryo EM reconstruction, consistent with a dynamic, intrinsically disordered interaction with the membrane surface. Even Mx proteins, which have a shorter (40-residue) loop at the end of the stalk domain, have been shown to bind lipids through this loop[12]. Thus, in the dynamin superfamily, there appears to be a common theme of membrane interaction occurring through the variable region at the tip of the stalk domain opposite the G domain, despite low sequence similarity in this region. Given the structural location of the Drp1 B

domain and the fact that Drp1 tubulates lipid membranes independent of cofactors[9], we suspect that the Drp1 B domain is responsible for binding lipid membranes.

Full-length Drp1 has been shown to bind membranes containing phosphatidylserine[13] and also cardiolipin[14]. In the case of phosphatidylserine binding, the interaction was not traced to a specific Drp1 domain. In the case of cardiolipin, the interaction was thought to occur through the G domain, as a point mutation in this domain diminished the interaction without hindering GTPase activity. Lipid membrane binding by an isolated B domain has not been reported.

We previously demonstrated that the B domain is intrinsically disordered and coacervates in the presence of the protecting osmolyte trimethylamine-N-oxide (TMAO). This capacity for coacervation may represent an important part of B domain function *in vivo*. A potential role for B domain coacervation may be to facilitate membrane interaction and controlled membrane-remodeling events. TMAO has been shown to favor native-like conformations in destabilized proteins, and thus we hypothesize that, in the case of the B domain, TMAO may favor a membrane-binding-competent state.

Here we use an isolated B domain construct from human Drp1 to test if the B domain has an intrinsic membrane binding ability. We show that the B domain is able to bind lipids autonomously and does so with specificity for cardiolipin. CD spectra show that cardiolipin binding by the B domain is accompanied by a slight change in secondary structure. We measure lipid binding in the presence of TMAO to determine if the binding competent state is the same as the TMAO-favored state. We find that a sub-critical amount of TMAO enhances B domain lipid binding without loss of specificity, suggesting that the TMAO-induced state is competent for membrane binding.

MATERIALS AND METHODS

Vesicle preparation - All synthetic lipids were obtained from Avanti Polar Lipids (Alabaster, AL). Lipids were measured from chloroform stocks using Hamilton syringes, mixed in the intended ratios, and dried in a thin film under a nitrogen stream. Excess chloroform was removed from dried films by lyophilization for at least 2 hours. The dried lipids were then resuspended in the appropriate amount of deionized water to make a 13.1 mM solution of lipids. Lipid solutions were subjected to 11 freeze-thaw cycles in a dry ice/ethanol bath and a 37°C water bath. Freeze-thawed solutions were extruded at least 31 times through a 100 nm nucleopore track etch membrane (Whatman), using an Avanti syringe extruder apparatus (Avanti Polar Lipids). Vesicle size, homogeneity and reproducibility were verified using dynamic light scattering and electron microscopy. All lipids had dioleoyl (DO) acyl chains with the exception of cardiolipin, which had tetraoleoyl (TO) acyl chains. Vesicles used for sedimentation included 0.25% 1,2-dioleoyl-sn-glycero-3-phosphoethanolamine-N-(lissamine rhodamine B sulfonyl) (Rh-DOPE) for easy visualization of lipid pellets.

Vesicle sedimentation - Vesicle sedimentation assays were performed with 5 μM protein and 2.5 mM lipid in a 100 μL volume of 50 mM Tris, 25 mM MES and 25 mM acetate, pH 7.4. Reactions were mixed by pipette and incubated for 30 minutes at 25°C, and then subjected to centrifugation for 3 hours at 55k rpm (rcf 186k x g) in a Beckmann Optima MAX ultracentrifuge equipped with a TLA-55 rotor (Beckman Coulter, Brea, CA). Immediately following centrifugation, the top 80 μL was removed by pipette and diluted into 4x SDS loading buffer ("supernatant"); the remaining 20 μL, which contained a mixture of soluble protein and trace lipids, was removed and discarded. The lipid pellet was resuspended in 100 μL of buffer, and diluted into 4x SDS loading buffer ("pellet"). Each supernatant and pellet was analyzed by SDS-PAGE and stained with coomassie G-250 Blue Silver stain overnight and destained in several

changes of water until background was negligible. Gels were scanned on a Canoscan flatbed scanner (Canon USA), band volume was calculated using Image Quant TL (Amersham). The fraction of protein partitioned (f_p) was calculated using equation 3.1:

$$f_p = \frac{V_{pellet}}{V_{pellet} + V_{supernatant}} \tag{3.1}$$

where V_{pellet} and $V_{supernatant}$ are the band volumes of the pellet and supernatant respectively. Fraction partitioned was measured for the B domain as a function of LUV composition (increasing fraction of acidic lipid in a DOPC background) and at a fixed LUV composition as a function of total lipid concentration.

Calculation of partition coefficients and free energy of partitioning - The lipid partition coefficient K_x[15] was calculated using equation 3.2 from partitioning data measured as a function of LUV composition (increasing fraction of acidic lipid in a DOPC background):

$$K_x = \frac{\frac{[P]_{partitioned}}{[L]}}{\frac{[P]_{free}}{[W]}} \tag{3.2}$$

The concentration of protein partitioned, $[P]_{partitioned} = f_p \times [P]_{total}$, and the concentration of free protein, $[P]_{free} = [P]_{total} - [P]_{partitioned}$. $[L]$ is the accessible acidic lipid concentration, taken to be half of the total acidic lipid concentration to account for the inaccessible lipids on the inner leaflet of the lipid bilayer. The concentration of water, $[W]$ was considered to be 55.3 M.

Using the partition coefficients obtained from equations 3.2, a free energy of lipid partitioning was obtained from equation 3.4:

$$\Delta G_p = -RT \ln(K_x) \tag{3.3}$$

R is the gas constant in kcal/mol T, and T is temperature in Kelvin. Since only half of the total acidic lipid concentration was used for calculations of K_x (described above), a correction factor of -0.41 kcal/mol was added to the calculated ΔG_p as suggested in by White et al.[15]

Circular dichroism - CD spectra were measured in a 0.1 cm quartz cuvette on a Jasco J-710 spectropolarimeter (Easton, MD) from 260 nm to 190 nm with a bandwidth of 1.0 nm, a scan step of 0.2 nm, and a scan rate of 50 nm/min. All spectra represent the average of 6 scans. All spectra were recorded in CD buffer (10 mM potassium phosphate, 100 mM potassium fluoride, 1 mM TCEP, pH 7.4) and corrected for the contribution of buffer. Data for which the HT voltage rose above 550 V were discarded.

RESULTS

B domain binds acidic lipid vesicles with a specificity for cardiolipin

To determine if the B domain has intrinsic membrane-binding ability, we measured protein-lipid membrane binding as a function of lipid composition using a sedimentation assay. As a positive control, we first measured the pH-dependent binding of the cytoplasmic domain of the mitochondrial fission protein Fis1 (Figure 3.1A). We found little evidence of binding to lipid vesicles at pH 7 regardless of lipid composition. By contrast, at pH 5, Fis1 bound only to lipid vesicles that contain the acidic phospholipid DOPG. These data are consistent with our earlier reports that demonstrated that Fis1 undergoes a dramatic membrane-induced conformational change upon binding, resulting in reversible membrane clustering[16]. As a negative control, we tested bovine serum albumin for its ability to bind lipid vesicles. Regardless of pH or lipid composition, BSA did not bind appreciably (Figure 3.1B).

We next tested the ability of the B domain to bind lipid vesicles at pH 7. Similar to Fis1, we found little evidence of the B domain binding to neutral 100% DOPC vesicles. By contrast,

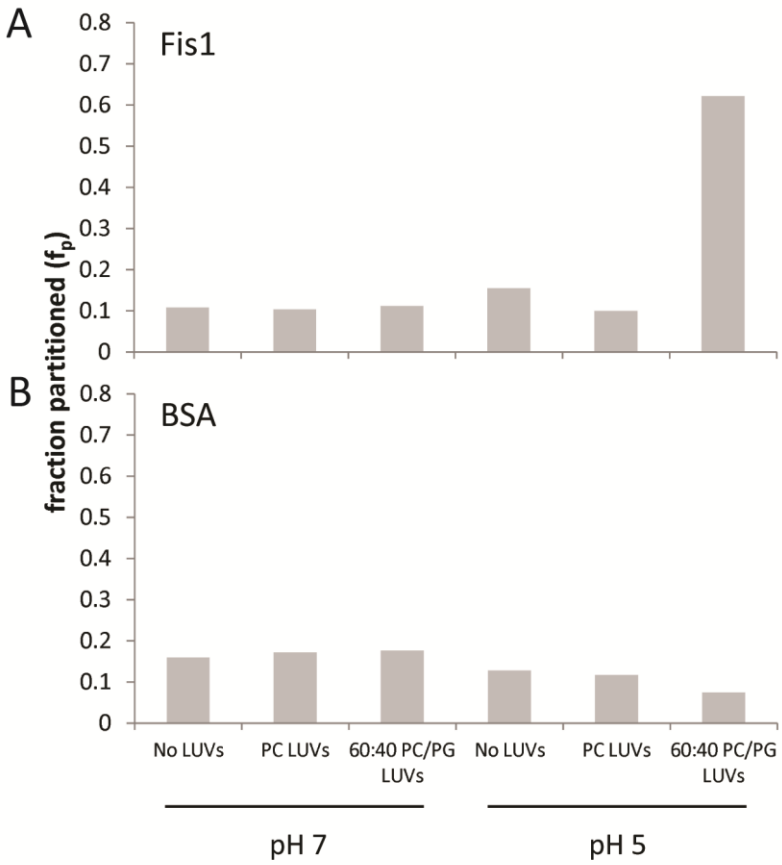

Figure 3.1 Sedimentation assay controls. Fis1 (A) and BSA (B) were sedimented with LUVs of the compositions specified at pH 7 or pH 5. As expected, Fis1 partitioned only with acidic lipid LUVs and at pH 5, and BSA did not partition under any conditions.

when we increased the acidic phospholipid content by adding DOPG, we observed increased binding of the B domain (Figure 3.2A). This binding was not specific to DOPG because we also observed binding in experiments with the acidic phospholipid DOPS (Figure 3.2B). However, we noticed a slight difference between the B domain's affinity for DOPG and DOPS even at identical concentrations of acidic phospholipid. These data suggest that B domain-lipid membrane binding is not solely the result of a non-specific electrostatic effect and may rise from a specific interaction between the phospholipid and the B domain. Given that *in vivo* Drp1 does not localize to the plasma membrane, which is rich in PS, but rather to the mitochondrial membrane, which contains the unique acidic lipid cardiolipin, we reasoned that membrane

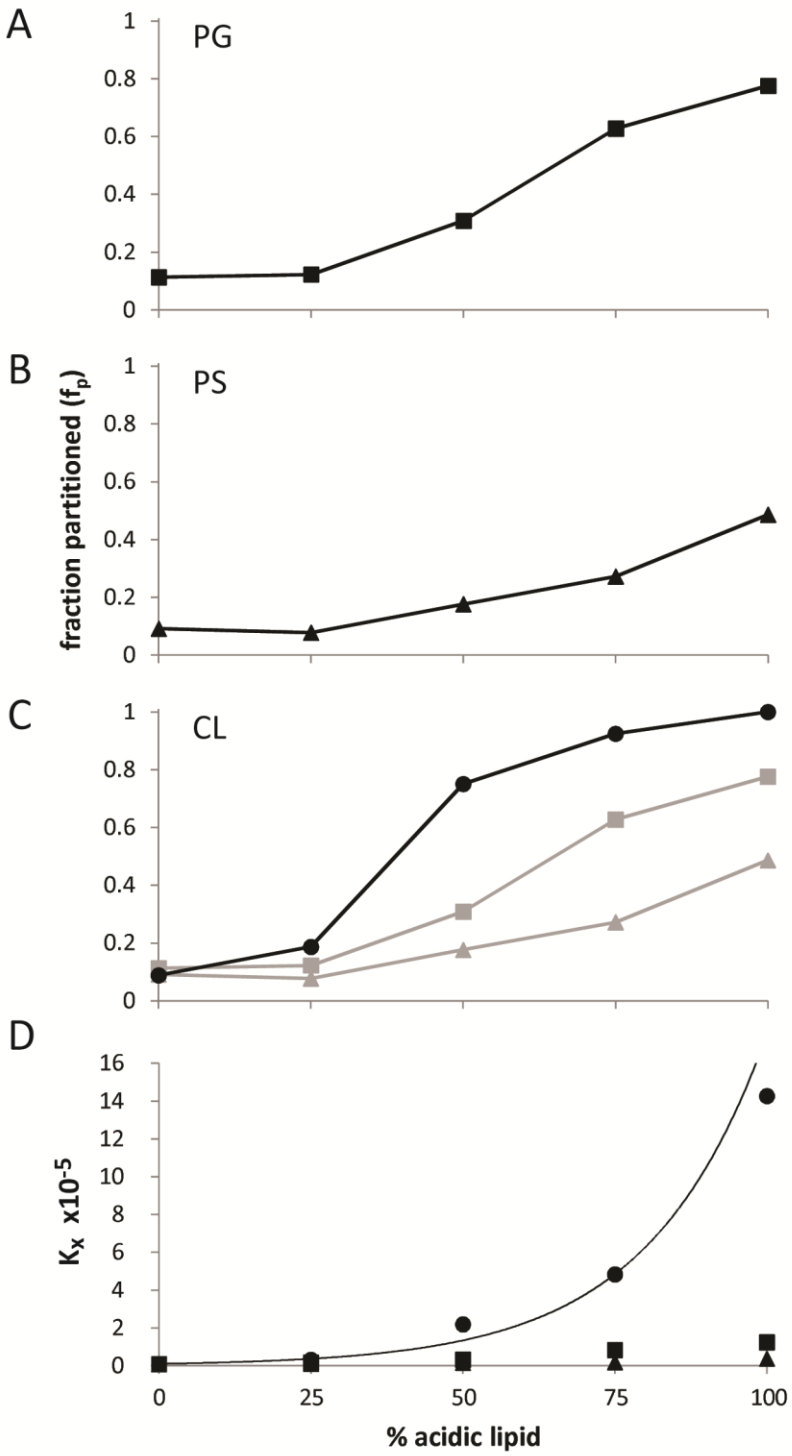

Figure 3.2 Partitioning of the B domain onto LUVs of various acidic lipid types and compositions. The fraction of B domain that partitioned with LUVs of each acidic lipid type and composition was determined by sedimentation (n = 2) and equation 3.1 as outlined in Methods. The acidic lipid types used were PG (A, squares), PS (B, triangles) and CL (C, circles). In all cases vesicle compositions were binary with PC. For (C), the PG and PS curves were reproduced in gray for comparison. Partition coefficients were calculated using equation 3.2 and plotted in (D) with the same symbols as A-C. The line is to guide the eye.

binding of the B domain may be enhanced in the presence of LUVs containing cardiolipin. Indeed we found enhanced binding in experiments with this mitochondria-specific acidic lipid (Figure 3.2C).

In order to quantify the strength of interaction between the B domain and lipid membranes of various compositions, we calculated a mole fraction partition coefficient (K_x) after the manner of White et al.[15]. As the fraction of DOPS was increased, the K_x remained relatively unchanged, with $K_x = 1.1 \times 10^4$ at 25% DOPS and $K_x = 3.7 \times 10^4$ at 100% DOPS. As the fraction of DOPG was increased, the K_x increased only slightly, from $K_x = 1.7 \times 10^4$ at 25% DOPG to $K_x = 1.2 \times 10^5$ at 100% DOPG. By contrast, as the fraction of cardiolipin was increased, the K_x increased significantly, from $K_x = 3.2 \times 10^4$ at 25% cardiolipin to $K_x = 1.4 \times 10^6$ at 100% cardiolipin (Figure 3.2D). This suggests that the B domain is significantly more sensitive to the concentration of cardiolipin in the membrane than the other acidic lipids, further confirming the specificity of the B domain for cardiolipin.

Only cardiolipin induces structural rearrangement in the B domain

To determine if lipid interaction is accompanied by structural change in the B domain, we measured the circular dichroism (CD) of B domain samples in the presence of LUVs composed of 100% DOPC, or 25% DOPC and 75% acidic lipid. As expected, 100% DOPC LUVs did not induce any changes in secondary structure in the B domain (Figure 3.3A). Interestingly, LUVs containing the acidic lipids DOPG and DOPS likewise had no appreciable effect on B domain secondary structure (Figs 3.3B and 3.3C, respectively). Cardiolipin LUVs, by contrast, resulted in a modest but clearly discernible change in the CD spectra near 200 nm (Figure 3.3D), suggesting that a change in secondary structure occurs upon interaction with cardiolipin-containing membranes. This result is consistent with the previously observed preference for cardiolipin

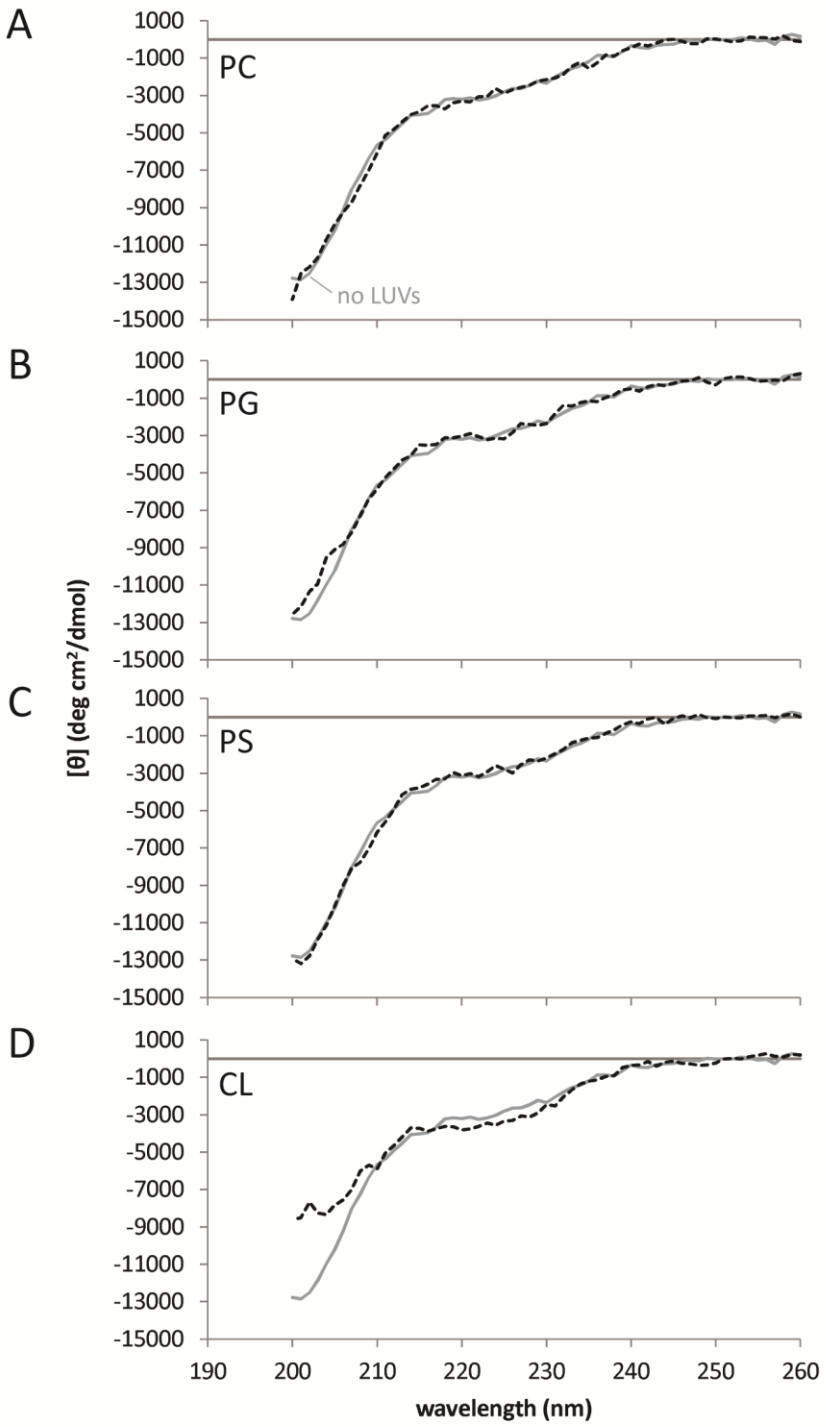

Figure 3.3 B domain secondary structure in the presence of LUVs. The CD spectrum of the B domain does not change in the presence of 100% DOPC LUVs (A, dashed line), 75% DOPG LUVs (B, dashed line), or 75% DOPS LUVs (C, dashed line), compared to its spectrum in the absence of LUVs (solid gray line, A-D). The B domain exhibits a change in secondary structure in the presence of 75% TOCL LUVs, as indicated by the change in molar ellipticity near 200 nm (D). See Table 3.1 for deconvolution data.

binding. Deconvolution of the CD spectra revealed that B domain interaction with lipid membranes containing cardiolipin results primarily in an increase in beta strand secondary structure (Table 3.1). This is similar to what was observed when the B domain was in the presence of TMAO (see chapter 2), suggesting that the secondary structure induced in the B domain by TMAO and by cardiolipin may be similar.

Table 3.1

	CONTIN-LL fit structural composition				
LUVs	**Helix**	**Strand**	**Turn**	**Unrd**	RMSD
100% PC	6.5	15.4	9.4	68.6	0.054
75% CL	7.9	20.3	11.9	60	0.063
Δ	1.4	4.9	2.5	-8.6	

B domain lipid membrane binding is enhanced in the presence of TMAO

Many intrinsically disordered proteins are known to adopt a folded structure upon binding. Protecting osmolytes such as trimethylamine-N-oxide (TMAO) have been shown to favor native-like folded states of intrinsically disordered proteins (IDPs) and the mutationally-denatured variants of natively folded proteins. Previous experiments demonstrated that the B domain undergoes a two-state-like transition in TMAO, with a transition midpoint around 2.8 M. We suspect that if the TMAO-induced state is competent for membrane binding, then membrane binding will be enhanced in the presence of TMAO. Furthermore, if the TMAO-induced state is competent for membrane binding, we need only lower the energy barrier to the membrane-binding-competent state slightly with a sub-critical concentration of TMAO in order to enhance binding. To test this idea, we measured B domain lipid membrane partitioning in the presence of 1.8 M TMAO, which is still on the unfolded baseline of the B domain TMAO titration. If our reasoning is correct, we should expect to see enhanced lipid membrane binding with the

specificity for cardiolipin intact. If TMAO favors a state other than a membrane-binding-competent state, then we should expect to see little to no enhancement, if not a decrease in binding, and possibly loss of the specificity for cardiolipin.

The presence of 1.8 M TMAO had no effect on the interaction of the B domain with 100% DOPC vesicles, nor did it result in increased sedimentation of B domain in the absence of vesicles, verifying that the presence of TMAO at this concentration does not cause sedimentable protein aggregation or non-specific interactions with neutral lipids. For vesicle compositions containing either DOPG or DOPS however, TMAO enhanced binding to a similar level as that observed for CL LUVs in the absence of TMAO (Figs 3.4A and 3.4B, respectively). The specificity for PG over PS that was observed in the absence of TMAO is preserved in the presence of TMAO, although slightly less pronounced. Cardiolipin specificity remains strongly intact in the presence of TMAO, with the partitioning of the B domain into CL LUVs dramatically enhanced in the presence of TMAO (Figure 3.4C). The fraction of B domain that partitioned onto 25% cardiolipin vesicles increased from 0.2 in the absence of TMAO, to 0.8 in the presence of 1.8 M TMAO. Accordingly, the partition coefficient at 25% cardiolipin increased from $K_x = 3.2 \times 10^4$ in the absence of TMAO to $K_x = 6.7 \times 10^5$ in the presence of 1.8 M TMAO. Using the linear extrapolation method, we determined a rough estimate of the free energy of membrane partitioning, $\Delta G_P = 5.9 \pm 0.1$ kcal/mol (Figure 3.4D). This represents the average extrapolated value of all the acidic lipid compositions and the corresponding standard deviation. We emphasize that this is a rough estimate, since each extrapolation was based on few data points and the linear transition regions of the partitioning curves were not well-defined. We conclude that the enhanced lipid binding and intact specificity for cardiolipin in the presence of TMAO verifies that a membrane-binding-competent state is inducible by TMAO. This suggests that the coacervated state of the B domain may be competent for membrane binding.

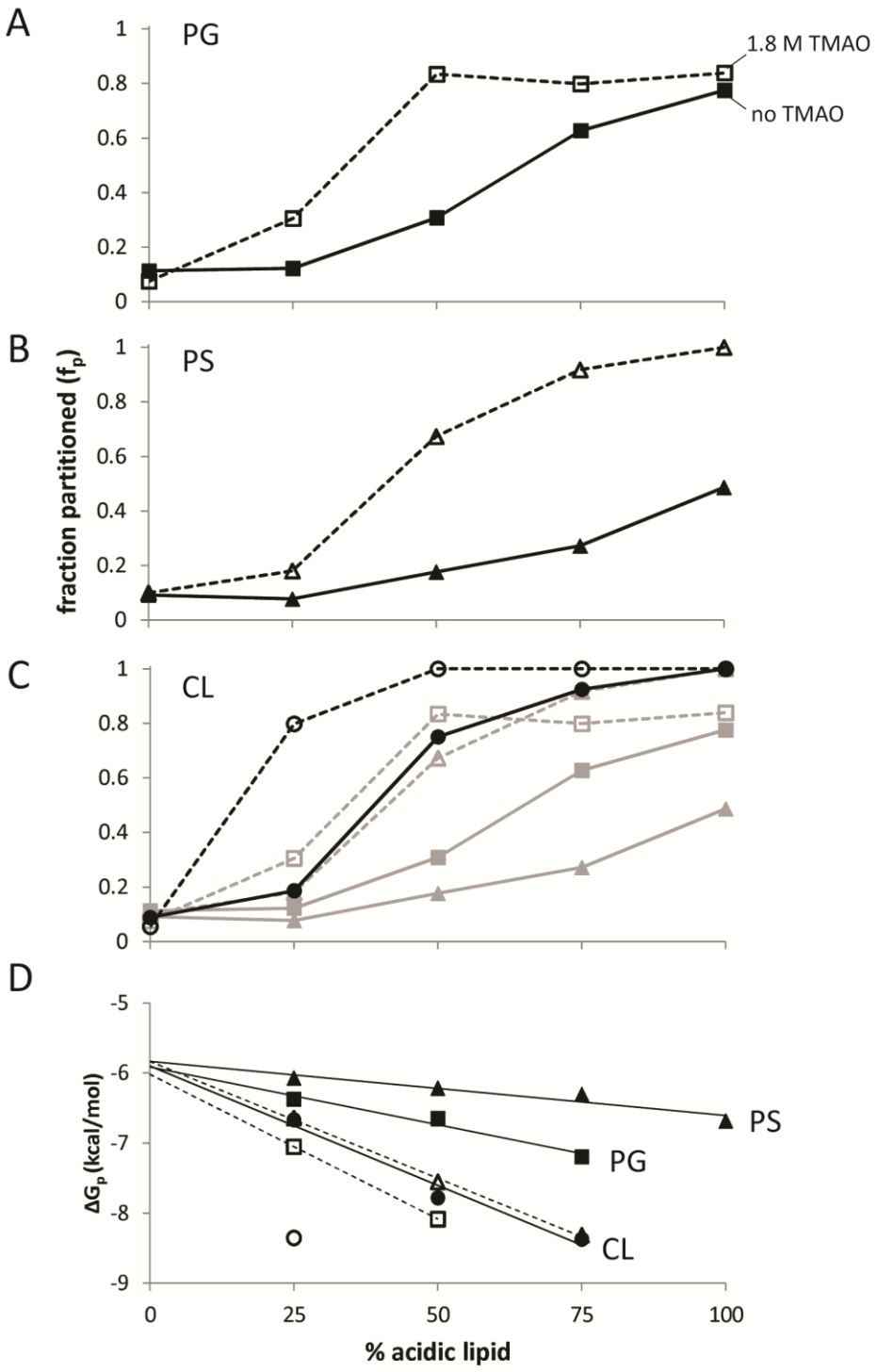

Figure 3.4 Partitioning of the B domain in the presence of 1.8 M TMAO. B domain partitioning with PG (A, squares), PS (B, triangles) and CL (C, circles) was determined as in Figure 3.2, but in the presence of TMAO (open shapes and dashed lines). Partitioning data in the absence of TMAO is reproduced here for comparison (solid shapes and lines). For (C), the PG and PS curves were reproduced in gray for comparison. Free energies of partitioning were calculated using equation 3.3 (D) and plotted with the same symbols as A-C. The linear extrapolation method was used to estimate ΔG_P in the absence of acidic lipid (see text).

DISCUSSION

Here we have presented data in support of the hypothesis that the Drp1 B domain has an intrinsic ability to bind lipid membranes. Our data show that the Drp1 B domain binds lipid membranes with specificity for cardiolipin, and that this interaction is accompanied by a modest change in secondary structure. Furthermore, we discovered that a membrane-binding-competent state is favored by TMAO, consistent with our hypothesis that the coacervated form of the B domain may facilitate membrane interaction. It is tempting to speculate that the presence of a cardiolipin-containing membrane may facilitate coacervation, but our data do not directly address this.

The B domain shows a sharp sensitivity to CL concentration, and solution conditions *in vivo* could shift the response to lower, biologically accessible CL concentrations. The membrane partitioning curve of the B domain as a function of %CL showed a sharp increase between 25% and 50% CL. This was in sharp contrast to the gradual increase in partitioning observed for both PG and PS membrane compositions. While the B domain has a clear specificity for CL over the other acidic lipid types, 25% to 50% CL is significantly higher than the %CL observed in mitochondrial membranes isolated from biological sources, which is on the order of 4-10% CL[17,18]. However, cardiolipin-enriched lipid rafts at Drp1 binding sites on mitochondria have been proposed[14,19,20], and the cardiolipin concentration in the outer mitochondrial membrane at contact sites between inner and outer mitochondrial membranes has been measured to be about 20-25%[21]. Thus, CL is probably not homogeneously distributed throughout the membrane, and local areas of high CL content appear to be likely. As we observed by the addition of TMAO in the partitioning measurements, solution conditions can shift the sensitive transition region of B domain membrane partitioning to lower concentrations of CL. In the presence of TMAO, the transition region was shifted to compositions below 25%

CL. Solution conditions or other factors *in vivo* may have a similar effect, bringing the CL sensitivity of the B domain into the relevant range of 4-25% CL.

The change in B domain secondary structure upon partitioning with CL membranes was modest and may represent a change in compactness or the formation of a "fuzzy" complex. Subtle changes in compactness, e.g. from a pre-molten globule state to a molten globule state, upon membrane interaction appear to be common in proteins that reversibly bind membranes[22]. Dynamic or "fuzzy" interactions have also been demonstrated in IDPs that do not undergo concomitant folding to a well-defined state upon binding[23–25]. The change in B domain secondary structure in the presence of CL LUVs was similar to the change in B domain secondary structure observed in the presence of TMAO (Chapter 2) in that the largest change in estimated secondary structure was an increase in beta sheet content. The overall change in the B domain spectra in the presence of CL LUVs appeared less dramatic than that observed in 3.1 M TMAO (see Figure 2.9A), though it appeared quite similar to the spectra observed in 1.5 M ammonium sulfate (see Figure 2.10C). Regardless, the enhanced CL binding and retention of CL specificity in the presence of TMAO suggests that the membrane-binding state and the TMAO-induced state are closely related. Coacervation in three dimensions (i.e. in the absence of a CL membrane) may be slightly different than coacervation restricted to two dimensions (i.e. on a CL membrane), and this may explain the slight differences in CD spectra.

Coacervation on membranes has been reported in other systems. A recent report discovered a previously unknown family of intrinsically disordered proteins in the fungus *Neurospora crassa* that aggregate on membranes to facilitate membrane wound healing[26]. Proteins from this family, known as septal pore-associated (SPA) proteins, were found to form both punctuate and ring-shaped aggregates at *N. crassa* septal pores *in vivo*, and formed coacervates and gels when purified. The membrane-water interface offers a unique

environment that seems to favor protein aggregation[27], and protein aggregation at membrane surfaces may be an important, though underappreciated aspect of membrane remodeling[28]. It has been independently demonstrated, both by theory[29] and experiment[30], that protein aggregation on the membrane surface can induce membrane curvature, and that protein insertion into the membrane is unnecessary for curvature induction. Thus, coacervation and peripheral "fuzzy" interactions with the membrane may be a viable means of membrane remodeling by the B domain, and perhaps by many more membrane-remodeling proteins than are currently appreciated.

REFERENCES

(1) Takei, K., Haucke, V., Slepnev, V., Farsad, K., Salazar, M., Chen, H., and De Camilli, P. (1998) Generation of coated intermediates of clathrin-mediated endocytosis on protein-free liposomes. *Cell 94*, 131–141.

(2) Sweitzer, S. M., and Hinshaw, J. E. (1998) Dynamin undergoes a GTP-dependent conformational change causing vesiculation. *Cell 93*, 1021–1029.

(3) Accola, M. A., Huang, B., Al Masri, A., and McNiven, M. A. (2002) The antiviral dynamin family member, MxA, tubulates lipids and localizes to the smooth endoplasmic reticulum. *J. Biol. Chem. 277*, 21829–35.

(4) Kochs, G., Reichelt, M., Danino, D., Hinshaw, J. E., and Haller, O. (2005) Assay and functional analysis of dynamin-like Mx proteins. *Methods Enzymol. 404*, 632–43.

(5) Smaczynska-de Rooij, I. I., Allwood, E. G., Mishra, R., Booth, W. I., Aghamohammadzadeh, S., Goldberg, M. W., and Ayscough, K. R. (2012) Yeast dynamin Vps1 and amphiphysin Rvs167 function together during endocytosis. *Traffic 13*, 317–28.

(6) Ban, T., Heymann, J. A. W., Song, Z., Hinshaw, J. E., and Chan, D. C. (2010) OPA1 disease alleles causing dominant optic atrophy have defects in cardiolipin-stimulated GTP hydrolysis and membrane tubulation. *Hum. Mol. Genet. 19*, 2113–22.

(7) Ingerman, E., Perkins, E. M., Marino, M., Mears, J. A., McCaffery, J. M., Hinshaw, J. E., and Nunnari, J. (2005) Dnm1 forms spirals that are structurally tailored to fit mitochondria. *J. Cell Biol. 170*, 1021–7.

(8) Mears, J. A., Lackner, L. L., Fang, S., Ingerman, E., Nunnari, J., and Hinshaw, J. E. (2011) Conformational changes in Dnm1 support a contractile mechanism for mitochondrial fission. *Nat. Struct. Mol. Biol. 18*, 20–6.

(9) Yoon, Y., Pitts, K. R., and McNiven, M. A. (2001) Mammalian dynamin-like protein DLP1 tubulates membranes. *Mol. Biol. Cell 12*, 2894–905.

(10) Zhang, P., and Hinshaw, J. E. (2001) Three-dimensional reconstruction of dynamin in the constricted state. *Nat. Cell Biol. 3*, 922–6.

(11) Salim, K., Bottomley, M. J., Querfurth, E., Zvelebil, M. J., Gout, I., Scaife, R., Margolis, R. L., Gigg, R., Smith, C. I., Driscoll, P. C., Waterfield, M. D., and Panayotou, G. (1996) Distinct specificity in the recognition of phosphoinositides by the pleckstrin homology domains of dynamin and Bruton's tyrosine kinase. *EMBO J. 15*, 6241–50.

(12) Von der Malsburg, A., Abutbul-Ionita, I., Haller, O., Kochs, G., and Danino, D. (2011) Stalk domain of the dynamin-like MxA GTPase protein mediates membrane binding and liposome tubulation via the unstructured L4 loop. *J. Biol. Chem. 286*, 37858–65.

(13) Fröhlich, C., Grabiger, S., Schwefel, D., Faelber, K., Rosenbaum, E., Mears, J. A., Rocks, O., and Daumke, O. (2013) Structural insights into oligomerization and mitochondrial remodelling of dynamin 1-like protein. *EMBO J. 32*, 1280–92.

(14) Montessuit, S., Somasekharan, S. P., Terrones, O., Lucken-Ardjomande, S., Herzig, S., Schwarzenbacher, R., Manstein, D. J., Bossy-Wetzel, E., Basañez, G., Meda, P., and Martinou, J.-C. (2010) Membrane remodeling induced by the dynamin-related protein Drp1 stimulates Bax oligomerization. *Cell 142*, 889–901.

(15) White, S. H., Wimley, W. C., Ladokhin, A. S., and Hristova, K. (1998) Protein folding in membranes: determining energetics of peptide-bilayer interactions. *Methods Enzymol. 295*, 62–87.

(16) Wells, R. C., and Hill, R. B. (2011) The cytosolic domain of Fis1 binds and reversibly clusters lipid vesicles. *PLoS One 6*, e21384.

(17) Getz, G. S., Bartley, W., Stirpe, F., Notton, B. M., and Renshaw, A. (1962) The lipid composition of rat-liver mitochondria, fluffy layer and microsomes. *Biochem. J. 83*, 181–91.

(18) Colbeau, A., Nachbaur, J., and Vignais, P. M. (1971) Enzymic characterization and lipid composition of rat liver subcellular membranes. *Biochim. Biophys. Acta 249*, 462–92.

(19) Sorice, M., Manganelli, V., Matarrese, P., Tinari, A., Misasi, R., Malorni, W., and Garofalo, T. (2009) Cardiolipin-enriched raft-like microdomains are essential activating platforms for apoptotic signals on mitochondria. *FEBS Lett. 583*, 2447–50.

(20) Landes, T., and Martinou, J.-C. (2011) Mitochondrial outer membrane permeabilization during apoptosis: the role of mitochondrial fission. *Biochim. Biophys. Acta 1813*, 540–5.

(21) Ardail, D., Privat, J. P., Egret-Charlier, M., Levrat, C., Lerme, F., and Louisot, P. (1990) Mitochondrial contact sites. Lipid composition and dynamics. *J. Biol. Chem. 265*, 18797–802.

(22) Halskau, Ø., Muga, A., and Martínez, A. (2009) Linking new paradigms in protein chemistry to reversible membrane-protein interactions. *Curr. Protein Pept. Sci. 10*, 339–59.

(23) Tompa, P., and Fuxreiter, M. (2008) Fuzzy complexes: polymorphism and structural disorder in protein-protein interactions. *Trends Biochem. Sci. 33*, 2–8.

(24) Fuxreiter, M., and Tompa, P. (2012) Fuzzy complexes: a more stochastic view of protein function. *Adv. Exp. Med. Biol. 725*, 1–14.

(25) Mittag, T., Kay, L. E., and Forman-Kay, J. D. (2010) Protein dynamics and conformational disorder in molecular recognition. *J. Mol. Recognit. 23*, 105–16.

(26) Lai, J., Koh, C. H., Tjota, M., Pieuchot, L., Raman, V., Chandrababu, K. B., Yang, D., Wong, L., and Jedd, G. (2012) Intrinsically disordered proteins aggregate at fungal cell-to-cell channels and regulate intercellular connectivity. *Proc. Natl. Acad. Sci. U. S. A. 109*, 15781–6.

(27) Gorbenko, G., and Trusova, V. (2011) Protein aggregation in a membrane environment. *Adv. Protein Chem. Struct. Biol.* 1st ed., pp 113–42. Elsevier Inc.

(28) Simunovic, M., Srivastava, A., and Voth, G. A. (2013) Linear aggregation of proteins on the membrane as a prelude to membrane remodeling. *Proc. Natl. Acad. Sci. U. S. A. 110*, 20396–401.

(29) Ramakrishnan, N., Kumar, P. B. S., and Ipsen, J. H. (2013) Membrane-Mediated Aggregation of Curvature-Inducing Nematogens and Membrane Tubulation. *Biophysj 104*, 1018–1028.

(30) Stachowiak, J. C., Schmid, E. M., Ryan, C. J., Ann, H. S., Sasaki, D. Y., Sherman, M. B., Geissler, P. L., Fletcher, D. A., and Hayden, C. C. (2012) Membrane bending by protein-protein crowding. *Nat. Cell Biol. 14*, 944–9.

Chapter 4

The effects of alternative splicing and post-translational modification on structure, folding and lipid binding of the B domain

INTRODUCTION

Alternative splicing and post-translational modification (PTM) are common in intrinsically disordered (ID) proteins and domains[1–5]. Because ID proteins and domains are often involved in signaling via interactions with multiple binding partners, alternative splicing in ID proteins and domains has been proposed to be a means of rewiring signaling networks[6,7]. PTMs may be a means of altering homotypic and heterotypic interactions of ID proteins and domains by altering properties of charge, hydrophobicity, or sterics[8].

Drp1 has an alternatively spliced region in the B domain that gives rise to five isoforms that vary only in the length of the B domain[9,10], and these isoforms appear to be differentially expressed in human tissues[10,11]. This may suggest that Drp1 activity can be modulated through the B domain to meet the differing needs of these tissue types, but this remains to be demonstrated. Little is known about how enzymatic properties vary from isoform to isoform, although it has been shown that some isoforms differ in their interaction with microtubules when phosphorylated[10].

The B domain contains several sites of PTM, including eight confirmed SUMOylation sites[12] and two confirmed phosphorylation sites, S616 and S637[13]. These phosphorylation sites have been shown to be involved in translocation of Drp1 to mitochondria from the cytosol[14,15] and may also play a role in coordinating mitochondrial fission with the cell cycle[16] and apoptotic signaling[17]. Dynamic cycling of Drp1 on and off the mitochondria may be directed by phosphorylation and dephosphorylation events[18].

These studies indicate that alternative splicing and phosphorylation have important effects on Drp1 activity. However, the mechanisms by which these modifications achieve their effects are unclear. We hypothesize that alternative splicing and/or phosphorylation may modulate the B domain conformational ensemble, thermodynamic properties and/or

interactions with potential binding partners (i.e. lipid membranes) in order to achieve their effects.

Here we monitor three properties of B domain isoforms to determine if these properties are affected by alternative splicing and phosphorylation: (1) secondary structure, monitored by CD, (2) folding/coacervation in TMAO, monitored by fluorescence and light-scattering, and (3) lipid binding, monitored by sedimentation assay. We compare wild-type Drp1 B domain (isoform 1) with isoform 3, and also with phosphomimetics S637D and S616D using these techniques.

MATERIALS AND METHODS

B domain cloning, expression and purification - The same primers used for the cloning of B domain isoform 1 as described in chapter 2 were used to clone the B domain from a full-length Drp1 isoform 3 construct. The S637D and S616D mutations were introduced into the B domain isoform 1 background using the Quikchange method (Agilent Stratagene). All constructs were verified by DNA sequencing (Retrogen, San Diego, CA). Otherwise, protein expression and purification was carried out as described in chapter 2.

Vesicle preparation and vesicle sedimentation assay - Vesicle preparation and sedimentation were performed as described in chapter 3.

Calculation of partition coefficients and free energy of partitioning - Protein/vesicle sedimentation data measured at a fixed LUV composition as a function of total lipid concentration were fit to equation 4.1 by nonlinear least-squares analysis to obtain an additional measure of the partition coefficient K_x[19]:

$$f_p = \frac{K_x[L]}{[W] + K_x[L]} \quad (4.1)$$

The fraction of protein partitioned, f_p, was determined as described in chapter 3. $[L]$ is the accessible acidic lipid concentration, taken to be half of the total acidic lipid concentration to account for the inaccessible lipids on the inner leaflet of the lipid bilayer. The concentration of water, $[W]$ was considered to be 55.3 M.

Using the partition coefficients obtained from equations 4.1, a free energy of lipid partitioning was obtained from equation 4.2:

$$\Delta G_p = -RT \ln(K_x) \tag{4.2}$$

R is the gas constant in kcal/mol T, and T is temperature in Kelvin. Since only half of the total acidic lipid concentration was used for calculations of K_x (described above), a correction factor of -0.41 kcal/mol was added to the calculated ΔG_p as suggested by White et al.[19]

The lipid partition coefficient K_x was calculated at each lipid concentration using equation 4.3 from partitioning data measured as a function of lipid concentration[19]:

$$K_x = \frac{\frac{[P]_{partitioned}}{[L]}}{\frac{[P]_{free}}{[W]}} \tag{4.3}$$

The concentration of protein partitioned, $[P]_{partitioned} = f_p \times [P]_{total}$, and the concentration of free protein, $[P]_{free} = [P]_{total} - [P]_{partitioned}$. $[L]$ and $[W]$ are the same as defined in equation 4.1.

Circular Dichroism - CD measurements were performed as described in chapter 3.

RESULTS

The B domain isoforms 1 and 3 vary in structural characteristics, but phosphorylation does not have an obvious structural effect

We selected isoforms 1 and 3 (hereafter referred to as B1 and B3) for comparison because they represent the longest (137 amino acids) and the shortest (100 amino acids)

isoforms, respectively. Since the m-value of folding or unfolding in osmolyte is strongly dependent on backbone volume and therefore polypeptide chain length[20–22], we expected isoforms 1 and 3 to be the most different of all possible pairs of isoforms, at least in folding-related properties. Secondary structure propensity and lipid-binding affinity cannot be reliably predicted *a priori*, so these were not used as selection criteria in choosing isoforms to compare.

We evaluated secondary structure content of B3 by circular dichroism (CD) and compared it to the CD spectrum of B1 (Figure 4.1A). Surprisingly, we observed a minimum near

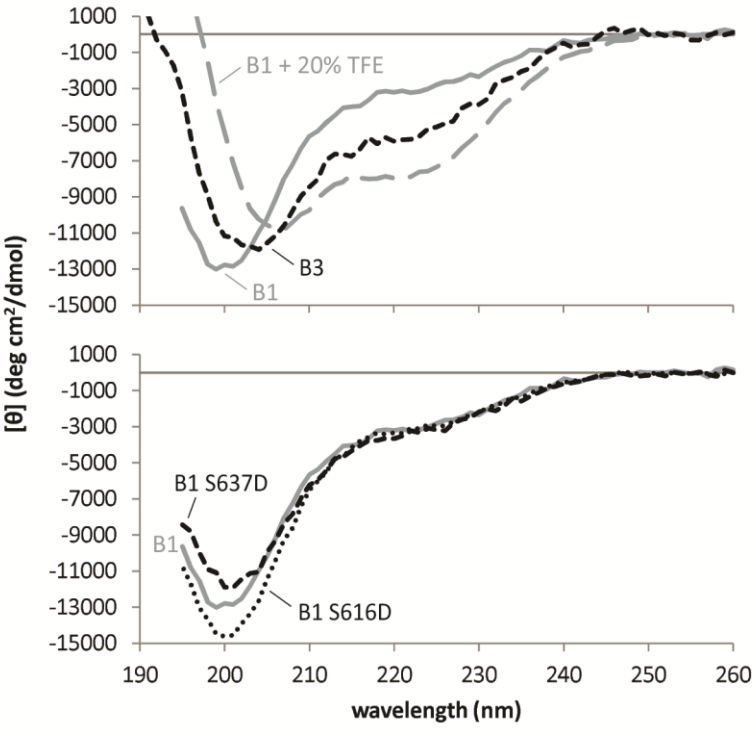

Figure 4.1 CD spectra of B3 and B1 phosphomimetics. (A) The minima at 204 nm and the enhanced shoulder near 222 nm in the spectrum of B3 indicates increased helicity compared to that of B1, but not as much helicity as B1 in 20% TFE. (B) The change in secondary structure due to the phosphomimetic mutations S637D and S616D appears to be minimal (see Table 4.1).

204 and a significant shoulder at 222 nm in the B3 CD spectrum, indicative of elevated helical content. For a helical comparison, we artificially induced helicity in B1 by the addition of 20% trifluoroethanol (TFE). Compared to the artificially induced helical B1 spectrum, the minimum in the B3 spectrum is slightly shifted toward lower wavelengths perhaps due to residual intrinsic

disorder. Indeed, the CONTIN-LL fit of the CD data estimates a helical content of 16% and unstructured content of 52% for B3, compared to a helical content of 24% and unstructured content of 42% for B1 in 20% TFE (Table 4.1). These spectra suggest that alternative splicing influences B domain structure.

Since phosphorylation at positions S616 and S637 in the B domain of Drp1 result in differences in translocation to mitochondria in vivo[14,15], we suspected that this could be a result of changes in structure in the B domain. To determine if phosphorylation influences secondary structure in the B domain, we evaluated the secondary structure content of the B1 phosphomimetics S616D and S637D (Figure 4.1B). The CD spectra of both phosphomimetics were similar to B1, but differed slightly in the magnitude of the minimum at 200 nm, with the minimum for S616D being slightly more pronounced, and the minimum for S637D being slightly less pronounced than that of B1. Secondary structure estimates based on CONTIN-LL fits of these spectra suggest minimal differences in secondary structure between B1 and the phosphomimetics (Table 4.1). Assuming that the phosphomimetic mutations accurately mimic phosphorylated protein, we conclude that phosphorylation in the B domain does not significantly influence B domain structure.

Table 4.1

	CONTIN-LL fit structural composition				
Construct	**Helix**	**Strand**	**Turn**	**Unrd**	RMSD
B1	8.4	18.5	12.5	60.6	0.037
B1 + 20% TFE	23.9	16.2	18	41.8	0.038
B3	16	18.3	13.9	51.7	0.067
B1 S637D	7.2	18.4	12	62.3	0.053
B1 S616D	6.7	16.4	10.2	66.7	0.046

The B domains isoforms 1 and 3 and the phosphomimetic S637D show modest variation in folding/coacervation behavior

Given the difference in secondary structure between B1 and B3, we suspected that B3 might respond differently to the protecting osmolyte TMAO. The folding/coacervation experiments previously performed on B1 (see chapter 2) were repeated with B3, wherein steady state tryptophan fluorescence and static right-angle light-scattering were observed as a function of increasing TMAO concentration. Comparison of the normalized center a spectral mass for B1 and B3 indicates that B3 is only slightly less destabilized compared to B1, with a concentration midpoint (Cm) of 2.7 ± 0.2 M for B3 and 2.8 ± 0.1 M for B1 (Figure 4.2A). We measured light-

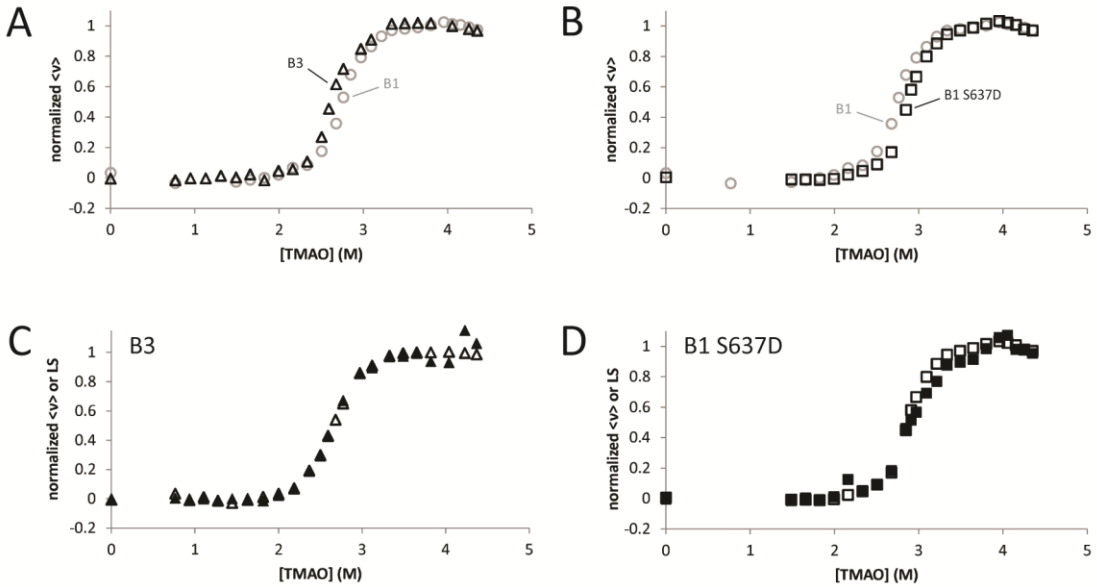

Figure 4.2 Steady-state tryptophan fluorescence and light scattering (LS) of B3 and B1 S637D as a function of TMAO. (A) B3 (open black triangles) undergoes a two-state transition as measured by fluorescence in TMAO. The transition closely resembles that of B1 (open gray circles) but the Cm at 2.7 ± 0.2 M for B3 is slightly shifted from that of B1 at 2.8 ± 0.1 M. (B) B1 S637D (open black triangles) also undergoes a two-state transition as measured by fluorescence in TMAO. Again, the transition closely resembles that of B1 (open gray circles) except that the Cm at 2.9 ± 0.2 M for B1 S637D is slightly shifted from that of B1 at 2.8 ± 0.1 M. (C) The same B3 samples as (A) followed by light scattering (filled triangles) show the same concentration dependence, and align with the B3 fluorescence data (open triangles). (D) The same B1 S637D samples as (B) followed by light scattering (filled squares) show the same concentration dependence, and align with the B1 S637D fluorescence data (open squares).

scattering as a function of TMAO in the same samples used for fluorescence to determine if B3 also exhibited assembly or phase-separation, as we observed for B1. The light-scattering of B3 in TMAO closely mimicked the fluorescence signal for B3 (Figure 4.2B), similar to what was observed previously for B1. These data suggest that B3 undergoes a process similar to that observed for B1, namely combined folding and phase separation.

We suspected that S637D would also behave similar to B1, given its similarity to B1 in secondary structure content. The steady-state fluorescence of S637D in TMAO was similar to that of B1, but surprisingly the phosphomimetic was slightly destabilized compared to B1, with the Cm for S637D at 2.9 ± 0.2 M compared to 2.8 ± 0.1 M for B1 (Figure 4.2C). As observed for B1 and B3, the light-scattering of S637D closely followed the fluorescence signal (Figure 4.2D). Thus, the S637D phosphomimetic appears to undergo a similar folding/phase separation behavior in TMAO as observed for B1.

Together these data suggest that the folding/phase separation behavior observed for the B domain in TMAO is an intrinsic property of the domain that is not strongly influenced by alternative splicing or phosphorylation.

The B domain isoforms 1 and 3 do not vary in lipid binding

To determine if alternative splicing in the B domain influences its affinity or specificity for lipids, we measured partitioning of B3 onto LUVs composed of binary compositions of dioleoylphosphatidylcholine (DOPC or PC) and one of three acidic lipids, dioleoylphosphatidylglycerol (DOPG or PG), dioleoylphosphatidylserine (DOPS or PS) or tetraoleoylcardiolipin (TOCL or CL), and compared it to the partitioning of B1 (see chapter 3). As observed for B1, B3 exhibited a hierarchy of affinities for the acidic lipids, with partitioning occurring most readily onto CL LUVs and least readily onto PS LUVs, with partitioning onto PG

LUVs lying in between (Figure 4.3A). Comparison of the B3 partitioning data for each acidic lipid type with that of B1 shows that the partitioning of B1 and B3 is very similar in all cases (Figures 4.3 B-D).

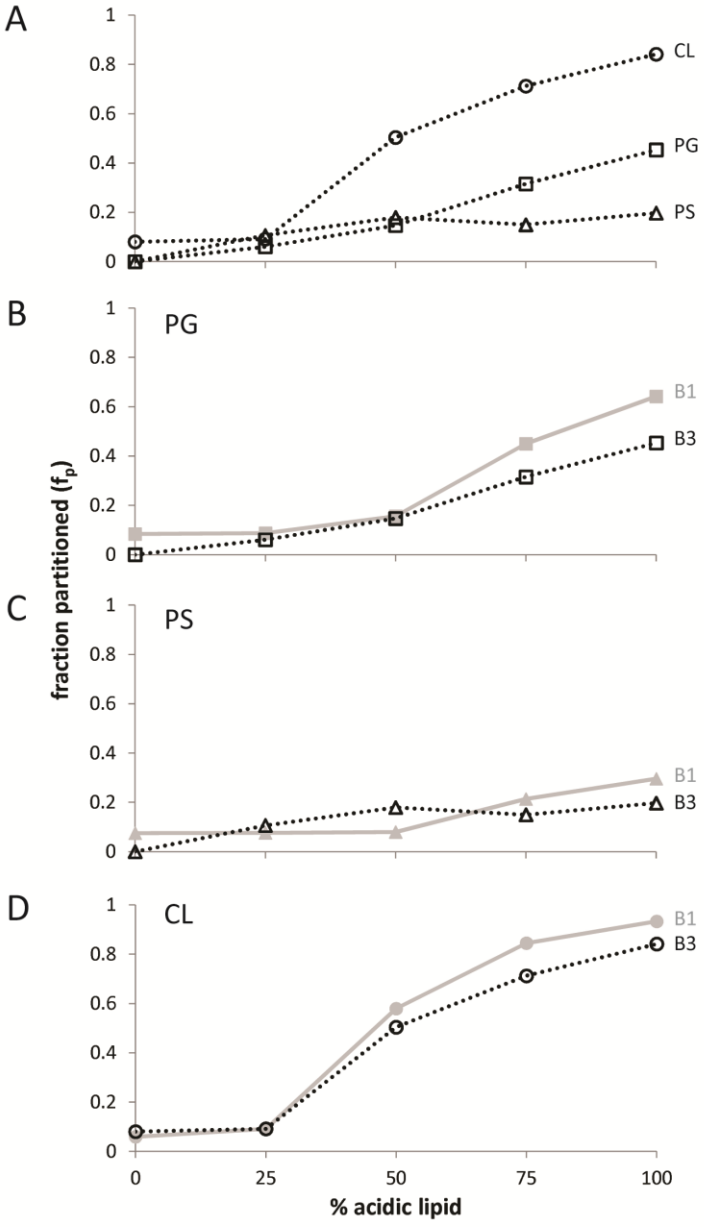

Figure 4.3 Partitioning of B3 onto LUVs of various acidic lipid types and compositions. The fraction of B3 that partitioned with LUVs of each acidic lipid type and composition was determined by sedimentation as described in Chapter 3. The acidic lipid types used were PG (squares), PS (triangles) and CL (circles). In all cases vesicle compositions were binary with PC. (A) B3 exhibited a clear specificity for CL LUVs over PG and PS LUVs. (B-D) Partitioning of B1 (gray) and B3 (black) is similar for each of the acidic lipid types: PG (B), PS (C), and CL (D).

In order to obtain a more accurate measure of the partition coefficient, we measured partitioning of B1 or B3 as a function of lipid:protein ratio with LUVs of a fixed composition (75% CL, 25% PC) (Figures 4.4A and 4.4B, respectively). The partitioning data were fit to equation 4.1 (see methods) as described by White[19]. The B1 and B3 partitioning curves were nearly identical, with the fits giving a K_x of $1.8 \times 10^6 \pm 0.2 \times 10^6$ and $2.1 \times 10^6 \pm 0.2 \times 10^6$, respectively. From these partition coefficients we calculated free energies of partitioning (ΔG_p) of -8.9 ± 1.0 kcal/mol and -9.0 ± 1.0 kcal/mol, respectively, using equation 4.2.

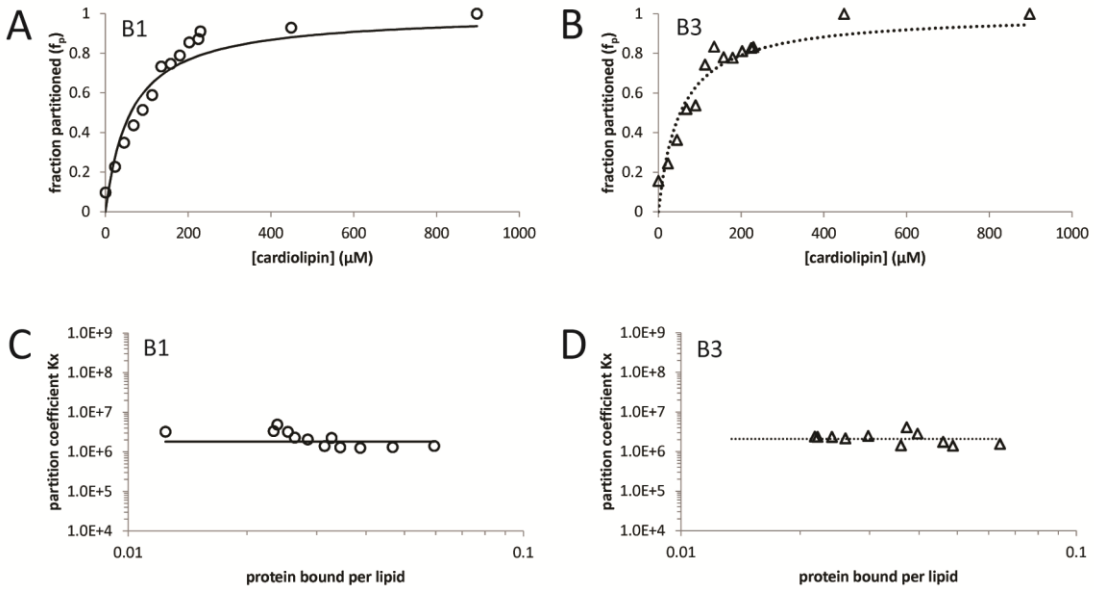

Figure 4.4 Lipid membrane partitioning of B1 and B3 as a function of total CL concentration. LUV composition was fixed at 75% CL, 25% PC. (A-B) The fraction of B1 partitioned (A, circles) or B3 partitioned (B, triangles) as a function of total CL concentration was fit to equation 4.1 (solid and dotted line for B1 and B3, respectively) to determine the partition coefficient (K_x) and the free energy of partitioning (ΔG_p) (see text). (C-D) A partition coefficient was calculated at each lipid concentration using equation 4.3, and plotted as a function of proteins bound per lipid for B1 (C) and B3 (D). The unchanging partition coefficient over a wide range of lipid concentrations indicates simple partitioning, rather than cooperative or anti-cooperative partitioning.

By also calculating K_x at each lipid concentration using equation 4.3, and plotting this as a function of proteins bound per lipid, we can determine whether the lipid interaction is the result of simple partitioning (resulting in a flat line), cooperative partitioning (K_x increases with proteins bound per lipid), or anti-cooperative partitioning (the K_x drops at high ratios of protein

bound per lipid)[19]. Our data show that the K_x remains relatively unchanged over the wide range lipid concentrations tested, suggesting that both B1 and B3 interact with CL LUVs through simple partitioning (Figures 4.4C and 4.4D, respectively). Lipid binding data were not collected for B domain phosphomimetics.

We previously showed that B1 undergoes a modest change in secondary structure upon binding CL LUVs, and that this change was primary an increase in beta structure, as estimated by CONTIN-LL deconvolution of the CD spectrum. Since B3 is more helical and less unstructured than B1, we were interested to see if CL LUVs would induce an increase in beta structure, perhaps at the expense of helicity. We measured the CD spectrum of B3 in the presence of 75% CL LUVs to determine if lipid binding results in a change in secondary structure in this isoform. In the presence of CL LUVs, the B3 CD spectrum showed, to our surprise, an enhanced shoulder at 222 nm and a shift of the minimum from 204 (in the absence of LUVs) toward longer wavelengths, indicative of increased helicity (Figure 4.5A). Light scattering from the LUVs prevented measurement of the spectrum to wavelengths below 205 nm, so a precise minimum could not be determined. The CONTIN-LL fit of the data suggests that some of the strand and unstructured content is replaced by helix and turn in the presence of CL LUVs, with the decrease in strand and unstructured content by about 5 points and 2 points, respectively, and the increase in helix and turn at about 6 points and 1 point, respectively (Table 4.2). The CD spectrum of B3 in the presence of LUVs closely resembles that of B1 in 20% TFE, but deviates at shorter wavelengths (Figure 4.5B).

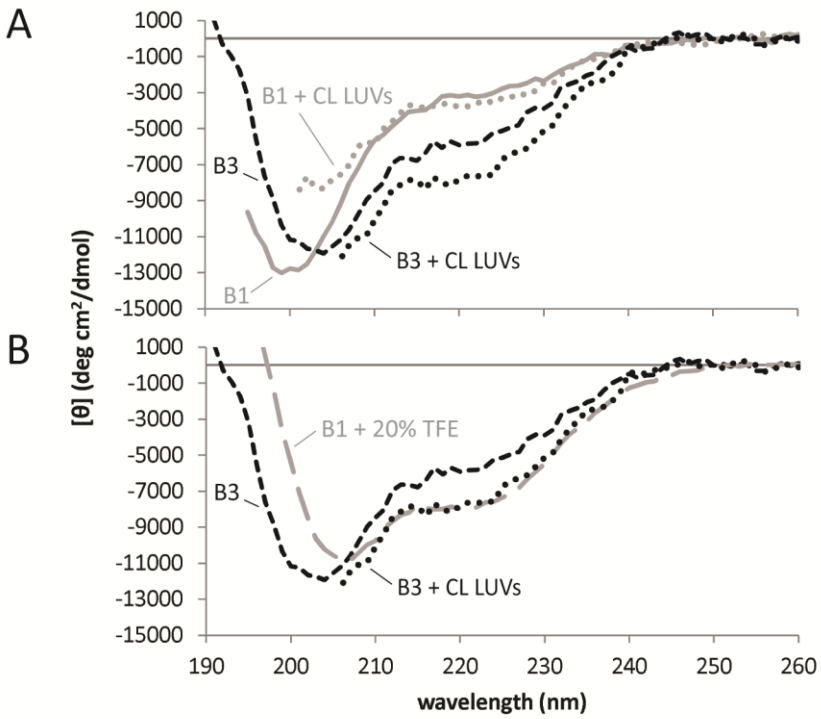

Figure 4.5 CD spectrum of B3 in the presence of 75% CL LUVs. (A) The CD spectrum of B3 in the presence of 75% CL LUVs (black dotted line) has a stronger shoulder near 222 nm and potentially a minimum that is shifted to higher wavelengths compared to B3 in the absence of LUVs (black dashed line). The spectrum is significantly different than that of B1 (gray solid line) and B1 in the presence of 75% CL LUVs (gray dotted line). (B) The CD spectrum of B3 in the presence of 75% CL LUVs (black dotted line) has a similar shoulder near 222 nm as B1 in 20% TFE (gray long-dashed line), but appears to deviate at shorter wavelengths.

Table 4.2

B3	CONTIN-LL fit structural composition				
LUVs	**Helix**	**Strand**	**Turn**	**Unrd**	RMSD
none	16	18.3	13.9	51.7	0.067
75% CL	22.4	13.2	14.9	49.6	0.071
Δ	6.4	-5.1	1	-2.1	

DISCUSSION

Here we have attempted to determine whether alternative splicing and/or phosphorylation result in altered structural and thermodynamic properties in the B domain and

thereby modulate B domain function. We found that although isoforms 1 and 3 have significant differences in secondary structure content, they vary only slightly in folding/coacervation, and they bind lipids with similar affinity and specificity. The phosphomimetics S637D and S616D were similar in structure to the unmodified B domain, suggesting that phosphorylation alone is not sufficient to induce significant structural changes. S637D showed only slight destabilization in its folding/phase separation energy compared to isoform 1.

These results suggest that the regions responsible for the folding/coacervation and lipid binding properties of the B domain are not located in the alternatively spliced region, and therefore are not modulated by alternative splicing. One interpretation of these findings is that the folding/coacervation and lipid binding properties may be intrinsic to all isoforms. However, we note that B1 and B3 are identical in net charge (+2) and fraction of charged residues (FCR) (0.270) (at neutral pH and assuming no shifted pKas of ionizable residues). It has shown that FCR and charge distribution within an amino acid sequence are important determinants of IDP behavior, including radius of gyration (or ensemble dimensions), and phase separation[23,24]. Based on these metrics, perhaps it should be expected that isoforms 1 and 3 have similarities in folding/coacervation and lipid binding properties. Other isoforms differ in FCR, with B5 having the lowest (0.252) and B2 having the highest (0.288). Future studies will explore whether these differences are large enough to modulate function.

Despite their similarity in folding/coacervation and lipid binding properties, we observed that isoforms 1 and 3 differ in secondary structure content, suggesting that the alternatively spliced region has some structural influence. A recent study showed that Drp1 isoforms varied in their ability to co-localize with microtubules, and this interaction is thought to be mediated by the B domain[10]. It may be that the differences in secondary structure reported here have a role in the Drp1-microtubule interaction. The same study also showed that the Drp1-microtubule

interaction was influenced by B domain phosphorylation. Thus, a combination of alternative splicing and phosphorylation appears to be important, and while phosphorylation does not appear to influence secondary structure in our B1 construct, it may have a different effect on other isoforms. Future work will explore this possibility.

Drp1 is involved in variety of pathways and processes, from "housekeeping" mitochondrial fission for the maintenance of mitochondrial homeostasis, to mitochondrial fission relating to apoptosis[25,26], and from peroxisomal fission[27] to bundling of microtubules[10]. It is therefore challenging to determine which of its roles is influenced by a particular change such as alternative splicing or post-translational modification. The possibility that different isoforms respond differently to a given post translational modification further complicates the picture, but opens a wide variety of possibilities for precise modulation of function in many different roles. A careful and methodical testing of the many possible combinations of alternative splicing and post-translational modification will be required to fully understand how Drp1 function is modulated.

REFERENCES

(1) Colak, R., Kim, T., Michaut, M., Sun, M., Irimia, M., Bellay, J., Myers, C. L., Blencowe, B. J., and Kim, P. M. (2013) Distinct types of disorder in the human proteome: functional implications for alternative splicing. *PLoS Comput. Biol. 9*, e1003030.

(2) Iakoucheva, L. M., Radivojac, P., Brown, C. J., O'Connor, T. R., Sikes, J. G., Obradovic, Z., and Dunker, A. K. (2004) The importance of intrinsic disorder for protein phosphorylation. *Nucleic Acids Res. 32*, 1037–49.

(3) Hagai, T., Azia, A., Tóth-Petróczy, Á., and Levy, Y. (2011) Intrinsic disorder in ubiquitination substrates. *J. Mol. Biol. 412*, 319–24.

(4) Xie, H., Vucetic, S., Iakoucheva, L. M., Oldfield, C. J., Dunker, A. K., Obradovic, Z., and Uversky, V. N. (2007) Functional anthology of intrinsic disorder. 3. Ligands, post-translational modifications, and diseases associated with intrinsically disordered proteins. *J. Proteome Res. 6*, 1917–32.

(5) Collins, M. O., Yu, L., Campuzano, I., Grant, S. G. N., and Choudhary, J. S. (2008) Phosphoproteomic analysis of the mouse brain cytosol reveals a predominance of protein phosphorylation in regions of intrinsic sequence disorder. *Mol. Cell. Proteomics 7*, 1331–1348.

(6) Buljan, M., Chalancon, G., Eustermann, S., Wagner, G. P., Fuxreiter, M., Bateman, A., and Babu, M. M. (2012) Tissue-specific splicing of disordered segments that embed binding motifs rewires protein interaction networks. *Mol. Cell 46*, 871–83.

(7) Buljan, M., Chalancon, G., Dunker, A. K., Bateman, A., Balaji, S., Fuxreiter, M., and Babu, M. M. (2013) Alternative splicing of intrinsically disordered regions and rewiring of protein interactions. *Curr. Opin. Struct. Biol. 23*, 443–50.

(8) Nishi, H., Fong, J. H., Chang, C., Teichmann, S. A., and Panchenko, A. R. (2013) Regulation of protein-protein binding by coupling between phosphorylation and intrinsic disorder: analysis of human protein complexes. *Mol. Biosyst. 9*, 1620–6.

(9) Howng, S.-L., Sy, W.-D., Cheng, T.-S., Lieu, A.-S., Wang, C., Tzou, W.-S., Cho, C.-L., and Hong, Y.-R. (2004) Genomic organization, alternative splicing, and promoter analysis of human dynamin-like protein gene. *Biochem. Biophys. Res. Commun. 314*, 766–772.

(10) Strack, S., Wilson, T. J., and Cribbs, J. T. (2013) Cyclin-dependent kinases regulate splice-specific targeting of dynamin-related protein 1 to microtubules. *J. Cell Biol. 201*, 1037–51.

(11) Chen, C. H., Howng, S. L., Hwang, S. L., Chou, C. K., Liao, C. H., and Hong, Y. R. (2000) Differential expression of four human dynamin-like protein variants in brain tumors. *DNA Cell Biol. 19*, 189–94.

(12) Figueroa-Romero, C., Iñiguez-Lluhí, J. A., Stadler, J., Chang, C.-R., Arnoult, D., Keller, P. J., Hong, Y., Blackstone, C., and Feldman, E. L. (2009) SUMOylation of the mitochondrial fission

protein Drp1 occurs at multiple nonconsensus sites within the B domain and is linked to its activity cycle. *FASEB J. 23*, 3917–27.

(13) Cribbs, J. T., and Strack, S. (2009) Functional characterization of phosphorylation sites in dynamin-related protein 1. *Methods Enzymol.* 1st ed., pp 231–53. Elsevier Inc.

(14) Chang, C.-R., and Blackstone, C. (2007) Cyclic AMP-dependent protein kinase phosphorylation of Drp1 regulates its GTPase activity and mitochondrial morphology. *J. Biol. Chem. 282*, 21583–7.

(15) Cereghetti, G. M., Stangherlin, A., Martins de Brito, O., Chang, C. R., Blackstone, C., Bernardi, P., and Scorrano, L. (2008) Dephosphorylation by calcineurin regulates translocation of Drp1 to mitochondria. *Proc. Natl. Acad. Sci. U. S. A. 105*, 15803–8.

(16) Taguchi, N., Ishihara, N., Jofuku, A., Oka, T., and Mihara, K. (2007) Mitotic phosphorylation of dynamin-related GTPase Drp1 participates in mitochondrial fission. *J. Biol. Chem. 282*, 11521–9.

(17) Cribbs, J. T., and Strack, S. (2007) Reversible phosphorylation of Drp1 by cyclic AMP-dependent protein kinase and calcineurin regulates mitochondrial fission and cell death. *EMBO Rep. 8*, 939–44.

(18) Merrill, R. A., Dagda, R. K., Dickey, A. S., Cribbs, J. T., Green, S. H., Usachev, Y. M., and Strack, S. (2011) Mechanism of neuroprotective mitochondrial remodeling by PKA/AKAP1. *PLoS Biol. 9*, e1000612.

(19) White, S. H., Wimley, W. C., Ladokhin, A. S., and Hristova, K. (1998) Protein folding in membranes: determining energetics of peptide-bilayer interactions. *Methods Enzymol. 295*, 62–87.

(20) Li, J., Motlagh, H. N., Chakuroff, C., Thompson, E. B., and Hilser, V. J. (2012) Thermodynamic dissection of the intrinsically disordered N-terminal domain of human glucocorticoid receptor. *J. Biol. Chem. 287*, 26777–87.

(21) Auton, M., and Bolen, D. W. (2005) Predicting the energetics of osmolyte-induced protein folding/unfolding. *Proc. Natl. Acad. Sci. U. S. A. 102*, 15065–8.

(22) Auton, M., Rösgen, J., Sinev, M., Holthauzen, L. M. F., and Bolen, D. W. (2011) Osmolyte effects on protein stability and solubility: a balancing act between backbone and side-chains. *Biophys. Chem. 159*, 90–9.

(23) Das, R. K., and Pappu, R. V. (2013) Conformations of intrinsically disordered proteins are influenced by linear sequence distributions of oppositely charged residues. *Proc. Natl. Acad. Sci. U. S. A. 110*, 13392–7.

(24) Mao, A. H., Crick, S. L., Vitalis, A., Chicoine, C. L., and Pappu, R. V. (2010) Net charge per residue modulates conformational ensembles of intrinsically disordered proteins. *Proc. Natl. Acad. Sci. U. S. A. 107*, 8183–8188.

(25) Cheung, E. C. C., McBride, H. M., and Slack, R. S. (2007) Mitochondrial dynamics in the regulation of neuronal cell death. *Apoptosis 12*, 979–92.

(26) Wasiak, S., Zunino, R., and McBride, H. M. (2007) Bax/Bak promote sumoylation of DRP1 and its stable association with mitochondria during apoptotic cell death. *J. Cell Biol. 177*, 439–50.

(27) Thoms, S., and Erdmann, R. (2005) Dynamin-related proteins and Pex11 proteins in peroxisome division and proliferation. *FEBS J. 272*, 5169–81.

Chapter 5

Conclusion: Intrinsic disorder, amphitropism and coacervation in the dynamin superfamily

In this dissertation we have examined the properties and function of the B domain in the mitochondrial fission mechanoenzyme Drp1. Specifically, we have provided evidence for an auto-inhibitory role of the B domain by showing that removal of the B domain from Drp1 resulted in enhanced assembly and GTP hydrolysis. We have demonstrated that the B domain is intrinsically disordered (ID) and undergoes phase separation or coacervation under conditions that induce other ID proteins to fold. We have discovered that the B domain binds lipid membranes with a preference for cardiolipin, and that this interaction is enhanced under conditions that favor the coacervated state.

Despite recent advances in understanding the structure and function of the stalk, BSE and G domains of Drp1[1,2], the structural and functional details of the B domain have largely remained a mystery. Recently, Strack and Cribbs proposed that the B domain may have an auto-inhibitory role in Drp1 function, based on experiments which showed that removal of the B domain resulted in punctuate mitochondria, indicative of increased mitochondrial fission[3]. However, the effect of the B domain on Drp1 GTP hydrolysis has not been measured directly, nor has the effect of the B domain on Drp1 assembly been measured quantitatively, so it has remained unclear if the B domain has a direct influence on Drp1 enzymatic activity. We have presented here the first measurements of these properties. Our results indicate that the B domain does indeed influence Drp1 GTPase activity as well as assembly, and that the GTPase activity in a Drp1 ΔB construct correlates with the extent of Drp1 ΔB assembly as modulated by salt concentration. Given that GTPase activity is known to be coupled to assembly in Drp1[2], this suggests that the B domain likely influences Drp1 GTP hydrolysis by directly modulating Drp1 assembly.

This dissertation presents the first direct experimental measures of B domain structural properties, and identifies an important difference between Drp1 and classical dynamins. The

variable domain in classical dynamins is a pleckstrin homology (PH) domain and has been studied in structural detail[4–7]. Given the overall similarities in sequence and function between classical dynamins and Drp1, one might reasonably suspect that the B domain could be a PH domain. Several factors make it difficult to predict from sequence whether the B domain might adopt a PH fold. First, PH domains are known to be conserved in structure but not sequence, with the exception of a single moderately conserved tryptophan[8,9]. Thus, the lack of sequence identity between the Drp1 B domain and the dynamin-1 PH domain does not exclude the possibility that the B domain could be a PH domain. Interestingly, the Drp1 B domain is similar in length to the dynamin-1 PH domain and possesses a single tryptophan in the appropriate location. Second, despite having a stable fold composed of both beta strands and an alpha helix, the dynamin-1 PH domain is nearly 60% solvent-exposed coil and turn. As a result, sequence-based intrinsic disorder prediction for the dynamin-1 PH domain accurately, but potentially misleadingly, gives a predicted probability of intrinsic disorder that is slightly above the threshold value of 0.5. If the B domain is a PH domain with a ratio of regular secondary structure and exposed loops similar to the dynamin-1 PH domain, intrinsic disorder prediction for the B domain could also be misleading. Finally, the Drp1 B domain has a similar mean net charge and mean hydrophobicity as the dynamin-1 PH domain, suggesting that the Drp1 B domain and the dynamin-1 PH domain have similarities in amino acid composition. In this dissertation, we have provided several lines of experimental evidence that eliminate the possibility that the B domain adopts a PH-like fold. Rather, the data suggest that the B domain is intrinsically disordered, and likely does not adopt significant secondary structure, even upon association with a binding partner.

The B domain of Dnm1, the yeast homolog of Drp1, was proposed by Mears et al. to be intrinsically disordered based on their observation that cryo-EM models of assembled Dnm1

lacked density at the expected location of the B domain[10]. However, the potential role of intrinsic disorder in Dnm1 or Drp1 function has not been previously speculated or explored. We unexpectedly found that the flavor of intrinsic disorder found in the B domain appears to lend itself to liquid-liquid phase separation, i.e. coacervation. We suspect that the ability to coacervate may be an important property of the B domain, and propose a model that suggests a role for both intrinsic disorder and coacervation in Drp1 function (see below).

The mode of membrane contact in Drp1 has been a topic of debate in the mitochondrial fission field. A prominent model suggests that Drp1-membrane contact is mediated only by adaptor proteins that are anchored to the membrane by a transmembrane helix[3]. While adapter proteins undoubtedly play an essential role in recruiting Drp1 to appropriate sites of scission, this model fails to account for the observation that Drp1 capably tubulates lipid membranes *in vitro*, in the absence of any other protein partners[11]. Thus, the force exerted by Drp1 that results in membrane remodeling is apparently applied through direct contact between Drp1 and the membrane. The region of Drp1 that is responsible for membrane contact has not been definitively identified. Interestingly, Montessuit et al. identified a point mutation in the G domain of Drp1 which diminished cardiolipin binding, suggesting the G domain may interact with membranes[12]. Alternatively, Mears et al. have suggested that the B domain is a likely candidate for membrane contact, based on the proposed orientation of yeast Dnm1 and human dynamin-1 assembled on membrane tubules in cryo-EM models[10]. In this dissertation we have demonstrated that the B domain possesses intrinsic lipid membrane binding ability, and has a preference for cardiolipin, a lipid that is unique to the mitochondrial membranes which Drp1 remodels. These data are consistent with the B domain being a site of contact between Drp1 and the mitochondrial membrane.

Finally, the structural consequences of alternative spicing and phosphorylation in the B domain have not been previously explored. Our preliminary results suggest that alternative splicing influences B domain secondary structure, while phosphorylation does not. Interestingly, alternative splicing does not appear to significantly impact coacervation or lipid membrane binding, suggesting that alternative splicing likely modulates some other property of the B domain, such as the availability of SUMOylation sites[13], or interaction with other binding partners (e.g. microtubules[14]). This remains an exciting area of future exploration.

To reconcile the findings presented in this dissertation, we propose a model (Figure 5.1) in which the random, thermally-driven motions of the intrinsically disordered B domain occlude the stalk domain assembly interfaces and thereby inhibit high-order assembly of Drp1 in

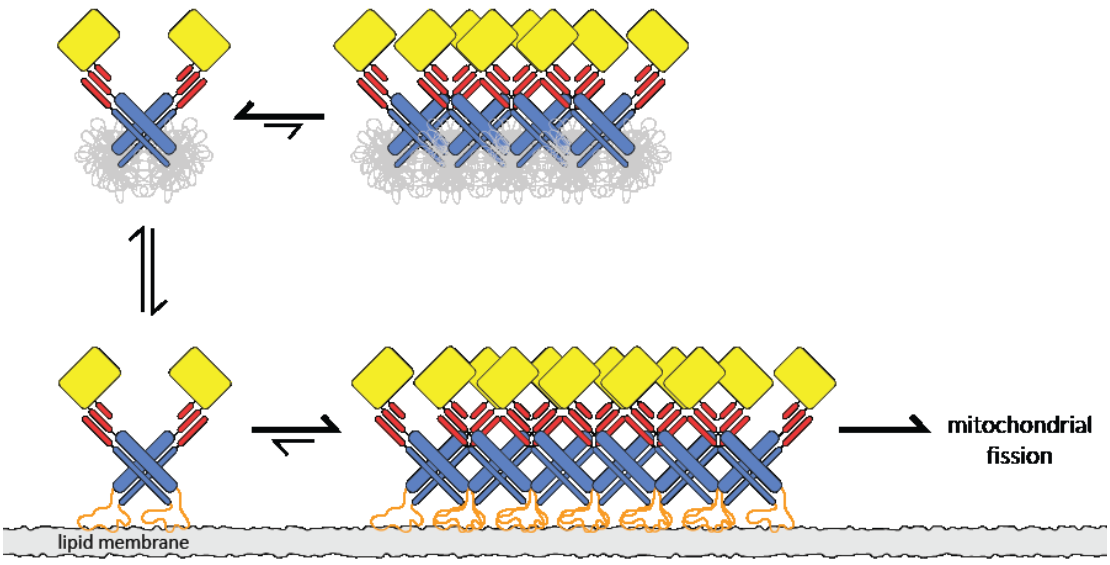

Figure 5.1 A model for the role of the B domain in Drp1 function. Thermally-driven motions of the intrinsically disordered B domain (gray lines) occlude the stalk domain assembly interfaces and thereby inhibit high-order assembly of Drp1 in the cell cytosol (upper panel). Upon recruitment of Drp1 to the mitochondrial membrane, the affinity of the B domain for cardiolipin favors B domain conformations which maximize interaction with the membrane (orange lines), essentially sequestering the B domain away from the stalk interfaces, and allowing higher-order assembly to proceed (lower panel). In this way, high-order assembly can proceed unhindered only at the mitochondrial membrane, and unproductive high-order assembly in the cytosol is prevented.

the cell cytosol. Upon recruitment of Drp1 to the mitochondrial membrane, the affinity of the B domain for cardiolipin favors B domain conformations which maximize interaction with the membrane (albeit a dynamic or "fuzzy" interaction), essentially sequestering the B domain away from the stalk interfaces, and allowing higher-order assembly to proceed. Furthermore, a high local Drp1 concentration resulting from the restriction of Drp1 to two dimensions at the membrane surface, and the confinement of the B domain to a relatively small volume between the stalk domains and the membrane surface will favor homotypic B domain interactions (i.e., the coacervated state), further freeing the stalk domain assembly interfaces from occlusion by the B domain. In this way, high-order assembly can proceed unhindered only at the mitochondrial membrane, and unproductive high-order assembly in the cytosol is prevented. This model is consistent with the present data and unifies the findings that (1) removal of the B domain results in enhanced assembly and GTP hydrolysis, (2) the B domain is intrinsically disordered, (3) the B domain coacervates, and (4) the B domain has an intrinsic membrane-binding ability that may be related to the coacervated state.

This model draws on the concept of the entropic bristle domain (EBD) proposed by Jan Hoh[15] and later revisited by Santner, et al.[16] According to the theory of Hoh and the experimental validation of Santner et al., an EBD is an intrinsically disordered region that improves the solubility of another other protein domain to which it is attached by providing a large hydrophilic surface area, and prevents aggregation or hyper-assembly of the other protein domain by excluding potential binding partners through its thermally-driven random motions. Not only does the B domain possess the necessary physical traits of an EBD, i.e. it is a relatively long, hydrophilic and intrinsically disordered sequence, but also its location at the tip of the stalk domain places it in an optimal position to block Drp1 assembly (which occurs primarily through the stalk domain) through random thermal motions.

Our model suggests the following testable predictions: (1) Drp1 isoforms may vary in their equilibrium oligomerization state and basal GTP hydrolysis rate in the absence of a lipid membrane. Because alternative splicing in the B domain alters the length and secondary structural properties of the B domain, the conformational ensemble of some B domain isoforms may be more effective than others at occluding assembly interfaces in the stalk, resulting in different propensities for oligomerization. Since assembly and GTP hydrolysis are coupled in Drp1, differences in oligomerization state should also be measurable as a difference in basal GTP hydrolysis. (2) Mutations in the B domain that alter flexibility, net charge, and distribution of ionizable residues will alter Drp1 activity. Flexibility, net charge, and distribution of ionizable residues are key determinants of intrinsic disorder and coacervation[17–25], which are the basis of auto-inhibition and membrane interaction in our model. Therefore, modulation of these properties in the B domain will influence Drp1 assembly, basal Drp1 GTP hydrolysis, membrane association, and membrane-stimulated GTP hydrolysis. (3) Cardiolipin-containing membranes will stimulate GTP hydrolysis in Drp1 more effectively than other acidic lipids. Cardiolipin will be more effective at sequestering the B domain away from stalk domain interfaces and thus will be more effective at allowing assembly at the membrane. This will be manifested in the degree of membrane stimulated GTP hydrolysis. (4) Highly concentrated assembly-deficient Drp1 variants may still associate via coacervation of the B domains, whereas assembly-deficient Drp1 ΔB variants will neither assemble nor coacervate under identical conditions. Future work will test each of these predictions.

This model of auto-inhibition of Drp1 assembly by the B domain may also apply to other dynamin superfamily members. If this is true, we might expect to see intrinsic disorder as a common feature at the tip of the stalk domains of various dynamin superfamily members. Indeed, we performed an intrinsic disorder prediction analysis of the dynamin superfamily and

found that nearly all of the dynamin superfamily members contain at least one extended region (> 25 residues) of intrinsic disorder, and interestingly, the ID region in all of the amphitropic dynamins is located at the tip of the stalk domain, in the location corresponding to the B domain in Drp1 (Figure 5.2). In the tethered dynamins, the ID regions do not appear to be located in regions that would facilitate occlusion of the stalk domain assembly interfaces, and thus our model probably does not apply in these proteins. Among the amphitropic dynamins, dynamin-1 appears to be slightly unique in that the ID regions attach the tip of the stalk to an independently folded PH domain. In this case, our model may still apply, but may be more accurately described as an entropic "ball-and-chain[s]" mechanism, where the PH domain is the "ball" and the flanking flexible linkers are the "chains". In fact, electron density for the PH domain was found in multiple locations in the dynamin crystal structure, including locations near the assembly region of the stalk domain[1,26]. This is consistent with the idea that the PH domain, with its flanking flexible linkers, may sweep out a large area around the stalk in order to prevent assembly. MxA and Vps1 both have a disordered loop for a variable domain at the tip of the stalk domain, similar to the B domain of Drp1, but of differing lengths (The ID regions of MxA, Vps1 and Drp1 are roughly 40, 95 and 135 residues in length, respectively). Thus our model may be equally as relevant to these proteins as it is to Drp1.

Based on this analysis, our model appears to apply specifically to the amphitropic dynamins, which include dynamin-1, MxA, Vps1 and Drp1 (Figure 5.3). We suspect, therefore, that the variable domains (VDs) of these proteins may also have a role in reversible membrane interaction. Specifically, we propose that interaction of the VD with the membrane may be a mechanism by which auto-inhibition of stalk assembly is relieved, by restricting the VD to conformations that are in contact with the membrane and therefore are not occluding the stalk domain assembly interfaces. This provides a means of preventing unproductive assembly in the

cytosol by only favoring it at the membrane surface. Given that the interaction of the B domain with lipid membranes was enhanced under conditions that favor a coacervated state,

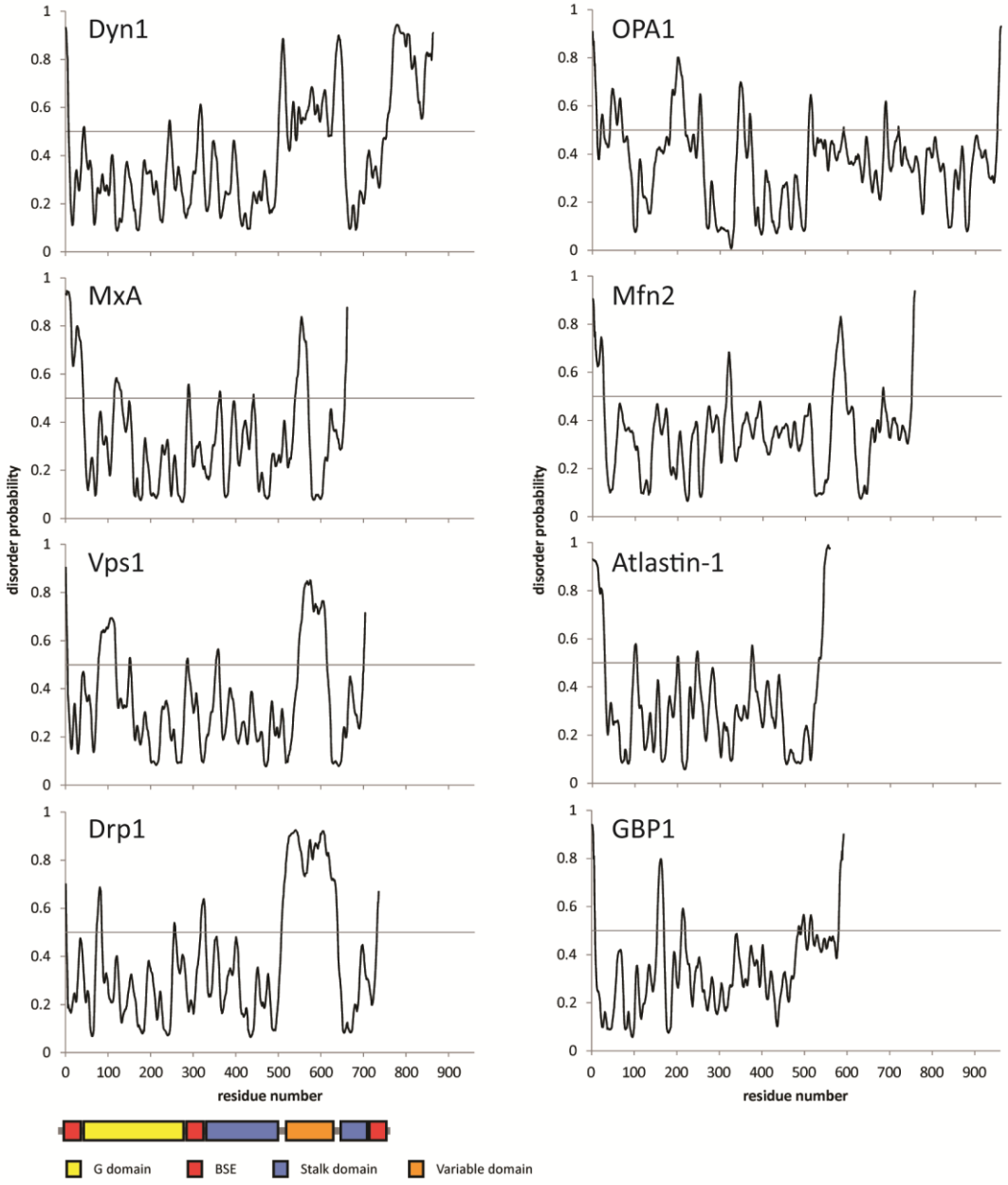

Figure 5.2 Prediction of intrinsic disorder in the dynamin superfamily. Amino acid sequences of the dynamin superfamily were analyzed using PrDOS[41]. A continuous segment of sequence with a disorder probability > 0.5 is considered to be a probable region of intrinsic disorder. Amphitropic dynamins are in the left column, tethered dynamins are in the right column. The approximate location of domains is indicated for the amphitropic dynamins below the left column of predictions. Predicted intrinsically disordered regions appear to coincide with the variable domains of these proteins. Dyn1 = dynamin-1.

coacervation may have a role in membrane interaction and therefore the relief of stalk assembly auto-inhibition. It is unknown if the VDs of MxA and Vps1 also exhibit a propensity for coacervation, but this is an intriguing possibility.

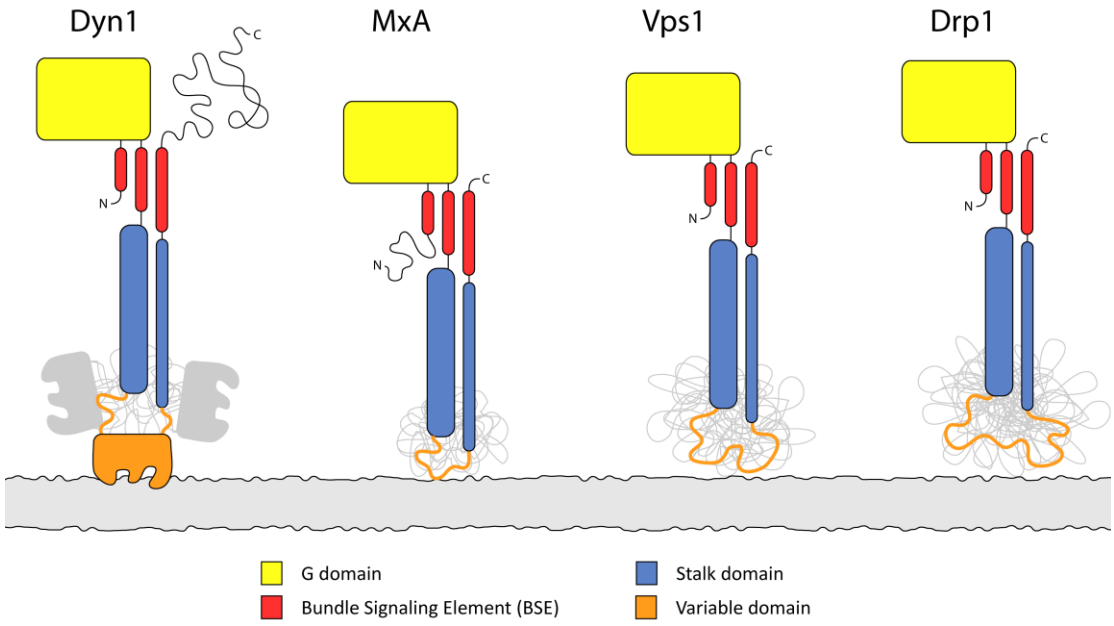

Figure 5.3 A model for the role of the variable domain (VD) in the amphitropic dynamins. The variable domains (orange lines) are depicted as intrinsically disordered regions that may prevent aggregation or hyper-assembly of the stalk domain via thermally-driven random motions (gray lines). Interaction of the VD with the membrane may be a mechanism by which auto-inhibition of stalk assembly is relieved, by restricting the VD to conformations which are in contact with the membrane and therefore are not occluding the assembly interfaces of the stalk domain. The proteins are shown as monomers for clarity, but in actuality are likely constitutive dimers.

Biologically, coacervation has long been appreciated as an important step in the formation of elastomeric materials[27], from ligaments and arterial walls[28,29], to spider silks[30] and the underwater adhesives of caddisfly larvae and mollusks[31,32]. Typically, these coacervates are exported from the cell where they coalesce further to form the final macroscopic tissue or substance[29]. Fewer instances are known of coacervation as a process that remains intracellular and microscopic, although several examples have emerged in recent years[33–36]. One of the functions of phase separation of this type appears to be spatial organization within the cell[37]. For example, ribonucleoprotein (RNP) granules are liquid droplets rich in protein and RNA and

represent a liquid-liquid phase separation that may be used as a means of subcellular compartmentalization[38–40]. Another example is found within the nuclear pore complex[34], where nucleoporin proteins form gels – an extensively networked liquid-liquid phase separation. A final example of intracellular coacervation is found in fungi, where the SPA proteins of Woronin bodies coacervate and line interseptal pores, facilitating resealing of damaged lipid membranes[35]. The membrane-remodeling function of the amphitropic dynamins may find parallels in the role of coacervation in protecting and sealing membranes found in SPA proteins.

REFERENCES

(1) Fröhlich, C., Grabiger, S., Schwefel, D., Faelber, K., Rosenbaum, E., Mears, J., Rocks, O., and Daumke, O. (2013) Structural insights into oligomerization and mitochondrial remodelling of dynamin 1-like protein. *EMBO J. 32*, 1280–92.

(2) Chang, C.-R., Manlandro, C. M., Arnoult, D., Stadler, J., Posey, A. E., Hill, R. B., and Blackstone, C. (2010) A lethal de novo mutation in the middle domain of the dynamin-related GTPase Drp1 impairs higher order assembly and mitochondrial division. *J. Biol. Chem. 285*, 32494–503.

(3) Strack, S., and Cribbs, J. T. (2012) Allosteric modulation of Drp1 mechanoenzyme assembly and mitochondrial fission by the variable domain. *J. Biol. Chem. 287*, 10990–1001.

(4) Ferguson, K. M., Lemmon, M. A., Schlessinger, J., and Sigler, P. B. (1994) Crystal structure at 2.2 A resolution of the pleckstrin homology domain from human dynamin. *Cell 79*, 199–209.

(5) Timm, D., Salim, K., Gout, I., Guruprasad, L., Waterfield, M., and Blundell, T. (1994) Crystal structure of the pleckstrin homology domain from dynamin. *Nat. Struct. Biol. 1*, 782–8.

(6) Fushman, D., Cahill, S., Lemmon, M. A., Schlessinger, J., and Cowburn, D. (1995) Solution structure of pleckstrin homology domain of dynamin by heteronuclear NMR spectroscopy. *Proc. Natl. Acad. Sci. U. S. A. 92*, 816–20.

(7) Kenniston, J. A., and Lemmon, M. A. (2010) Dynamin GTPase regulation is altered by PH domain mutations found in centronuclear myopathy patients. *EMBO J. 29*, 3054–67.

(8) Blomberg, N., Baraldi, E., Nilges, M., and Saraste, M. (1999) The PH superfold: a structural scaffold for multiple functions. *Trends Biochem. Sci. 24*, 441–5.

(9) Blomberg, N., and Nilges, M. (1997) Functional diversity of PH domains: an exhaustive modelling study. *Fold. Des. 2*, 343–55.

(10) Mears, J., Lackner, L. L., Fang, S., Ingerman, E., Nunnari, J., and Hinshaw, J. E. (2011) Conformational changes in Dnm1 support a contractile mechanism for mitochondrial fission. *Nat. Struct. Mol. Biol. 18*, 20–6.

(11) Yoon, Y., Pitts, K. R., and McNiven, M. A. (2001) Mammalian dynamin-like protein DLP1 tubulates membranes. *Mol. Biol. Cell 12*, 2894–905.

(12) Montessuit, S., Somasekharan, S. P., Terrones, O., Lucken-Ardjomande, S., Herzig, S., Schwarzenbacher, R., Manstein, D. J., Bossy-Wetzel, E., Basañez, G., Meda, P., and Martinou, J.-C. (2010) Membrane remodeling induced by the dynamin-related protein Drp1 stimulates Bax oligomerization. *Cell 142*, 889–901.

(13) Figueroa-Romero, C., Iñiguez-Lluhí, J. A., Stadler, J., Chang, C.-R., Arnoult, D., Keller, P. J., Hong, Y., Blackstone, C., and Feldman, E. L. (2009) SUMOylation of the mitochondrial fission

protein Drp1 occurs at multiple nonconsensus sites within the B domain and is linked to its activity cycle. *FASEB J. 23*, 3917–27.

(14) Strack, S., Wilson, T. J., and Cribbs, J. T. (2013) Cyclin-dependent kinases regulate splice-specific targeting of dynamin-related protein 1 to microtubules. *J. Cell Biol. 201*, 1037–51.

(15) Hoh, J. H. (1998) Functional protein domains from the thermally driven motion of polypeptide chains: a proposal. *Proteins 32*, 223–8.

(16) Santner, A. A., Croy, C. H., Vasanwala, F. H., Uversky, V. N., Van, Y.-Y. J., and Dunker, A. K. (2012) Sweeping away protein aggregation with entropic bristles: intrinsically disordered protein fusions enhance soluble expression. *Biochemistry 51*, 7250–62.

(17) Radivojac, P., Obradovic, Z., Smith, D. K., Zhu, G., Vucetic, S., Brown, C. J., Lawson, J. D., and Dunker, A. K. (2004) Protein flexibility and intrinsic disorder 71–80.

(18) Rauscher, S., and Pomès, R. (2012) Structural disorder and protein elasticity. *Adv. Exp. Med. Biol. 725*, 159–83.

(19) Dobrynin, A. V., and Rubinstein, M. (1995) Flory Theory of a Polyampholyte Chain. *J. Phys. II 5*, 677–695.

(20) Kantor, Y., and Kardar, M. (1995) Instabilities of charged polyampholytes. *Phys. Rev. E 51*, 1299–1312.

(21) Mohanty, B., Gupta, A., Bohidar, H. B., and Bandyopadhyay, S. (2007) Effect of gelatin molecular charge heterogeneity on formation of intermolecular complexes and coacervation transition. *J. Polym. Sci. Part B Polym. Phys. 45*, 1511–1520.

(22) Das, R. K., and Pappu, R. V. (2013) Conformations of intrinsically disordered proteins are influenced by linear sequence distributions of oppositely charged residues. *Proc. Natl. Acad. Sci. U. S. A. 110*, 13392–7.

(23) Mao, A. H., Crick, S. L., Vitalis, A., Chicoine, C. L., and Pappu, R. V. (2010) Net charge per residue modulates conformational ensembles of intrinsically disordered proteins. *Proc. Natl. Acad. Sci. U. S. A. 107*, 8183–8188.

(24) Mao, A. H., Lyle, N., and Pappu, R. V. (2013) Describing sequence-ensemble relationships for intrinsically disordered proteins. *Biochem. J. 449*, 307–18.

(25) Kizilay, E., Kayitmazer, A. B., and Dubin, P. L. (2011) Complexation and coacervation of polyelectrolytes with oppositely charged colloids. *Adv. Colloid Interface Sci. 167*, 24–37.

(26) Ford, M. G. J., Jenni, S., and Nunnari, J. (2011) The crystal structure of dynamin. *Nature 477*, 561–6.

(27) Tatham, A. S., and Shewry, P. R. (2000) Elastomeric proteins: biological roles, structures and mechanisms. *Trends Biochem. Sci. 25*, 567–71.

(28) Urry, D. W., Okamoto, K., Harris, R. D., Hendrix, C. F., and Long, M. M. (1976) Synthetic, crosslinked polypentapeptide of tropoelastin: an anisotropic, fibrillar elastomer. *Biochemistry 15*, 4083–4089.

(29) Yeo, G. C., Keeley, F. W., and Weiss, A. S. (2011) Coacervation of tropoelastin. *Adv. Colloid Interface Sci. 167*, 94–103.

(30) Vollrath, F., and Porter, D. (2006) Spider silk as archetypal protein elastomer. *Soft Matter 2*, 377.

(31) Stewart, R. J., and Wang, C. S. (2010) Adaptation of caddisfly larval silks to aquatic habitats by phosphorylation of h-fibroin serines. *Biomacromolecules 11*, 969–74.

(32) Lim, S., Choi, Y. S., Kang, D. G., Song, Y. H., and Cha, H. J. (2010) The adhesive properties of coacervated recombinant hybrid mussel adhesive proteins. *Biomaterials 31*, 3715–22.

(33) Kato, M., Han, T. W., Xie, S., Shi, K., Du, X., Wu, L. C., Mirzaei, H., Goldsmith, E. J., Longgood, J., Pei, J., Grishin, N. V, Frantz, D. E., Schneider, J. W., Chen, S., Li, L., Sawaya, M. R., Eisenberg, D., Tycko, R., and McKnight, S. L. (2012) Cell-free formation of RNA granules: low complexity sequence domains form dynamic fibers within hydrogels. *Cell 149*, 753–67.

(34) Milles, S., Huy Bui, K., Koehler, C., Eltsov, M., Beck, M., and Lemke, E. A. (2013) Facilitated aggregation of FG nucleoporins under molecular crowding conditions. *EMBO Rep. 14*, 178–83.

(35) Lai, J., Koh, C. H., Tjota, M., Pieuchot, L., Raman, V., Chandrababu, K. B., Yang, D., Wong, L., and Jedd, G. (2012) Intrinsically disordered proteins aggregate at fungal cell-to-cell channels and regulate intercellular connectivity. *Proc. Natl. Acad. Sci. U. S. A. 109*, 15781–6.

(36) Tompa, P. (2013) Hydrogel formation by multivalent IDPs: A reincarnation of the microtrabecular lattice? *Intrinsically Disord. Proteins 1*, e24068.

(37) Li, P., Banjade, S., Cheng, H.-C., Kim, S., Chen, B., Guo, L., Llaguno, M., Hollingsworth, J. V, King, D. S., Banani, S. F., Russo, P. S., Jiang, Q.-X., Nixon, B. T., and Rosen, M. K. (2012) Phase transitions in the assembly of multivalent signalling proteins. *Nature 483*, 336–40.

(38) Brangwynne, C. P., Eckmann, C. R., Courson, D. S., Rybarska, A., Hoege, C., Gharakhani, J., Jülicher, F., and Hyman, A. A. (2009) Germline P granules are liquid droplets that localize by controlled dissolution/condensation. *Science 324*, 1729–32.

(39) Han, T. W., Kato, M., Xie, S., Wu, L. C., Mirzaei, H., Pei, J., Chen, M., Xie, Y., Allen, J., Xiao, G., and McKnight, S. L. (2012) Cell-free formation of RNA granules: bound RNAs identify features and components of cellular assemblies. *Cell 149*, 768–79.

(40) Brangwynne, C. P. (2013) Phase transitions and size scaling of membrane-less organelles. *J. Cell Biol. 203*, 875–81.

(41) Ishida, T., and Kinoshita, K. (2007) PrDOS: prediction of disordered protein regions from amino acid sequence. *Nucleic Acids Res. 35*, W460–4.

AMMON E. POSEY

Born September 12, 1979 in Murray, UT

T. C. Jenkins Department of Biophysics
101 Jenkins Hall
3400 N. Charles Street
Baltimore, MD 21218

(410) 870-5976 aeposey@gmail.com

EDUCATION

PhD, Biophysics — Aug 2014
Johns Hopkins University, Baltimore, MD

MA Medical and Biological Illustration — Apr 2008
Johns Hopkins University School of Medicine, Baltimore, MD

BS Biophysics, minor in visual arts — Apr 2006
Brigham Young University, Provo, UT
3.69 GPA

HONORS AND AWARDS

Teaching Assistantship, Department of Biology, Johns Hopkins University	2010, 2011, 2012, 2014
Carlson Fellowship, Department of Biophysics, Johns Hopkins University	2008
Didusch Scholarship, Johns Hopkins University School of Medicine	2006 – 2008
NASA Langley Aerospace Research Student Scholar (LARSS)	2004, 2005
Best Research Presentation, NASA LARSS Advanced Materials Branch	2004
Heritage Scholarship (4 year full-tuition), Brigham Young University	2001 – 2004
Spring Scholarship, Department of Biology, Brigham Young University	2003
Sterling Scholar State Finalist	1998

RESEARCH EXPERIENCE

PhD thesis, Laboratories of R. Blake Hill and Vincent J. Hilser — Aug 2009 – May 2014
Program in Molecular Biophysics, Johns Hopkins University, Baltimore MD

- Demonstrated that a protein domain of unknown function is intrinsically disordered using size exclusion chromatography, circular dichroism and NMR
- Used light scattering, analytical ultracentrifugation, steady-state fluorescence and circular dichroism to show that protecting osmolytes drive reversible aggregation of an intrinsically disordered domain in a beta-turn-rich conformation
- Developed a lipid binding assay and used it to show that a protein domain of interest binds lipid membranes with specificity for cardiolipin over other anionic lipids
- Devised a proteomic screen to identify proteins that reversibly bind lipid membranes
- Scripted programs in Python for data mining, data simulation, fitting and analysis
- Instructed undergraduate and graduate lab members on instrument operation and experimental techniques

RESEARCH EXPERIENCE (continued)

Master's thesis, Advised by Jennifer Fairman and Peter L. Pedersen — Aug 2007 – Mar 2008
Dept of Art as Applied to Medicine and Dept of Biological Chemistry
Johns Hopkins University School of Medicine, Baltimore, MD
- Assimilated literature relating to the molecular determinants of cancer cell immortalization and the aberrant metabolism of cancer cells (the Warburg effect)
- Created an animated molecular model of a protein megacomplex thought to contribute to the aberrant metabolism of cancer cells

Research Assistant, Langley Aerospace Research Student Scholars program — May 2005 – Aug 2005
NASA Langley Research Center, Hampton, VA — May 2004 – Aug 2004
- Examined gold-protein interactions and protein-monolayer interactions using electrochemical cell, AFM and EM
- Contributed to the development of a glucose sensor and a glucose fuel cell, resulting in a patent
- Developed a novel technique for gold nanoshell fabrication, resulting in a publication
- Delivered research presentations, defended posters and authored two research reports

Research Assistant, Laboratory of Gerald D. Watt — Feb 2004 – Apr 2006
Dept of Chemistry and Biochemistry, Brigham Young University, Provo, UT
- Investigated ferritin protein iron sequestration using stopped-flow spectroscopy and inductively coupled plasma optical emission spectrometry
- Developed method of symmetrically attaching gold nanoparticles to ferritin protein, confirmed nanoparticle attachment by electron microscopy
- Acquired proficiency in UV/Vis spectroscopy and liquid chromatography

PUBLICATIONS AND PATENTS

Posey, A. E., and R. B. Hill. 2014. Intrinsic disorder in the dynamin protein superfamily. (In preparation, to be submitted August 2014)

Posey, A. E., C. M. Manlandro, V. J. Hilser, R. B. Hill. 2014. The B domain of the mechanoenzyme Drp1 inhibits hydrolysis and assembly, is intrinsically disordered and coacervates in protecting osmolyte. (In preparation, to be submitted August 2014)

Koppenol-Raab, M., **A. E. Posey,** R. B. Hill. 2014. Identification of a functionally important residue at a protein interface through pKa measurements of a single protein. (Submitted)

Chang, C.-R., C. M. Manlandro, D. Arnoult, J. Stadler, **A. E. Posey**, R. B. Hill, C. Blackstone. 2010. A lethal de novo mutation in the middle domain of the dynamin-related GTPase Drp1 impairs higher order assembly and mitochondrial division. Journal of Biological Chemistry. 285(42):32494-32503.

Kim, J.-W., **A. E. Posey**, G. D. Watt, S. H. Choi, P. T. Lillehei. 2010. Gold nanoshell assembly on a ferritin protein employed as a bio-template. Journal of Nanoscience and Nanotechnology 10(3):1771-1777.

Posey, A. E. 2008. Visualization of a novel protein megacomplex and its roles in the aberrant metabolism and immortalization of cancer cells. Johns Hopkins University School of Medicine, Baltimore, MD (master's thesis).

PUBLICATIONS AND PATENTS (continued)

Posey, A. E., and J.-W. Kim. 2005. Catalysis of glucose oxidation by gold oxide: Interference in enzyme-catalyzed fuel cells. NASA LARSS Internal Publication (8/05/2005).

Kim, J.-W., **A. E. Posey**, S.-H. Choi, S.-H. Chu, Y. Park, G. C. King, and J. R. Elliot. 2004. Ferritin-based glucose sensor. NASA case # LAR-19009-1 (8/18/2004). (patent disclosure)

Posey, A. E., J.-W. Kim, and S.-H. Choi. 2004. The Use of Ferritin as an Electron Transfer Mediator for Biofuel Cell and Biosensor Applications. NASA LARSS Internal Publication (8/12/2004).

PRESENTATIONS

Posey, A. E., V. J. Hilser, and R. B. Hill. The B domain of the mitochondrial fission mechanoenzyme Drp1 is intrinsically disordered. Biophysical Society 57th Annual Meeting, Philadelphia, PA, February 2013. (poster presentation)

Posey, A. E., and R. B. Hill. Toward identification of pH-sensitive amphitropic proteins. Biophysical Society 55th Annual Meeting, Baltimore, MD, March 2011. (poster presentation)

Posey, A. E., E. Li, L. Chen, J. Lin, E. J. Denning, T. B. Woolf, and K. Hristova. The Effect of Membrane Thickness on the Dimerization Energy of Transmembrane Helices. Biophysical Society 53rd Annual Meeting, Boston, MA, March 2009. (poster presentation)

Posey, A. E. Gold Nanoshells for Application in Thermoelectric Materials. NASA LARSS Research Meeting, Langley Research Center, Advanced Materials Branch, Hampton, VA, August 2005. (oral presentation)

Posey, A. E. Ferritin as an Electron Transfer Mediator and Electrocatalyst Cage for Biofuel Cell Applications. NASA LARSS Research Meeting, Langley Research Center, Advanced Materials Branch, Hampton, VA, August 2004. (oral presentation)

PROGRAMMING, COMPUTATION & SOFTWARE

Python, PyLab (NumPy, SciPy, Matplotlib, IPython), Linux/Unix, Mathematica
PyMOL, DeepView/Swiss-PDBViewer, sequence alignment and sequence analysis tools
Origin, Kaleidagraph, Excel, Powerpoint, Word, Adobe Photoshop, Adobe Illustrator, Adobe Flash

TEACHING EXPERIENCE

Teaching Assistant, **Department of Biology, Johns Hopkins University, Baltimore, MD**

Graduate Biophysical Chemistry — Spring 2012
- Held regular office hours, led recitation/review sections

Genetics Lab — Fall 2011
- Provided weekly laboratory instruction

Cell Biology — Spring 2011, 2014
- Led recitation/review section

Biochemistry — Fall 2010, 2012
- Led recitation/review section

LEADERSHIP AND SERVICE

Youth Group Counselor & Advisor 2011 – 2013
The Inner Harbor Ward, Baltimore, MD 2008 – 2009
▪ Planned/supervised weekly activities for Baltimore City youth

Volunteer Representative, India Bangalore Mission 1999 – 2001
▪ Trained volunteers, organized theological discussions and taught English

ASSOCIATIONS

The Protein Society 2013 – present
Biophysical Society 2009 – present
Association of Medical Illustrators 2007 – 2008